UNIVERSITÀ DEGLI STUDI DI MILANO

Scuola di Dottorato in Fisica, Astrofisica e Fisica Applicata

Dipartimento di Fisica

Corso di Dottorato in Fisica, Astrofisica e Fisica Applicata

Ciclo XXX

Dynamics and characterization of quantum systems interacting with classical noise

Settore Scientifico Disciplinare FIS/03

Supervisore: Prof. Matteo G. A. Paris

Co-supervisore: Prof. Bassano Vacchini

Coordinatore: Prof. Francesco Ragusa

Tesi di Dottorato di:

Matteo Rossi

Anno Accademico 2016/2017

Commission of the final examination:

External Referees:
Dr. Jyrki Piilo (University of Turku, Finland)
Dr. Paola Verrucchi (Istituto dei sistemi complessi-CNR, Firenze)

External Members:
Prof. Marco Barbieri (Università degli Studi Roma Tre)
Prof. Sandro Wimberger (Università degli Studi di Parma)

Internal Member:
Prof. Matteo G. A. Paris

Final examination:

Date: 7 November 2017

Dipartimento di Fisica
Università degli Studi di Milano
via Celoria 16, 20133 Milano, Italy

Cover illustration:

Tunnard, John. *Psi*. Venice: Peggy Guggenheim Collection; 1938.

MIUR subjects:

FIS/03

To my parents

Contents

Acknowledgments

This journey as a PhD student has been very intense and rewarding. It would have never be possible without the help of the amazing people that I met throughout these years, and that have been invaluable for my growth, both as a scientist and as a person. I wish to express my sincere gratitude to all of them.

First of all, I would like to thank my supervisor Matteo Paris for his guidance and deep insights, the precious advice he has given throughout these years, and his constant support to my research. It has been a honor working with him.

I would also like to thank my co-suvpervisor Bassano Vacchini and all the former and current members of the Applied Quantum Mechanics Group at the Università di Milano: my fellow PhD students Antonio Mandarino, Jacopo Trapani, Francesco Albarelli and Luigi Seveso, the post-docs Claudia Benedetti, Matteo Bina and Marco Genoni, and the senior members Simone Cialdi, Stefano Olivares and Dario Tamascelli. It has been a pleasure to work and spend time with these incredible people.

I would also like to thank Gerardo Adesso and Sabrina Maniscalco and all the members of their respective groups in Nottingham, UK and Turku, Finland for their hospitality and for giving me the possibility to learn interesting new topics and work in very active and stimulating research environments.

Besides those already mentioned above, I would like to thank all the people with I had the pleasure to work with throughout these years: Caterina Foti, Paola Verrucchi, Alessandro Cuccoli, Massimo Borrelli and Tommaso Tufarelli.

Finally, and most importantly, I want to thank my family for their unconditional love and help, and, in particular, my parents Mara and Giuseppe that have supported me during my studies with their sacrifices and work. This thesis is dedicated to them.

List of publications

Most of the material presented in this thesis has been published in these papers:

1. M. A. C. Rossi, C. Benedetti, M. Borrelli, S. Maniscalco, M. G. A. Paris
   "Continuous-time quantum walks on spatially correlated noisy lattices"
   Phys. Rev. A **96**, 040301(R) (2017)

2. S. Cialdi, M. A. C. Rossi, C. Benedetti, B. Vacchini, D. Tamascelli, S. Olivares, and M. G. A. Paris
   "All-optical quantum simulator of qubit noisy channels"
   Appl. Phys. Lett. **110**, 081107 (2017)

3. M. A. C. Rossi and M. G. A. Paris
   "Non-Markovian dynamics of single- and two-qubit systems interacting with Gaussian and non-Gaussian fluctuating transverse environments"
   J. Chem. Phys. **144**, 024113 (2016)

4. M. A. C. Rossi and M. G. A. Paris
   "Entangled quantum probes for dynamical environmental noise"
   Phys. Rev. A **92**, 010302(R) (2015)

5. M. A. C. Rossi, C. Benedetti, and M. G. A. Paris
   "Engineering decoherence for two-qubit systems interacting with a classical environment"
   Int. J. Quantum Inf. **12**, 1560003 (2014)

Other published papers:

6. M. A. C. Rossi, C. Foti, A. Cuccoli, J. Trapani, P. Verrucchi, and M. G. A. Paris
   "Effective description of the short-time dynamics in open quantum systems"
   Phys. Rev. A **96**, 032116 (2017)

7. L. Seveso, M. A. C. Rossi, and M. G. A. Paris
   "Quantum metrology beyond the quantum Cramér-Rao theorem"
   Phys. Rev. A **95**, 012111 (2017)

8. M. A. C. Rossi, M. Bina, M. Paris, M. Genoni, G. Adesso, and T. Tufarelli
   "Probing the diamagnetic term in light-matter interaction"
   Quantum Sci. Technol. **2**, 01LT01 (2017)

9. M. A. C. Rossi, T. Giani, and M. G. A. Paris
"Probing deformed quantum commutators"
Phys. Rev. D **94**, 024014 (2016)

10. M. A. C. Rossi, F. Albarelli, and M. G. A. Paris,
"Enhanced estimation of loss in the presence of Kerr nonlinearity"
Phys. Rev. A **93**, 053805 (2016)

Other unpublished material:

1. F. Albarelli, M. A. C. Rossi, M. G. A. Paris, and M. G. Genoni,
"Ultimate quantum limits for noisy magnetometry via time-continuous measurements"
arXiv:1706.00485

2. M. A. C. Rossi, C. Benedetti, S. Cialdi, D. Tamascelli, S. Olivares, B. Vacchini, and M. G. A. Paris
"Non-Markovianity by undersampling"
arXiv:1705.05852 (To appear in *Int. J. Quantum Inf.*)

Introduction

In the last decades, tremendous progress has been made in the quest for quantum technologies, both from the theoretical and experimental side. Various algorithms and protocols have been designed that take advantage of quantum resources for computation, communication and metrology; we are testing quantum communication through space with satellites, we are building quantum computers with more and more qubits and some researchers believe that we are only a few years away from showing the "quantum supremacy", that is, seeing a quantum device perform a particular task that's beyond the reach of any conventional computer.

Since the early years of quantum mechanics, physicists have studied with interest the weird nature of quantum correlations, especially from a fundamental point of view. Eventually, the new field of quantum information theory emerged with the goal of investigating how quantum systems can be used to store, transmit and elaborate information and how the non-classical nature of their correlations allows to define protocols that outperform their classical counterparts. A lot of effort has been put into classifying quantum correlations and exploring their properties, fostered by the fact that correlations often stand as key resource for secure communication [1], quantum computation [2], and metrological problems [3]. Traditionally, entanglement was the only known form of quantum correlations. Nowadays, the existence of more general forms of non-classical correlations as discord or steering is accepted, limiting entanglement to capture aspects of correlations based on non-separability [4]. For instance, quantum discord, an information-deficit between quantum and classical correlations, has been shown to be a resource for computation [5] and quantum information protocols [6].

However, many challenges lie ahead for practical implementations of quantum technologies. One of the most important of those challenges comes from the fact that quantum systems are unavoidably affected by the interaction with their surrounding. The coupling to the environment is generally detrimental to the quantum information contained in the system as it undergoes decoherence. Thus, beside the undeniable fundamental interest in understanding the dynamics of quantum systems interacting with an environment, a great deal of attention has been devoted to the study of *open quantum systems* [7]: it is fundamental, for developing quantum technologies, to overcome the problem of decoherence and loss of information. An interesting result of this scrutiny of the dynamics of open quantum systems is the recognition of another figure of merit as resource for quantum technology: the concept of quantum non-Markovianity. While Markovianity is well defined for a classical stochastic process, it does not generalize in a straightforward

way to the quantum world. The effort to find a generalization for quantum system led to many different definitions and measures to quantify its degree [8–10]. Qualitatively, the non-Markovianity is connected to the presence of memory effects in the environment, that allow for temporary recoherence and revival of quantum correlations. Thus, a proper description and understanding of the environment and, possibly, its engineering, may prove extremely important in the realization of quantum devices.

When treating the interaction of a quantum system with its surroundings, it is natural to describe the environment quantum-mechanically as well. However, systems of interest in quantum information generally interact with complex environments, with many degrees of freedom, and a full quantum description may be challenging or even unfeasible. To this end, a classical model of the environment usually represents a valid alternative and may provide good results. A random unitary evolution, that is, a unitary evolution that depends on stochastic classical fields, may describe equally well the resulting irreversible dynamics of the open system without the need to invoke a quantum environment at all. A general understanding of whether and under which conditions the two descriptions are equivalent still lacks, with an ongoing debate in the literature [11–13]. Parametric representation has also been used to show that classical variables can emerge in quantum Hamiltonians as environmental degrees of freedom [14–18]. Moreover, it has recently been shown that for certain kinds of interactions a classical description can be found that is completely equivalent to the quantum one. For instance, Crow and Joynt proved [11] an explicit construction method for a random-classical-field description of one-qubit dephasing maps.

Besides theoretical interest, the interaction with classical noise is extremely important in physical implementations. There are indeed various experimental evidences of interaction with classical forms of noise, typically Gaussian noise or colored noise with spectrums of the form $1/f^{\alpha}$. This is a particularly relevant phenomenon in nanodevices and solid-state qubits [19]. Solid-state systems can be used to represent qubits by using *quantum dots*, i.e. nanostructures made of semiconductors that generate a tridimensional potential well that spatially confines charged particles, such as electrons and holes. The charge or spin of the trapped particle can then be used as a physical realization of a qubit, and can be measured and manipulated, for instance by applying voltages or magnetic fields, to process quantum information. The main advantage of solid-state qubits is that it is easier, compared to other physical implementations, to tune the parameters that control the state of the system and thus to perform operations on the qubit. This tunability, however, comes at the cost of greater sensitivity to fluctuations in the control parameters and to local electromagnetic fields. Various experiments have observed that those fluctuations can be described as $1/f$ noise and that they have a detrimental effect on decoherence. Also superconductive devices can be used for implementing qubits, for instance by using the number of Cooper pairs in electrostatic box as quantum numbers and Josephson junctions to control the interaction between qubits. Recently, also experiments with superconducting circuits evidenced $1/f$ low-frequency fluctuations of various physical observables.

Because of these reasons, classical system-environment interactions have attracted considerable attention in the field of quantum information [20]. Examples include studies

of the dynamics of quantum correlations [21–30], the simulation of motional averaging [31], decoherence of spin systems in magnetic fields [32, 33] or in solid state qubits [34–36]. Also continuous-variable systems have been object of extensive studies [37–39].

The very sensitivity of quantum systems to external influences is on one hand a problem for quantum information processing tasks. However, on the other hand, it also provides an effective tool to characterize unknown parameters of a given environment by exploiting quantum probes, as opposed to classical ones, usually macroscopic and more intrusive. Indeed, in many metrological tasks one aims at the highest possible precision, but at the same time the measurement device can alter or damage the sample. Quantum probes have the advantage of being microscopic and very sensitive, and moreover one can exploit quantum correlations to achieve even higher precision. It is indeed known that entanglement is a resource for various estimation problems [40–42], as it allows to overcome the classical limit to sensitivity. Quantum metrology is now an affirmed research field [43], with applications that extend to gravitational wave detection [44]. It is thus natural to use quantum systems as probes to determine the properties of their complex environments [45, 46], and a study of possible enhancements given by entanglement or other forms of quantum correlations.

Another class of systems that has attracted much interest in the last decades is that of quantum walks. Quantum walks are the generalization of classical random walks and describe the propagation of a particle on a discrete graph. Their quantum nature, with quantum superposition and interference, allows for features and properties that are not seen in their classical counterparts and that are relevant in quantum information processing: for example, the faster propagation speed of the walker is relevant in quantum search algorithms [47], universal quantum computation [48] or transport on complex networks [49]. Experimental implementations of quantum walks have been realized or proposed with various physical systems including trapped ions [50], atoms [51] and optical waveguides [52], which inevitably suffer from noise coming from the interaction with the environment and imperfections in the setup. The decoherence induced may limit the propagation of the walker, restoring the classical diffusion speed, or even localize the walker. It is thus fundamental to address the effects of noise on quantum walks, and a description of the noise in terms of a classical stochastic field may again prove extremely useful [53, 54].

This PhD thesis contains a detailed study of the dynamics of quantum systems interacting with classical noise. In particular, we focus on finite dimensional quantum systems and we consider environments that are modeled by Gaussian stochastic processes and we compare them to a prototypical non-Gaussian process, the random telegraph noise, characterized by a bistable fluctuator. In fact, generally, the noise affecting solid-state devices is non-Gaussian, generated by a large number of fluctuators, with a broad spectrum of switching rates. However, Gaussian processes are much easier to describe, being entirely defined by their second-order statistics, and provide a good approximation of more complex fluctuating environments, thus allowing for a reasonably self-contained description of systems where a full analytical solution of the dynamics is not avoidable.

Our aim is to analyze the dynamics of quantum correlations, and to establish a connection between the features of the evolution, in particular the presence of recoherence

effects, and the non-Markovianity of the quantum map. We will first review the state of the art regarding dephasing noise, which involves typical frequencies of the environment that are much smaller than the natural frequency of the quantum system. In this case, fluctuations can cause decoherence in a superposition of states, without inducing transitions between different energy levels. Afterwards, we will move to the analysis of the so-called transverse noise, which induces relaxation and excitation of the quantum systems, and has a richer phenomenology.

We will then present the first implementation of an optical quantum simulator of single-qubit noisy dephasing channels. The simulator uses single photons generated by parametric down-conversion as information carriers, and encodes the qubit into the polarization degree of freedom. The optical setup permits to apply many random unitary transformations in parallel, thus allowing us to sample the probability space of the stochastic process describing the noise. We will present and discuss the results of simulations involving Gaussian and non-Gaussian noise, commenting on drawbacks and possible extensions of the experimental apparatus.

Then, we will describe the use of qubit systems as probes for detecting properties of the classical environment, and show that the use of entangled probes can give quantum enhancement to the precision of the estimation under proper experimental conditions. Finally, we will address the dynamics of a continuous-time quantum walk affected by spatially correlated classical noise.

This thesis is structured as follows.

- In Chapter 1 we review the general properties of stochastic processes, we introduce Gaussian processes and the prototypical Ornstein-Uhlenbeck process, and then we introduce the random telegraph noise. We also discuss the numerical simulation of these two stochastic processes.

- In Chapter 2 we review the basic concepts of quantum mechanics and quantum information, focusing on the definitions and measures of quantum correlations. We also discuss the general formalism for the description of open quantum systems and introduce the concept of quantum non-Markovianity. We finally introduce the formal tools of quantum estimation theory, needed to infer the value of an unknown parameter from measurements on a quantum system.

- In Chapter 3 we review the description of the random unitary quantum channel, that describes the dynamics of a quantum system under the effect of classical noise. We then review the analytical solutions to dephasing noise and the transfer matrix method, that allows for an analytical solution to transverse random telegraph noise. We then discuss the numerical simulation of the dynamics in the general case. Finally, we show some original results involving the study of the dynamics of quantum correlations and the characterization of the quantum map in the case of transverse Gaussian and random telegraph noise.

- In Chapter 4 we describe the experimental implementation of an optical simulator of a single-qubit classical noise channel. We describe the apparatus and present the

results obtained with the simulation of Ornstein-Uhlenbeck and random telegraph noise.

- In Chapter 5 we describe a probing scheme where we use qubits to infer the spectral width of classical Gaussian noise. After reviewing the single-qubit probing scheme, we show that the preparation of an entangled state allows for quantum-enhanced precision in the estimation procedure.
- In Chapter 6 we study the dynamics of continuous-time quantum walks affected by random telegraph noise with spatial correlations and we discuss the properties of the dynamics.

Chapter 1

Stochastic processes and classical noise

In this chapter we review the main concepts related to the theory of stochastic processes and classical noise. The topic is very broad and, inevitably, the discussion here will be limited to the notions that are required in the understanding of the following discussion. First, we will revise the main concepts involving random variables and stochastic processes, then we will specialize to Gaussian processes, with particular attention to the Ornstein-Uhlenbeck process, and to the random telegraph process. We will also give the classical definition of non-Markovianity, which we will generalize to the quantum case in Chapter 2. A more exhaustive discussion can be found on reference books on the topic such as [55].

1.1 Random variables and stochastic processes

A stochastic process describes the dynamics of a physical property of a system that evolves with some indeterminacy, instead of obeying a deterministic law. Stochastic processes are widely employed in many disciplines, including biology, chemistry, finance, computer science, engineering, and, of course, physics.

Random variables Without the need to deal with formal mathematical definitions, we can say that a *random variable* X is an object defined by a set of possible outcomes $\{x_i\}$, called sample space. To each outcome is a assigned a probability $p(X = x_i) \equiv p(x_i)$, which satisfies the property $\sum_i p(x_i) = 1$, with $p(x_i) \geq 0$. The sample space can be discrete or continuous: in that case, we will have a continuous probability distribution $p(x)$.

Assuming that X has value in a continuous sample space, we define the expected value of X as

$$\mathbb{E}[X] = \int dx\ x p(x) \tag{1.1}$$

and its variance

$$\mathrm{Var}[X] = \mathbb{E}\left[(X - \mathbb{E}[X])^2\right] = \mathbb{E}\left[X^2\right] - \mathbb{E}[X]^2 . \tag{1.2}$$

If the sample space is discrete, the integral in Eq. (1.1) is replaced by a sum over all the elements in the space. In general, the quantity $\mathbb{E}[X^m]$ is called the *m-th moment* of X. The average is thus the first moment and the variance is the difference between the second moment and the square of the first one.

A random variable is entirely specified by its sample space and the probability distribution $p(x)$, but is also described completely by the *characteristic function*

$$\chi(\xi) = \mathbb{E}\left[e^{i\xi X}\right] = \int e^{i\xi x} p(x) dx. \tag{1.3}$$

$\chi(\xi)$ is the Fourier transform of the probability distribution $p(x)$.

The moments of X can be expressed in terms of the characteristic function:

$$\mathbb{E}[X^m] = (-i)^m \left.\frac{d^m \chi(\xi)}{d\xi^m}\right|_{\xi=0}. \tag{1.4}$$

In general, a random variable is characterized by an infinite number of moments. Random variables characterized by a Gaussian probability distribution, or simply Gaussian random variables, are described by only the first and second moment.

The probability distribution for a Gaussian random variable is

$$p(x) = \frac{1}{\sqrt{2\pi\sigma^2}} e^{-\frac{(x-\mu)^2}{2\sigma^2}}. \tag{1.5}$$

One can easily check that the expected value is $\mathbb{E}[X] = \mu$ and the variance is $\mathrm{Var}[X] = \sigma^2$. The characteristic function is also Gaussian:

$$\chi(\xi) = e^{i\xi\mu - \frac{1}{2}\sigma^2\xi^2}. \tag{1.6}$$

Stochastic processes A stochastic process is a collection of random variables, indexed by a time parameter t: $\{X(t), t \in T\}$. Each of the $X(t)$ is defined on the same sample space and its value represents the observed value of the stochastic process at time t. More formally, $\{X(t), t \in T\}$ is a function of two arguments: $\{X(t,s), t \in T, s \in S\}$, where S is the probability space. For a fixed value of t, $X(t,\cdot)$ is a function defined on the probability space, i.e. a random variable. If, on the other hand, we fix S, then $X(\cdot, s)$ is a function of time that represents a specific observation of the stochastic process, that we call *realization* of the process.

In other words, we assume that a set of joint probabilities $p(x_1, t_1; x_n, t_2; \ldots)$ exists, that fully characterizes the stochastic process. In terms of these joint probabilities, we can also define conditional probability densities:

$$p(x_1, t_1; x_2, t_2; \ldots | y_1, \tau_1; y_2, \tau_2; \ldots) = \frac{p(x_1, t_1; x_2, t_2; \ldots; y_1, \tau_1; y_2, \tau_2; \ldots)}{p(y_1, \tau_1; y_2, \tau_2; \ldots)}. \tag{1.7}$$

In particular, the conditional probability $p(x_n, t_n | x_1, t_1; \ldots; x_{n-1}, t_{n-1})$ tells us the probability density for the value of the stochastic process at time t_n, given its previous history $x_1(t_1), \ldots, x_{n-1}(t_{n-1})$. It is in this context that the notion of Markovianity, which we will discuss in the quantum formalism in Subsection 2.3.1, is introduced at the classical level.

We say that a stochastic process is *Markovian* if the following equality holds for any set of n successive times:

$$p(x_n, t_n | x_1, t_1; \ldots; x_{n-1}, t_{n-1}) = p(x_n, t_n | x_{n-1}, t_{n-1}), \tag{1.8}$$

that is, the state of the stochastic process only depends on the last assumed value and not on the previous history. In this sense, it is said that a Markov process is memoryless. If the above property does not hold, we say that the process is non-Markovian.

The Markov property (1.8) implies that the conditional transition property satisfies the *Chapman-Kolmogorov equation* [55]

$$p(x,t|y,s) = \sum_z p(x,t|z,\tau)p(z,\tau|y,s). \tag{1.9}$$

The Markov property is relatively easy to verify for processes that have a discrete time domain (which are usually referred to as *Markov chains*), but it is a bit trickier for continuous-time processes.

An important quantity in the characterization of stochastic processes is the *autocorrelation function*, defined as

$$C(t_1,t_2) = \mathbb{E}\left[X(t_1)X(t_2)\right], \tag{1.10}$$

where t_1 and t_2 are two instants of time.

A stochastic process is said to be *stationary* if any joint probability is invariant under translations in time

$$p(x_1,t_1;\ldots;x_n,t_n) = p(x_1,t_1+\tau;\ldots;x_n,t_n+\tau), \qquad \forall\tau. \tag{1.11}$$

If a process is stationary, its moments are time-independent, and its autocorrelation function only depends on the difference $|t_2 - t_1|$: $C(t_1,t_2) = C(|t_2-t_1|) \equiv C(\tau)$. It can thus be defined by its Fourier transform, which is the *power spectral density* (or simply, the spectrum) of the process

$$S(\omega) = \int d\tau\ C(\tau)e^{-i\omega\tau}. \tag{1.12}$$

The spectrum and autocorrelation function are extremely important in the characterization of a stochastic process, because, together with the mean and variance, are one of the easiest functions to measure experimentally, by directly sampling.

Finally, we introduce the *noise phase*, that will be employed in the following chapters:

$$\phi(t) = \int_{t_0}^{t} X(s)ds. \tag{1.13}$$

$\phi(t)$ is itself a stochastic process. Its characteristic function, defined as

$$\mathbb{E}\left[e^{i\nu\phi}\right] = \mathbb{E}\left[e^{i\nu\int_{t_0}^{t} X(s)ds}\right], \tag{1.14}$$

will be useful in the description of the dynamics of quantum systems interacting with classical noise.

In the following, we are going to focus on the class of Gaussian stochastic processes, by looking in particular at the Ornstein-Uhlenbeck process, and then to another process that is relevant in the study of physical implementations of quantum systems: the random telegraph noise.

1.2 Gaussian processes

A stochastic process is said to be Gaussian if any joint probability distribution is a Gaussian distribution. Using the characteristic function, the Gaussian property can be expressed with the following equation

$$\chi_{X(t_1),\dots,X(t_n)}(\xi_1,\dots,\xi_n) = \mathbb{E}\left[\exp\left(i\sum_{j=1}^{n}\xi_j X(t_j)\right)\right] = \exp\left[i\sum_{j=1}^{n}\xi_j\mu_j - \frac{1}{2}\sum_{j,k=1}^{n}\xi_j\xi_k K(t_j,t_k)\right], \tag{1.15}$$

where $\mu_i = \mathbb{E}[X(t_i)]$ and we define the *covariance kernel*

$$K(t_1,t_2) = \mathbb{E}\left[(X(t_1)-\mu_1)(X(t_2)-\mu_2)\right] = \mathbb{E}[X(t_1)X(t_2)] - \mu_1\mu_2. \tag{1.16}$$

For a stationary process, the covariance kernel only depends on the difference between t_1 and t_2 and it equals the autocorrelation function plus the mean value of the process. Since in this thesis we deal with stationary, zero-mean processes, we will use the two notions interchangeably.

For a continuous time Gaussian process, Eq. (1.15) becomes

$$\mathbb{E}\left[e^{i\int_{t_0}^{t} ds\ \xi(s)X(s)}\right] = \exp\left[i\int_{t_0}^{t} ds\ \xi(s)\mu(s) - \frac{1}{2}\iint_{t_0}^{t} ds ds'\ \xi(s)\xi(s')K(s,s')\right], \tag{1.17}$$

Equations (1.15) and (1.17) show us that a Gaussian process is entirely characterized by its first and second moments, i.e. the mean value and the covariance kernel.

A special case of Eq. (1.17) that is relevant for us is that of $\xi(s) \equiv \xi$ time independent. We have

$$\mathbb{E}\left[e^{i\xi\int_{t_0}^{t} ds\ X(s)}\right] = \exp\left[i\xi\int_{t_0}^{t} ds\ \mu(s) - \frac{\xi^2}{2}\beta(t)\right], \tag{1.18}$$

where we have introduced the β function

$$\beta(t) = \int_{t_0}^{t} ds \int_{t_0}^{t} ds'\ K(s,s'). \tag{1.19}$$

1.2.1 Wiener process

The Wiener process is the stochastic process that describes the Brownian motion of a particle suspended in a fluid. It is the simplest example of Gaussian process, and a building block for other stochastic processes. It is defined as the process with initial value $W(t=0) = 0$ and independent Gaussian increments. That is, $dW = W(t+dt) - W(t)$ is a normally distributed random variable with mean $\mu_{dW} = 0$ and variance $\mathrm{Var}[dW] = dt$, and mean and variance do not depend on t. The increments dW are often referred to as Wiener increments.

From the defining properties, it is easy to see that the mean value of the process is $\mathbb{E}[W(t)] = 0$, while the variance is $\mathrm{Var}[W(t)] = t$. It is characterized by the autocorrelation function [55]

$$C_W(t_1, t_2) = \min(t_1, t_2). \tag{1.20}$$

1.2.2 Ornstein-Uhlenbeck process

The Ornstein-Uhlenbeck (OU) process is the simplest stochastic process with non-trivial dynamics. It was introduced by Uhlenbeck and Ornstein in 1930 [56] to describe the velocity of a particle undergoing Brownian motion with friction, but it is widely used in modelling general noise with a finite correlation time [57].

It is defined via the stochastic differential equation

$$dX = \gamma(\mu - X)dt + \sqrt{\Gamma}\gamma dW, \tag{1.21}$$

where dW is a Wiener increment, μ is the stationary mean value, Γ is called damping rate and γ is the inverse of the autocorrelation time τ_C, and is also called spectral width. The first term of Eq. (1.21) is a friction term that keeps the value of X around the mean value μ.

Since the Wiener process is Gaussian, the Ornstein-Uhlenbeck process is Gaussian as well. It can be shown that it is stationary, with mean and variance

$$\mathbb{E}[X] = \mu, \qquad \mathrm{Var}[X] = \frac{\gamma\Gamma}{2}. \tag{1.22}$$

The initial condition of Eq. (1.21) can be chosen to be a fixed point X_0, or a random point extracted from the stationary distribution (1.22). Assuming, as we will do in the following chapters, that the mean value of the process is $\mu = 0$, the autocorrelation function of the process becomes

$$K_{\mathrm{OU}}(\tau) = \frac{\gamma\Gamma}{2} e^{-\gamma|\tau|}. \tag{1.23}$$

This in turn allows us to calculate the β function,

$$\beta_{\mathrm{OU}}(t) = \frac{\Gamma\left(\gamma t + e^{-\gamma t} - 1\right)}{\gamma}, \tag{1.24}$$

and the power spectral density, which is a Lorentzian

$$S_{\mathrm{OU}}(\omega) = \frac{\Gamma\gamma^2}{\sqrt{2\pi}(\gamma^2 + \omega^2)}. \tag{1.25}$$

From Eq. (1.23) we can see that the Ornstein-Uhlenbeck process has a finite correlation time $\tau_C = \gamma^{-1}$. Finally, it can be shown that it is a Markovian process in the sense of Eq. (1.8). In the limit of $\gamma \to \infty$ ($\tau_C \to 0$), the stochastic process becomes completely uncorrelated. The autocorrelation function and the power spectral density become respectively a Dirac delta and constant and we obtain Gaussian white noise:

$$K_{\mathrm{WN}}(t_1 - t_2) = \Gamma\delta(t_1 - t_2) \tag{1.26}$$

$$\beta_{\mathrm{WN}}(t) = \Gamma t. \tag{1.27}$$

1.3 Non-Gaussian processses

Gaussian processes are completely characterized by their first and second moments, i.e. by their mean and autocorrelation function. Although they play a central role in the theory of stochastic processes, due to their simple analytical properties, and to the fact that they can give god approximations in most situations, in some situations it is necessary to specify the model for the noise source in more details, thus requiring non-Gaussian processes [58]. Non-Gaussian noise cannot be approximated by any Gaussian model, such as a bath of harmonic oscillators, because of the central role played by the microscopic structure of the environment in determining the quantum dynamics of the system subject to the noise.

The key ingredient in the non-Gaussian noise models that are relevant in quantum devices is that of two-level fluctuators (TLF), i.e. quantities that switch randomly between two values with a certain switching rate. The effect of a single fluctuator is to produce the random telegraph noise, while a proper collection of TLFs gives rise to colored noise. In the following we review the random telegraph noise. More general forms of noise, and their effect on the dynamics of quantum systems, are discussed in Ref. [20] and refs. therein.

1.3.1 Random telegraph noise

The random telegraph noise (RTN) is a continuous time stochastic process $\{B(t), t \in [0, \infty]\}$, where the variable B can take two possible values. Without loss of generality we can assume $B = \pm 1$. The fluctuator jumps between the two states with a switching rate γ, i.e. in such a way that the average number of flips in a time interval $[t, t + \tau]$ is $\gamma\tau$.

The probability that, after a time t, the fluctuator has switched n times follows a Poisson distribution with parameter γt

$$p_n(t) = \frac{(\gamma t)^n}{n!} e^{-\gamma t}. \tag{1.28}$$

The RTN can thus be expressed as $B(t) = (-1)^P(t)$, where $P(t)$ is the Poisson process.

To obtain the mean value, the variance and the autocorrelation function of the process, we start by solving the Chapman-Kolmogorov equation for the transition probability. Assuming that the initial condition is $B(t_0) = x_0$, we can write

$$\frac{d}{dt} p(+1, t|x_0, t_0) = -\gamma p(+1, t|x_0, t_0) + \gamma p(-1, t|x_0, t_0) \tag{1.29a}$$

$$\frac{d}{dt} p(-1, t|x_0, t_0) = \gamma p(+1, t|x_0, t_0) - \gamma p(-1, t|x_0, t_0), \tag{1.29b}$$

together with the normalization condition $p(+1, t|x_0, t_0) + p(-1, t|x_0, t_0) = 1$. Eqs. (1.29) have the solution [55]

$$p(+1, t|x_0, t_0) = \frac{1}{2}\left[1 + e^{-2\gamma(t-t_0)}(\delta_{+1,x_0} - \delta_{-1,x_0})\right] \tag{1.30a}$$

$$p(-1, t|x_0, t_0) = \frac{1}{2}\left[1 - e^{-2\gamma(t-t_0)}(\delta_{+1,x_0} - \delta_{-1,x_0})\right]. \tag{1.30b}$$

The process clearly has a stationary solution, obtained by letting $t \to \infty$:

$$p_s(\pm 1) \equiv p(\pm 1, t \to \infty) = \frac{1}{2}. \tag{1.31}$$

The mean of the process and its variance can now be easily computed. The mean is

$$\mathbb{E}\left[B(t)\right] = \sum_{x=\pm 1} xP(x,t|x_0,t_0) = x_0 \exp[-2\gamma(t-t_0)], \tag{1.32}$$

while the variance has a cumbersome expression. The stationary values are, respectively:

$$\mathbb{E}\left[B(t)\right]_s = 0, \qquad \mathrm{Var}\left[B(t)\right]_s = 1 \tag{1.33}$$

The stationary expression for the autocorrelation function is given by (assuming $t_2 \geq t_1$)

$$K_{\text{RTN}}(t_1,t_2) = \sum_{x_1,x_2} x_2 x_1 P(x_2,t_2|x_1,t_1)P_s(x_1) \tag{1.34}$$

$$= \frac{1}{2}\sum_{x_1=\pm 1} x_1^2 \exp[-2\gamma(t_2-t_1)] = \exp[-2\gamma(t_2-t_1)], \tag{1.35}$$

where we have used Eq. (1.32). Given the stationarity of the process, we can write

$$K_{\text{RTN}}(\tau) = \exp[-2\gamma|\tau|]. \tag{1.36}$$

We immediately notice that the autocorrelation function of the RTN has the same time dependence as that of the Ornstein-Uhlenbeck process. The spectrum is a Lorentzian as well

$$S_{\text{RTN}}(\omega) = \frac{4\gamma}{(2\gamma)^2 + \omega^2}. \tag{1.37}$$

We thus have two processes with the same spectral properties, but with completely different probabilities distributions, to model noise sources that are relevant in the study of open quantum systems.

We finally write the probability distribution for the noise phase (1.13) and its characteristic function (1.14). We simply report the final results. The proof, which is rather complicated, is sketched in [20] and addressed in detail in [58, 59].

Instead of evaluating $\phi(t)$ we evaluate the quantity $\phi_\nu(t) = \nu\phi(t)$, and find that

$$p(\phi_\nu,t) = \frac{1}{2}e^{-\gamma t}[\delta(\phi_\nu+\nu t)+\delta(\phi_\nu-\nu t)] + \frac{\gamma}{2\nu}e^{-\gamma t}[\Theta(\phi_\nu+\nu t)-\Theta(\phi_\nu-\nu t)]$$
$$\times\left[\frac{I_1\left(\gamma t\sqrt{1-(\phi_\nu/\nu t)^2}\right)}{\sqrt{1-(\phi_\nu/\nu t)^2}} + I_0\left(\gamma t\sqrt{1-(\phi_\nu/\nu t)^2}\right)\right], \tag{1.38}$$

where $\delta(x)$ is the Dirac delta function, $\Theta(x)$ is the Heaviside step function, and $I_n(x)$ is the modified Bessel function of the first kind [60, §10.25]. A plot of $p(\phi_n,t)$ for a few values of γt is shown in Fig. 1.1a. The two Dirac deltas represent the probability for the

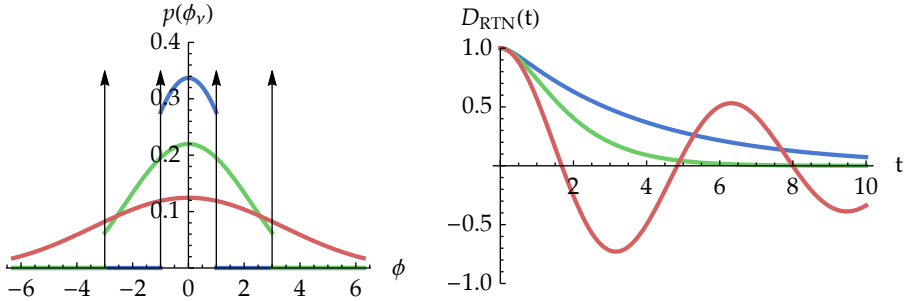

Figure 1.1: (a) The probability distribution $p(\phi_\nu, t)$ for $t = 1$ (blue), 5 (green), 10 (red) for $\gamma = \nu = 1$. The arrows represent the Dirac deltas. (b) shows the function $D_{\text{RTN}}(t)$ defined in Eq. (1.40) as a function of t for $\nu = 1$ and $\gamma = 2$ (blue), $\gamma = 1$ (green), $\gamma = 0.1$ (red). When $\gamma > \nu$ the function is monotonically decaying, while it is oscillating for $\gamma > \nu$.

fluctuator to be in the same state during time t, while the From Eq. (1.38), one obtains the expression for the characteristic function

$$D_{\text{RTN}}(t) \equiv \mathbb{E}\left[e^{i\nu\phi(t)}\right] = \frac{1}{2}e^{-\gamma t}\left[\left(1+\frac{\gamma}{2\delta}\right)e^{\delta t} + \left(1-\frac{\gamma}{2\delta}e^{-\delta t}\right)\right], \tag{1.39}$$

where we defined $\delta = \sqrt{\gamma^2 - \nu^2}$. δ is real if $\gamma^2 \geq \nu^2$, but it is imaginary in the other case, thus we have two qualitatively different behaviors for $\mathbb{E}\left[e^{i\nu\phi(t)}\right]$. We have

$$D_{\text{RTN}}(t) = \begin{cases} e^{-\gamma t}\left[\cosh|\delta|t + \frac{\gamma}{|\delta|}\sinh|\delta|t\right] & \gamma > \nu \\ e^{-\gamma t}\left[\cos|\delta|t + \frac{\gamma}{|\delta|}\sin|\delta|t\right] & \gamma < \nu. \end{cases} \tag{1.40}$$

As shown in Fig. 1.1b, when $\gamma > \nu$ the function is monotonically decaying, but in the opposite regime it has an oscillating behavior.

1.4 Numerical simulation of stochastic processes

Some of the results presented in this thesis require the numerical simulation of the classical noise affected by the quantum systems. In this section we report on the methods used for generating realizations of the OU and RTN processes. The methods are also used in the optical quantum simulator described in Chapter 4. The result of a simulation is a realization of the stochastic process in the time interval $[0, T]$, sampled at n time instants $t_0 = 0, t_1, t_2, \ldots, t_n = T$, separated by a time step $\Delta t = T/n$.

Ornstein-Uhlenbeck In general, stochastic processes defined by a stochastic differential equation can be simulated by means of Euler-Maruyama method, i.e. the generalization of the well-known Euler first order method for ordinary differential equations. A large body of literature deals with the study of convergence and stability of this method, see

for instance [55]. In the case of the Ornstein-Uhlenbeck we can avoid all this because the stochastic differential equation (1.21) can be solved [55, 57]. The solution reads

$$X(t) = \mu + e^{-\gamma t}(X(0) - \mu) + \gamma\sqrt{\Gamma}\int_0^t e^{-\gamma(t-t')}dW(t'). \tag{1.41}$$

The simulation thus amounts to generating n Wiener increments with variance Δt, $\Delta W \sim \mathcal{N}(0, \sqrt{\Delta t})$ and numerically evaluating the integral in Eq. (1.41). An example of implementation with MATLAB/Octave code is the following:

```
function X = ornsteinUhlenbeck(t, ... % time vector
                               mu, ... % mean value
                               gamma, ... % spectral width
                               Gamma) % damping rate

   % time step
   dt = t(2) - t(1);

   % Set initial condition
   % For fixed initial condition: X0 = 0;
   % Stationary initial condition:
   X0 = mu + gamma * sqrt(Gamma)/sqrt(2*gamma) * randn();

   % Vector of Wiener increments
   dW = [0 sqrt(dt) * randn(1, length(t) - 1)];

   % Sampling of the Ornstein-Uhlenbeck process
   X = X0 * exp(-gamma * t) + mu * (1 - exp(-gamma*t)) ...
      + gamma * sqrt(Gamma) * exp(- gamma * t) ...
        .* cumsum(exp(gamma * t) .* dW]);
end
```

Random telegraph noise As we have seen in Subsection 1.3.1, the RTN can be obtained from the Poisson process. If P is the variable describing the latter, then the RTN is simply given by $X = (-1)^P$, i.e. it switches its state at each event of the Poisson process. If you have a Poisson process with rate γ, then the time intervals δ between two events are independent and exponentially distributed with mean γ^{-1}. So the probability density function for δ is $p(\delta) = \gamma\exp(-\gamma\delta)$, and the cumulative distribution function is $F(\delta) = 1-\exp(-\gamma\delta)$. Thus we can generate the time intervals between events by drawing δ from the probability distribution above. By inverting the cumulative function, we obtain that $\delta = -\log(R)/\gamma$, where R is drawn from a uniform distribution in $[0, 1]$.

The following MATLAB/Octave code generates a realization of RTN sampled at the time instants of the vector `t`. It first generates a vector `delta` of intervals δ of length $N_\delta = \lfloor 2 * \gamma T \rfloor$, where T is the final time and $\lfloor\cdot\rfloor$ means the integer part. As there are on

average $\gamma * \Delta t$ events in the time interval Δt, this choice of N_δ guarantees that we generate events until the end of the sampling time.

```
function X = rtn(t, gamma)
% t is the vector of time steps
% gamma is the switching rate.
% X is a vector of the length of t containing the sampled process

   dt = t(2) - t(1);
   % Number of time intervals to generate
   % (twice the expected value gamma * T)
   Ndelta = max(1, floor(2 * t(end) * gamma));

   % Vector of the time intervals between events
   delta = - log(rand(Ndelta, 1)) / (dt * gamma);

   % The time instants of the events
   ct = cumsum(floor(delta)) + 1;

   % Finds the index of the first time outside the t vector
   ix = sum(ct <= length(t));

   % Create the signal by setting s to 1 at each event time
   % and then performing a cumulative sum.
   poisson = zeros(length(t),1);
   poisson(ct(1:ix)) = 1;
   poisson = cumsum(poisson);

   % This is for setting the initial condition
   % 1 and -1 with equal probability
   r = randi(2);

   % Here we obtain the RTN from the Poisson process
   X = (-1).^(r+poisson);
```

Summary

- A stochastic process is a collection of random variables, indexed by a discrete or continuous parameter t: $\{X(t), t \in T\}$. Stochastic processes are useful to describe classical fluctuations and noise in physical systems.

- Stochastic processes are in general characterized by the joint probability distributions of the random variables $X(t)$. A relevant class is that of Gaussian processes, where these probability distributions are Gaussian and are thus entirely described by their first and second moments. This means that a Gaussian process is entirely

characterized by its mean value and its autocorrelation function, or equivalently by its power spectral density.

- A paradigmatic Gaussian process is the Ornstein-Uhlenbeck process, characterized by an exponentially decaying autocorrelation function and thus a Lorentzian spectrum. The OU process can be easily simulated numerically by solving its stochastic differential equation
- A non-Gaussian stochastic process that is relevant for our discussion is the random telegraph noise, a process that jumps between two values at a certain switching rate. As the OU, it is characterized by an exponentially decaying autocorrelation function and a Lorentzian spectrum. It can be simulated by extracting the intervals between jumps from an exponential distribution.

Chapter 2

Basic tools of quantum theory

This chapter is meant as a quick reference for the fundamental notions of quantum mechanics, quantum information and quantum estimation theory, in order to set the notation for the following discussion. We start by reviewing the basics of quantum mechanics in Section 2.1. We then discuss the basic tools of quantum information theory and the measures of quantum correlations that we will employ in the following chapters in Section 2.2. In Section 2.3 we review the tools for describing the dynamics of open quantum systems, i.e. quantum systems that interact with an environment. We finally look at the tools of quantum estimation theory that are used in quantum metrology tasks, in Section 2.4.

2.1 Review of quantum mechanics

Quantum mechanics provides a mathematical description of physical systems at a fundamental level. To provide such description what we need is to specify states, evolutions and measurements. These concepts are given via postulates that we outline here.

2.1.1 Postulates

Like all physical theories, quantum mechanics is based on a few mathematical assumptions or postulates. Here we enumerate them, referring the reader to standard textbooks on the topic for a more exhaustive discussion of the postulates, the mathematical subtleties and their implications.

Postulate 1 (State space)

> Any isolated physical system is associated to a Hilbert space $\mathcal{H}$. The system is completely described by its *state vector* $|\psi\rangle$, also known as the wave function, which is a unit vector of $\mathcal{H}$.

The Hilbert space is a complex vector space endowed with an inner product $\langle\varphi|\psi\rangle$ with values in $\mathbb{C}$, that defines the norm $\|.\|$ in the space, such that $\big\||\psi\rangle\big\|^2 = \langle\psi|\psi\rangle$. A unit vector is thus a state with norm 1.

Being a vector space, $\mathcal{H}$ admits the superposition principle, i.e. any linear combination of states is also a state:

$$|\psi\rangle = \sum_n^d c_n |\psi_n\rangle \tag{2.1}$$

where $\{\psi_n\}_{n=1}^d$ is an orthonormal basis of $\mathcal{H}$ and d is its dimension. Requiring $|\psi\rangle$ to be a unit vector amounts to imposing the condition

$$\sum_n^d |c_n| = 1, \tag{2.2}$$

to the coefficients of Eq. (2.1).

If the system is composite, i.e. made of smaller subsystem, then its state space is the tensor product of the Hilbert spaces corresponding to subsystems:

$$\mathcal{H} = \mathcal{H}_1 \otimes \cdots \otimes \mathcal{H}_n. \tag{2.3}$$

Postulate 2 (Time evolution)

The evolution of an isolated quantum system is described by a unitary transformation. If the system is in the state $|\psi(t_0)\rangle$ at an initial time t_0 then its state $|\psi(t)\rangle$ at the time t is given by

$$|\psi(t)\rangle = U(t, t_0) |\psi(t_0)\rangle , \tag{2.4}$$

where $U(t, t_0)$ is a unitary operator ($UU^\dagger = \mathbb{I}$) depending only on t and t_0.

The time-evolution operator $U(t, t_0)$, also known as propagator, is related to the Hamiltonian of the system. It is the formal solution to the Schrödinger equation, a linear differential equation that describes the time evolution of the state:

$$i\hbar \frac{d}{dt} |\psi(t)\rangle = H(t) |\psi(t)\rangle . \tag{2.5}$$

By plugging Eq. (2.4) into Eq. (2.5), we obtain an operator differential equation for U

$$i\hbar \frac{d}{dt} U = H(t)U, \tag{2.6}$$

with the initial condition $U(t_0, t_0) = \mathbb{I}$.

We can write the formal solution to (2.6):

$$U(t, t_0) = \mathbb{I} - \frac{i}{\hbar} \int_{t_0}^{t} H(t_1)U(t_1, t_0)dt_1. \tag{2.7}$$

By iterating, we obtain a series expansion for the evolution operator

$$U(t, t_0) = \mathbb{I} - \frac{i}{\hbar} \int_{t_0}^{t} H(t_1)U(t_1, t_0)dt_1 + \left(-\frac{i}{\hbar}\right)^2 \int_{t_0}^{t} dt_1 \int_{t_0}^{t_1} dt_2 H(t_1)H(t_2) + \ldots \tag{2.8}$$

$$= \sum_{n=0}^{\infty} \frac{1}{n!} \left(-\frac{i}{\hbar}\right)^n \int_{t_0}^{t} dt_1 \int_{t_0}^{t_1} dt_2 \cdots \int_{t_0}^{t_n} dt_n H(t_1) \cdots H(t_n) , \tag{2.9}$$

where $t_n < \ldots < t_2 < t_1$. In general, being H an operator, the order in which $H(t_1), H(t_2), \ldots$ appear in the integral is relevant. In the case in which H commutes with itself at different times, the above equation can be simplified by noting that

$$\int_{t_0}^{t} dt_1 \int_{t_0}^{t_1} dt_2 H(t_1)H(t_2) = \frac{1}{2!}\int_{t_0}^{t} dt_1 \int_{t_0}^{t} dt_2 H(t_1)H(t_2), \tag{2.10}$$

and so on, allowing us to write

$$U(t,t_0) = \sum_{n=0}^{\infty} \frac{1}{n!}\left(-\frac{i}{\hbar}\right)^n \int_{t_0}^{t} dt_1 \cdots \int_{t_0}^{t} dt_n H(t_1)\cdots H(t_n) \tag{2.11}$$

$$= \exp\left[-\frac{i}{\hbar}\int_{t_0}^{t} H(t')dt'\right]. \tag{2.12}$$

This is the exact solution for the evolution operator when the Hamiltonian commutes with itself at different times. This includes the relevant case of a closed and isolated quantum system, for which the Hamiltonian is constant in time.

The solution for a general Hamiltonian can be written formally in a compact way by introducing the time ordering operator $\mathcal{T}$, and reads

$$U(t,t_0) = \sum_{n=0}^{\infty} \frac{1}{n!}\left(-\frac{i}{\hbar}\right)^n \int_{t_0}^{t} dt_1 \cdots \int_{t_0}^{t} dt_n \mathcal{T}[H(t_1)\cdots H(t_n)] \tag{2.13}$$

$$\equiv \mathcal{T}\exp\left[-\frac{i}{\hbar}\int_{t_0}^{t} H(t')dt'\right]. \tag{2.14}$$

Equation (2.9) is known as Dyson series expansion of the evolution operator, and its truncation up to some order N gives an approximate solution to the Schrödinger equation.

Postulate 3 (Measurement) In the quantum theory, the act of measurement of the system is a central topic. Whereas in classical mechanics it is assumed that the measurement of any quantity of the system can happen without perturbing it, in quantum mechanics the measurement is an irreversible operation that affects the state of the system.

> A quantum measurement is described by a collection of operators $\{M_m\}$ acting on the Hilbert space $\mathcal{H}$ of the system, where the index m labels the possible outcomes of the experiment. If $|\psi\rangle$ is the state of the system, the probability that result m occurs is
>
> $$p_m = \langle\psi|M_m^\dagger M_m|\psi\rangle \tag{2.15}$$
>
> and the state of the system immediately after the measurement is
>
> $$|\psi'\rangle = \frac{M_m|\psi\rangle}{\sqrt{\langle\psi|M_m^\dagger M_m|\psi\rangle}}. \tag{2.16}$$

Since the probabilities of all the outcomes must add to one, independently of the state of the system, we require that the set of measurement operators satisfy the completeness relation

$$\sum_m M_m^\dagger M_m = \mathbb{I}. \tag{2.17}$$

Since most of the times one is not interested in the state of the system after the measurement, it is customary in the literature to define the experiment with a set of operators $\{\Pi_m\}$ that are positive-semidefinite

$$\langle\psi|\Pi_m|\psi\rangle \qquad \forall\,|\psi\rangle \tag{2.18}$$

and complete

$$\sum_m \Pi_m = \mathbb{I}. \tag{2.19}$$

The measurement process is called positive-operator valued measurement (POVM). The probability that the measurement yields the outcome m is then

$$p_m = \langle\psi|\Pi_m|\psi\rangle\,. \tag{2.20}$$

The state of the system after the measurement depends on the specific implementation of the experiment, as, given a positive-semidefinite operator Π_m, there is an infinite number of operators M_m such that $\Pi_m = M_m M_m^\dagger$.

A relevant class of measurements is that of projective measurements, i. e. those measurements described by a Hermitian operator M acting on $\mathcal{H}$. Being Hermitian, M admits a spectral decomposition

$$M = \sum_i m_i P_i, \tag{2.21}$$

where the P_i are projectors onto the eigenvectors $|i\rangle$ of M, i.e. the solutions to the eigenvalue equation $M|i\rangle = m_i|i\rangle$. The projectors P_i satisfy the orthogonality condition $P_iP_j = \delta_{ij}P_i$ and the completeness relation $\sum_i P_i = \mathbb{I}$.

The probability of obtaining the outcome m_i is $p_i = \langle\psi|P_i|\psi\rangle$ and the expected value of the observable M is then given by

$$\langle M\rangle = \sum_i m_i p_i = \langle\psi|\sum_i m_i P_i|\psi\rangle = \langle\psi|M|\psi\rangle\,. \tag{2.22}$$

2.1.2 Mixed states and density matrix

In most cases we are not able to know with certainty in which state the system is. This happens in particular when we are considering a component of a composite system, or when the system of interest is interacting with an environment, as we will see in Section 2.3.

In the most general way, our knowledge of the system is represented by a statistical distribution $\{p_i, |\psi_i\rangle\}$, which means that the system has the probability p_i of being in the state $|\psi_i\rangle$, where obviously $\sum p_i = 1$. We say that the system is in a mixed state. We can

then define the quantum counterpart of the classical density function of a probability distribution, which is called density operator and is defined as

$$\rho = \sum_i p_i \left|\psi_i\right\rangle \left\langle\psi_i\right| . \tag{2.23}$$

The density operator defined in Eq. (2.23) is Hermitian, positive definite and $\mathrm{Tr}\,\rho = 1$. Conversely, any operator with these three properties may be used as a density operator for a certain system. We label the set of all possible density operators for a Hilbert space $\mathcal{H}$ by $\mathcal{S}(\mathcal{H})$.

If and only if the system is in a pure state the density operator is a projector and hence $\mathrm{Tr}\,\rho^2 = 1$. When the system is in a mixture, $\mathrm{Tr}\,\rho^2 < 1$. It is then useful to define the purity of the state as

$$\mu = \mathrm{Tr}\,\rho^2, \qquad \text{with } \frac{1}{d} \leq \gamma \leq 1 \tag{2.24}$$

where d is the dimensionality of the Hilbert space. The minimum value for γ is reached when the system is in a mixture of d states with probability $1/d$ each: we call such a state *completely mixed* and the corresponding density operator is $\mathbb{I}/d$.

The system is completely described by the density operator formalism. The evolution of the system is given by the *Liouville-von Neumann equation*, which is equivalent to the Schrödinger equation,

$$i\hbar\frac{\partial\rho}{\partial t} = [H, \rho], \tag{2.25}$$

where H is the Hamiltonian of the system in the Schrödinger picture. Equivalently, we can write

$$\rho(t) = U(t, t_0)\rho(t_0)U^\dagger(t, t_0), \tag{2.26}$$

where $U(t, t_0)$ is the evolution operator defined in Eq. (2.14).

The measurement process is easily described as well. We consider a measurement $\{M_m\}$ The probability of getting the outcome m is given by

$$p(m) = \mathrm{Tr}(M_m \rho M_m^\dagger) = \mathrm{Tr}(M_m^\dagger M_m \rho) \tag{2.27}$$

and if the result is m, the system will be in the state

$$\rho' = \frac{M_m \rho M_m^\dagger}{\mathrm{Tr}(M_m^\dagger M_m \rho)} \tag{2.28}$$

after the measurement.

The expectation value for an observable M is therefore given by

$$\langle M \rangle = \mathrm{Tr}[M\rho], \tag{2.29}$$

which reduces to Eq. (2.22) for a pure state, as can be easily checked.

2.1.3 Composite systems and partial trace

As we briefly discussed in Subsection 2.1.1, if the system is composite of more than one system, then its state space is the tensor product of the Hilbert spaces corresponding to subsystems: $\mathcal{H} = \mathcal{H}_1 \otimes \cdots \otimes \mathcal{H}_n$. Most of the times, however, we are interested in a part (or just one) of the subsystems: this happens, for instance, when we want to study quantum communication protocols, in which the quantum system is split between the two parties, or when we want to describe a principal quantum system interacting with an environment. The latter, in particular, is the central topic of this thesis. In these situations, the density matrix formalism comes in handy for the mathematical description of the system.

For simplicity, we restrict the discussion to a bipartite system, i.e. a Hilbert space $\mathcal{H} = \mathcal{H}_A \otimes \mathcal{H}_B$, where, adopting the standard notation in (quantum) information theory, $\mathcal{H}_A$ and $\mathcal{H}_B$ are held by two parties Alice and Bob. The discussion can be generalized to system with an arbitrary number of components.

The space $\mathcal{H}$ is spanned by the set of product states constructed from the orthonormal bases of the constituent Hilbert spaces,

$$|ij\rangle \equiv |i\rangle_A \otimes |j\rangle_B \,. \tag{2.30}$$

The most general expression for the density matrix is then

$$\rho = \sum_{ij} \sum_{hk} \rho_{ij,hk} \, |ij\rangle \langle hk| \,. \tag{2.31}$$

What is the density matrix ρ_A that describes the knowledge that Alice has of her subsystem? The mathematical tool that is needed here is the *partial trace*:

$$\begin{aligned} \rho_A \equiv \mathrm{Tr}_B[\rho] &= \sum_l {}_B\langle l|\rho|l\rangle_B = \sum_l \sum_{ij} \sum_{hk} \rho_{ij,hk} \;\; {}_B\langle l|ij\rangle \langle hk|l\rangle_B \\ &= \sum_l \sum_{ih} \rho_{il,hl} \, |i\rangle_A \langle h|_A \,, \end{aligned} \tag{2.32}$$

where we used the orthonormality of the basis of $\mathcal{H}_B$, $\langle i|j\rangle_B = \delta_{ij}$. The density matrix ρ_A is called the reduced density matrix for system A. An analogous definition can be given for the partial trace with respect to the subsystem A, that gives the reduced density matrix for ρ_B.

The partial trace is the correct operation to correctly describe the state of the system A, because it gives the right expectation values for measurements made on this subsystem. To understand this, let's consider a measurement operator O_A on Alice's system. Since the measurement does not affect Bob's subsystem, the operator acting on the whole Hilbert space is $O = O_A \otimes \mathbb{I}_B$. We then have

$$\begin{aligned}\langle O\rangle = \mathrm{Tr}[\rho O] &= \sum_{ij}\langle ij|\rho O|ij\rangle \\ &= \sum_{ij}\langle ij|\left(\sum_{lm}\sum_{hk}\rho_{lm,hk}\,|lm\rangle\langle hk|\right)(O_A\otimes\mathbb{I})|ij\rangle \\ &= \sum_{ij}\sum_{h}\rho_{ij,hj}\langle h|O_A|i\rangle = \sum_{ih}\langle i|\rho_A|h\rangle\langle h|O_A|i\rangle \\ &= \sum_{i}\langle i|\rho_A O_A|i\rangle = \mathrm{Tr}[\rho_A O_A],\end{aligned} \tag{2.33}$$

where we used Eqs. (2.31) and (2.32).

2.1.4 The qubit and two-qubit systems

The state space of a quantum system can have any finite or infinite dimension d but, in the framework of quantum information theory, quantum systems with $d = 2$ are of paramount importance as they generalize the classical *bit*. The *bit* is the fundamental unit of classical information. It is an abstract object that can have two discrete states, labeled by the binary digits 0 and 1. Information is encoded in sets of bits of arbitrary dimension. A two-level quantum system is called *qubit*. There are many possible physical realizations of a qubit. Any two-level quantum system, such as the polarization state of a photon, the spin $\frac{1}{2}$ of an electron or a nucleus, is a natural candidate for the implementation of a qubit. Systems with higher-dimensional spaces can be used as well, if a pair of energy states can be effectively decoupled from the rest of the spectrum.

We label the two states of an orthonormal basis of the system as $|0\rangle$ and $|1\rangle$ in analogy with the classical bit, and we refer to this basis as the *computational basis*. A pure qubit state is a superposition of these two states,

$$|\psi\rangle = \alpha\,|0\rangle + \beta\,|1\rangle\,, \tag{2.34}$$

where α and β are two complex numbers that satisfy the normalization relation $|\alpha|^2 + |\beta|^2 = 1$. Since the state is invariant with respect to an overall complex phase, a pure qubit state is identified by two real components.

A natural parametrization comes from the theory of angular momentum of spin-$\frac{1}{2}$ particles (a spin-$\frac{1}{2}$ particle can indeed be a physical representation of a qubit). We introduce the Pauli matrices, that are generators of $SU(2)$,

$$\sigma_x = \begin{pmatrix}0 & 1\\ 1 & 0\end{pmatrix}, \quad \sigma_y = \begin{pmatrix}0 & -i\\ i & 0\end{pmatrix}, \quad \sigma_z = \begin{pmatrix}1 & 0\\ 0 & -1\end{pmatrix}. \tag{2.35}$$

These matrices are traceless matrices that satisfy the commutation relation $[\sigma_i, \sigma_j] = i\epsilon_{ijk}\sigma_k$, with ϵ_{ijk} the totally antisymmetric tensor. Moreover, they satisfy the relation $\sigma_i^2 = \mathbb{I}$.

We consider $|0\rangle$ and $|1\rangle$ as, respectively, the eigenstates $|\uparrow\rangle$ and $|\downarrow\rangle$ of the projection of the spin onto the z axis, i.e. the eigenstates of σ_z. We now can visualize the qubit state

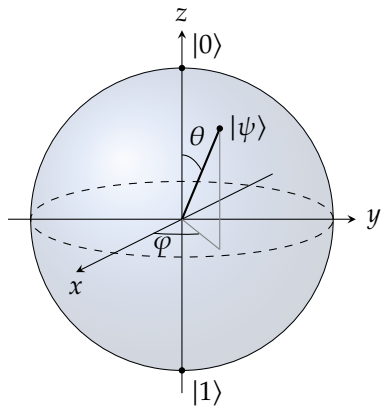

Figure 2.1: Bloch sphere. The pure state $|\psi\rangle$ is identified by the two angles $\theta \in [0, \pi]$ and $\varphi \in [0, 2\pi]$ and lies on the boundary of the sphere. Mixed states located in the bulk of the sphere, with the maximally mixed state in lying at the center.

as versor in $\mathbb{R}^3$, $\mathbf{n} = (\sin\theta\cos\varphi, \sin\theta\sin\varphi, \cos\theta)$, parametrized by the angles $\theta \in [0, \pi]$ and $\varphi \in [0, 2\pi]$. The state is thus identified by a point on a sphere with radius 1, called the *Bloch sphere*, Fig. 2.1. The corresponding parametrization in the computational basis is given by

$$|\psi\rangle = \cos\frac{\theta}{2}|0\rangle + e^{i\varphi}\sin\frac{\theta}{2}|1\rangle\,. \tag{2.36}$$

When a qubit system is in a mixed state, i.e. is described by a general density matrix ρ, it is represented as a non-unit vector $\boldsymbol{n}$ in the Bloch sphere, called the *Bloch vector*. The components of the vector are given by the projection onto each axis:

$$n_i = \mathrm{Tr}[\sigma_i\rho], \qquad i = x, y, z\,. \tag{2.37}$$

The density operator can thus be written in the form

$$\rho = \frac{1}{2}(\mathbb{I} + \boldsymbol{n}\cdot\boldsymbol{\sigma}), \tag{2.38}$$

where $\boldsymbol{\sigma} = (\sigma_x, \sigma_y, \sigma_z)$ is the vector of Pauli matrices defined in Eq. (2.35).

Some properties of the qubit state have an interesting interpretation in the Bloch representation. For instance, the purity of the state is proportional to the square of the Euclidean norm of the Bloch vector:

$$\mu = \frac{1}{2} + \frac{1}{2}\|\boldsymbol{n}\|^2. \tag{2.39}$$

The maximally mixed state, in the Bloch representation, lies at the center of the sphere.

A system made of more than one qubit is represented as the tensor product of the single-qubit Hilbert spaces

$$\mathcal{H} = \mathcal{H}_1 \otimes \ldots \otimes \mathcal{H}_n. \tag{2.40}$$

The computational basis for a multi-qubit system is given by the product states

$$|a_0\ a_1\ \ldots\ a_n\rangle = |a_0\rangle \otimes |a_1\rangle \ldots \otimes |a_n\rangle\,, \qquad \text{where } a_i \in \{0, 1\}. \tag{2.41}$$

In this thesis, we will limit the discussion to two-qubit systems, the simplest bipartite quantum system, where most of the results involving quantum correlations, that we will discuss in the following section, can be obtained analytically.

A two-qubit Hilbert space has dimension 4, and is thus described by $2^4 - 1 = 15$ real parameters. One possible parametrization of a two qubit state is based on the Pauli matrices:

$$\rho = \frac{1}{4} \sum_{i,j=0}^{3} a_{ij} \sigma_i^{(1)} \otimes \sigma_j^{(2)}, \tag{2.42}$$

where $\sigma_0 \equiv \mathbb{I}$, and the coefficient $a_{00} = \mathrm{Tr}[\rho] = 1$. The real coefficients a_{ij} form a 4×4 matrix that generalizes the Bloch vector for the single qubit, and is sometimes referred to as the Bloch matrix. A convenient representation of the Bloch matrix is

$$N = \begin{pmatrix} 1 & \boldsymbol{a} \\ \boldsymbol{b}^T & R \end{pmatrix}, \tag{2.43}$$

where $a = (a_{10}, a_{20}, a_{30})$ and $b = (a_{01}, a_{02}, a_{03})$ are the Bloch vectors of the reduced density operators $\rho_{1(2)} = \mathrm{Tr}_{1(2)}[\rho]$, as can be easily checked. The 3×3 matrix R, on the other hand, accounts for the correlations between the two qubits.

We introduce here the four *Bell states*, named after John S. Bell because they are the states for which the inequality for local realistic theories is maximally violated [2]:

$$\begin{aligned} |\Phi^+\rangle &= \frac{1}{\sqrt{2}}(|00\rangle + |11\rangle) \\ |\Phi^-\rangle &= \frac{1}{\sqrt{2}}(|00\rangle - |11\rangle) \\ |\Psi^+\rangle &= \frac{1}{\sqrt{2}}(|01\rangle + |10\rangle) \\ |\Psi^-\rangle &= \frac{1}{\sqrt{2}}(|01\rangle - |10\rangle). \end{aligned} \tag{2.44}$$

These states are relevant in the study of quantum information processing, and will be used in the following chapters.

A relevant subset of two-qubit states is that of the *X states* [61, 62], characterized by an X-shaped density operator with non-zero entries only in the two diagonals:

$$\rho = \begin{pmatrix} \rho_{11} & 0 & 0 & \rho_{14} \\ 0 & \rho_{22} & \rho_{23} & 0 \\ 0 & \rho_{23}^* & \rho_{33} & 0 \\ \rho_{14}^* & 0 & 0 & \rho_{44} \end{pmatrix}. \tag{2.45}$$

As can be immediately seen, these states are described by 7 real parameters.

In particular we will be interested in the subset of X states with maximally mixed marginals, i.e. those where the reduced density matrices for both qubits are the maximally mixed state:

$$\rho = \frac{1}{4} \left(\mathbb{I}_2 + \sum_i a_i \sigma_i \otimes \sigma_i \right), \tag{2.46}$$

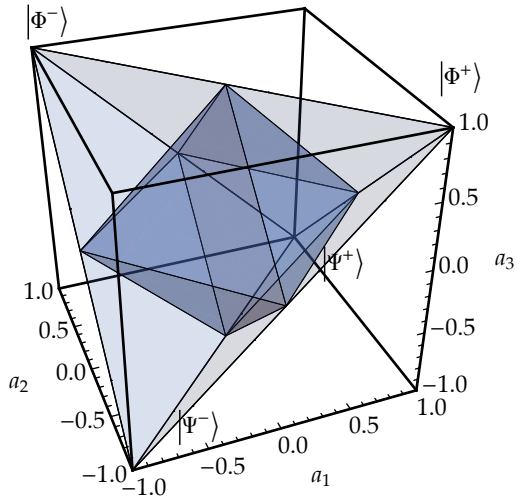

Figure 2.2: The Horodecki tetrahedron. On the axes are the three parameters a_i of Eq. (2.46). The four Bell states are at the vertices of a tetrahedron. The points of the tetrahedron are the Bell diagonal states. The blue octahedron inside the tetrahedron is the set of separable states

where the real coefficients satisfy $-1 \leq a_i \leq$. These states are also know as *Bell diagonal states*, because they can be parametrized as follows

$$\rho = c_1 |\Phi^+\rangle \langle\Phi^+| + c_2 |\Phi^-\rangle \langle\Phi^-| + c_3 |\Psi^+\rangle \langle\Psi^+| + c_4 |\Psi^-\rangle \langle\Psi^-| , \tag{2.47}$$

where the real coefficients satisfy the conditions $0 \leq c_i \leq 1$ and $\sum_i c_i = 1$. To go from one parametrization to the other

$$c_1 = \frac{1}{4}(1 + a_1 - a_2 + a_3) \tag{2.48}$$

$$c_2 = \frac{1}{4}(1 - a_1 + a_2 + a_3) \tag{2.49}$$

$$c_3 = \frac{1}{4}(1 + a_1 + a_2 - a_3) \tag{2.50}$$

$$c_4 = \frac{1}{4}(1 - a_1 - a_2 - a_3) . \tag{2.51}$$

Bell diagonal states can be visualized in a 3D plot, known in the literature as the *Horodecki diagram*. Using the parametrization (2.46), the Bell diagonal states lie at the vertices of a tetrahedron, with the Bell states (2.44) on the vertices. The Horodecki diagram is depicted in Fig. 2.2.

2.2 Quantum information and quantum correlations

The ultimate goal of quantum information theory is to determine how the peculiar features of quantum systems can be exploited to store, process and transmit information better than how it is possible with classical systems. The quantitative tools of quantum

information theory are thus generalizations of the classical tools developed since the foundation of classical information theory laid by Shannon in 1948. These involve, among the others, measures of the amount of information contained in a quantum state, and distance measures between states. In Subsection 2.2.1, we will in particular define two distance measures that are useful in our discussion, the trace distance and the fidelity.

The key feature of quantum systems that makes them so interesting for information theory, is the presence of form of correlations that are not possible in classical systems. A fundamental part of research is thus devoted to the study of how correlations between the components of a system are different in the quantum regime compared to the classical one. The typical non-classical form of correlation is *entanglement*. It is the crucial resource for a number of quantum-information-processing protocols, such as quantum key distribution, teleportation, and superdense coding [2, 63]. Though it is quite simple to define what an entangled state is, the characterization of the set of entangled states is not an easy task, especially for mixed states. A number of criteria and measures of entanglement have been proposed, but a general theory still lacks. Two-qubit systems, however, are simple enough to allow a complete characterization. In Subsection 2.2.2 we describe *negativity*, a measure of entanglement for bipartite systems that is easy to compute [64] and specialize it to the two-qubit case.

Despite being the most notable, entanglement is not the only form of quantum correlations. Some composite systems can be prepared in states that are separable, but are correlated in such a way that can't be entirely described by classical probability theory. In Subsection 2.2.3 we describe *quantum discord*, a measure of the amount of non-classical correlations [65], and how it can be evaluated for two-qubit systems.

2.2.1 Distance measures in the Hilbert space

Trace distance

One central question in quantum information theory regards the distinguishability between two quantum states. How close are two quantum states in the state space? How easy is it to discriminate between them with a quantum measurement? These are very important tasks in information processing, for instance in quantum communication, or to test the quality of quantum gates or quantum channels. Quantitative answers to these questions are given by distance measures. A few measures have been developed over the years, with different operational meanings and classical counterparts. The most commonly employed quantities are the *fidelity* and the *trace distance*. In this subsection we focus on the latter, as it will be used in Subsection 2.3.1 to define a measure of quantum non-Markovianity.

The trace distance between two quantum states ρ_1 and ρ_2 is defined as

$$D(\rho_1, \rho_2) = \frac{1}{2}\|\rho_1 - \rho_2\|, \tag{2.52}$$

where $\|A\| = \mathrm{Tr}\sqrt{A^\dagger A}$ is the trace norm of a square matrix. The matrix $\sqrt{A^\dagger A}$ is defined as the positive semidefinite matrix B such that $B^2 = A^\dagger A$. Being $A^\dagger A$ a positive semidefinite matrix, its square norm is well defined. In particular, since the density operators are

Hermitian, Eq. (2.52) can also be written

$$D(\rho_1, \rho_2) = \frac{1}{2} \operatorname{Tr} \sqrt{(\rho_1 - \rho_2)^2} = \frac{1}{2} \sum_i |\lambda_i|, \tag{2.53}$$

where λ_i are the eigenvalues of the Hermitian, but not necessarily positive matrix $\rho_1 - \rho_2$.

The trace distance has the properties of a metric distance, i.e.: it is zero if and only if $\rho_1 = \rho_2$, it is symmetric and the triangle inequality holds: $D(\rho_1, \rho_3) \leq D(\rho_1, \rho_2) + D(\rho_2, \rho_3)$. Its maximum value of one is reached for states that have orthogonal supports. Moreover, it is preserved under unitary transformations, i.e. $D(U\rho_1 U^\dagger, U\rho_2 U^\dagger) = D(\rho_1, \rho_2)$ for any unitary operator U.

For qubits, the trace distance has a nice geometrical interpretation: it is half the Euclidean distance in the Bloch representation. That is, if $\boldsymbol{r}_1$ and $\boldsymbol{r}_2$ are the Bloch vectors of ρ_1 and ρ_2,

$$D(\rho_1, \rho_2) = \frac{\|\boldsymbol{r}_1 - \boldsymbol{r}_2\|}{2}. \tag{2.54}$$

The operational interpretation of the trace distance is related to the probability of distinguishing the two states: Suppose that Alice prepares a quantum system in the state ρ_1 with probability 1/2 and in the state ρ_2 with probability 1/2. She gives the states to Bob, who performs a quantum measurement to discriminate between the two states. It can be seen [66] that Bob can identify the state with maximum probability

$$P_{\max} = \frac{1}{2}[1 + D(\rho_1, \rho_2)]. \tag{2.55}$$

From Eq. (2.55) we can see that the limiting case of zero trace distance (i.e. $\rho_1 = \rho_2$) gives a maximum probability $P_{\max} = 1/2$, meaning that any quantum measurement can't be better than randomly guessing between the two states. On the contrary, a trace distance of one, gives a maximum probability of one, i.e. perfect discrimination between the states.

Fidelity and the Bures distance

Another commonly employed distance measure is the *fidelity* [2], defined as

$$\mathcal{F}(\rho, \sigma) = \operatorname{Tr} \sqrt{\sqrt{\rho}\sigma\sqrt{\rho}}, \tag{2.56}$$

where ρ and σ are two quantum states. The fidelity is equal to one when $\rho = \sigma$ and it is zero for orthogonal states. For pure states, it coincides with the overlap between the two states:

$$\mathcal{F}(|\psi\rangle, |\varphi\rangle) = \operatorname{Tr} \sqrt{\sqrt{|\psi\rangle\langle\psi|}\,|\varphi\rangle\langle\varphi|\sqrt{|\psi\rangle\langle\psi|}} = |\langle\psi|\varphi\rangle|. \tag{2.57}$$

It is invariant under unitaries and it is monotonically decreasing under CPT maps

$$\mathcal{F}(\rho, \sigma) = \mathcal{F}(U\rho U^\dagger, U\sigma U^\dagger) \tag{2.58}$$

$$\mathcal{F}(\rho, \sigma) \geq \mathcal{F}(\mathcal{E}(\rho), \mathcal{E}(\sigma)). \tag{2.59}$$

Unlike the trace distance, the fidelity is not a metric distance, but we can introduce the Bures distance, which is a function of the fidelity and is indeed a metric distance:

$$D_B(\rho_1, \rho_2) = \sqrt{2(1 - \mathcal{F}(\rho_1, \rho_2))}. \tag{2.60}$$

The metric of the Bures distance is relevant in the field of quantum estimation theory, as we will note ins Section 2.4.

2.2.2 Entanglement

Given the Hilbert space $\mathcal{H} = \mathcal{H}_1 \otimes \ldots \otimes \mathcal{H}_n$ the pure state $|\psi\rangle \in \mathcal{H}$ is entangled if it can't be written as a product state:

$$|\psi\rangle \neq |\psi_1\rangle \otimes \ldots \otimes |\psi_n\rangle \qquad \forall\, |\psi_i\rangle \in \mathcal{H}_i \ ; \tag{2.61}$$

otherwise, the state is said to be *separable*.

We say that the mixed state ρ is separable if it can be written as a convex mixture of product states, that is

$$\rho = \sum_i p_i \rho_1^i \otimes \ldots \otimes \rho_n^i, \tag{2.62}$$

where the p_is are probabilities (i.e. $0 \leq p_i \leq 1$ and $\sum_{p_i} = 1$) and $\rho_m^i \in \mathcal{S}(\mathcal{H}_m)$. If this is not possible then the state is *entangled*.

The physical meaning of Eq. (2.62) is that separable states may be prepared by using only local operations and classical communications (LOCC). If the state is entangled, this can't be done, meaning that the correlations between the two systems are genuinely quantum, and they have been created with a global quantum operation.

Despite the definition being quite simple, in general it is not an easy task to determine whether a state is separable or not. The set of separable states, in fact, does not constitute a subspace of $\mathcal{S}(\mathcal{H})$ and the only mathematical characterization available is its convexity. Many different criteria have been introduced that partially characterize the set of entangled states for different Hilbert spaces. For two qubit systems, the characterization is complete, thanks to the so-called positive partial transpose (PPT) criterion, which provides a necessary condition for a state to be separable in a bipartite system. This condition is also sufficient for $2 \otimes 2$ and $2 \otimes 3$ Hilbert spaces.

In the following we introduce the PPT criterion and *negativity*, a quantitative measure of entanglement which we will employ in this thesis. We remark that besides negativity there are other measures of entanglement that rely on different features of the states (a thorough discussion of those measures and the relations between them can be found in [63]). Nevertheless, we can concentrate on negativity because it is easy to compute and it can be shown that in two-qubit systems all the measures are monotone functions with respect to each other and thus equivalent in characterizing the states.

The PPT criterion The positive partial transpose criterion was introduced by Peres in 1996 as a necessary condition for a state to be separable in bipartite systems [67]. In the same year, it was shown that the criterion was also a sufficient condition in $2 \otimes 2$ and $2 \otimes 3$

Hilbert spaces [68]. If ρ is a bipartite density operator, the *partial transposition map* with respect to system B is defined as

$$\rho^{T_B} = (\mathbb{I}_A \otimes T_B)(\rho), \tag{2.63}$$

where T_B is the transposition map on the system B.

If we write

$$\rho = \sum_{ijkl} p_{kl}^{ij} |i\rangle\langle j| \otimes |k\rangle\langle l|, \tag{2.64}$$

then, by applying the map (2.63), we get

$$\rho^{T_B} = \sum_{ijkl} p_{kl}^{ij} |i\rangle\langle j| \otimes |l\rangle\langle k|. \tag{2.65}$$

Obviously the partial transposition may be defined on system A too. Moreover, $\rho^{T_A} = (\rho^{T_B})^T$. Specializing to two-qubit systems, if we write the density operator as a block matrix

$$\rho = \begin{pmatrix} \rho_{11} & \rho_{12} \\ \rho_{21} & \rho_{22} \end{pmatrix}, \tag{2.66}$$

where the ρ_{ij}s are 2×2 matrices, its partial transpose with respect to system B is

$$\rho^{T_B} = \begin{pmatrix} \rho_{11}^T & \rho_{12}^T \\ \rho_{21}^T & \rho_{22}^T \end{pmatrix}. \tag{2.67}$$

The partial transpose of a Hermitian matrix is Hermitian, as can be easily checked. However, the partial transpose of a density matrix is not, in general, a positive definite matrix: some of its eigenvalues may be negative. It is on this fact that the PPT criterion is based:

> A necessary condition for the state ρ of a bipartite system $\mathcal{H} = \mathcal{H}_A \otimes \mathcal{H}_B$ to be separable is that its partial transpose has non-negative eigenvalues. If $\dim \mathcal{H}_A = 2$ and $\dim \mathcal{H}_B = 2$ or 3 then the condition is also sufficient.

While the proof of the sufficiency of the PPT criterion is rather involved (see [68]), we can easily show the necessity condition. If the state $\rho \in \mathcal{H}$ is separable, by definition it can be written as

$$\rho = \sum_i p_i \rho_A^i \otimes \rho_B^i. \tag{2.68}$$

The partial transpose of ρ with respect to system B is thus simply

$$\rho^{T_B} = \sum_i p_i \rho_A^i \otimes (\rho_B^i)^T, \tag{2.69}$$

but since the transposition preserves the eigenvalues of a matrix, ρ^{T_B} has the same eigenvalues as ρ, which are non-negative by the definition of density operator.

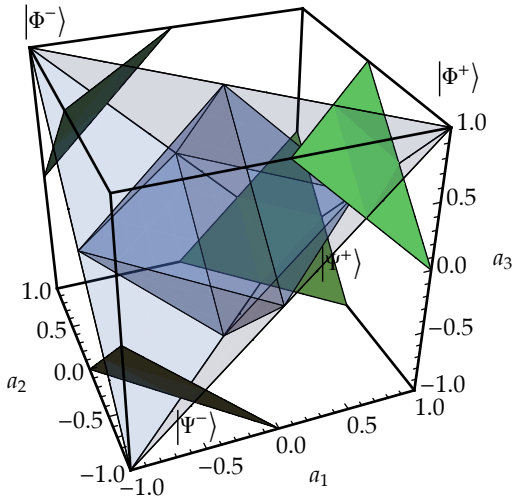

Figure 2.3: In green, surfaces of negativity $\frac{1}{2}$ in the Horodecki diagram. The planes are parallel to the faces of the octahedron of separable states.

Negativity The *negativity* is a quantitative version of the PPT criterion. It measures the extent to which the partial transpose ρ^{T_B} fails to be positive definite. Its advantage compared to other measures of entanglement, is that it is easy to compute with linear algebra and does not require any optimization procedure.

The negativity of a bipartite state ρ is defined as the quantity

$$N(\rho) = \frac{\|\rho^{T_A}\|_1 - 1}{2}, \tag{2.70}$$

where

$$\|A\|_1 = \sqrt{A^\dagger A} \tag{2.71}$$

is the trace norm of the matrix A.

When the matrix A is Hermitian, $\|A\|_1$ equals the sum of the absolute values of its eigenvalues. Since ρ^{T_B} is Hermitian and $\mathrm{Tr}(\rho^{T_B}) = \mathrm{Tr}(\rho) = 1$, we can rewrite (2.70) as

$$N(\rho) = 2\left|\sum_i \lambda_i^-\right|, \tag{2.72}$$

where λ_i^- are the negative eigenvalues of ρ^{T_B}. We thus see that $N(\rho) = 0$ if and only if the eigenvalues of ρ^{T_B} are all non-negative and hence ρ is separable, according to the PPT criterion.

For entangled states, $N(\rho) > 0$. The maximum is achieved for maximally entangled states, for which $N(\rho) = 1$. In the two-qubit case, the maximally entangled states are the four Bell states and all the states that are obtained from them by a local change of basis. In Fig. 2.3 we show how surfaces of equal negativity for Bell-state mixtures appear in the Horodecki diagram. They are planes parallel to the surfaces of the octahedron of separable states. The negativity of a point is proportional to its distance to the nearest surface of the octahedron, with the maximum of 1 reached for pure Bell states.

2.2.3 Quantum discord

Entanglement is certainly the most prominent example of quantum correlations, and it had long been believed to be an essential feature for any quantum computing algorithm to outperform its classical counterpart. This belief was also motivated by foundational reasons: neither classical or quantum superpositions violate Bell's inequalities and entanglement is required to exceed the bound to correlations imposed by any local and realist theory.

At the beginning of the 21st century some theoretical works started to cast doubt on the fact that entanglement was the only form of non-classical correlations for a quantum system. A measure of the difference between the total correlations and the classical correlations was proposed in 2001 by Ollivier and Zurek [65] and was named *quantum discord*: a system with non-zero quantum discord has correlations that cannot be accounted for entirely classically, and this is can be seen as a signature that the subsystems are genuinely quantum.

Remarkably, there are separable states that have a non-zero measure of quantum discord, so this means that the quantumness of the system allows the existence of non-classical correlations that are not related to entanglement. Whether these correlations could be a resource for quantum information processing is still an object of active research. An operational meaning of discord has been shown for a number of quantum information protocols [5, 6, 69].

In the following, we define quantum discord and see how it can be calculated for two-qubit systems. Analytical formulae exist only for certain classes of two-qubit states, while in general an optimization procedure is required.

We say that two systems are correlated if together they contain more information than taken separately. We begin by considering a classical bipartite system, made of the two subsystems A and B (measured by Alice and Bob).

Shannon entropy is a measure of the lack of information of a system, so we can define the *mutual information*

$$I(A:B) \equiv H(A) + H(B) - H(AB) \tag{2.73}$$

to be a measure of the correlations of the system AB. For classical variables, we may apply Bayes's rule $p_{x|y} = p_{xy}/p_y$ to obtain an equivalent definition of the mutual information

$$J(A:B) \equiv H(B) - H(B|A), \tag{2.74}$$

which involves the conditional entropy, defined as

$$H(B|A) = \sum_a p_a H(B|a) = \sum_a p_a \left(- \sum_b p_{b|a} \log p_{b|a} \right), \tag{2.75}$$

where the indices a and b denote the possible outcomes of the variables A and B, respectively. Classically, $I(A:B)$ and $J(A:B)$ are thus two equivalent expressions for the mutual information of the composite system AB.

For quantum systems, we can still define the mutual information as in equation (2.73), where the probability distributions are replaced by appropriate density matrices (ρ_A, ρ_B

and ρ_{AB}) and Shannon entropy H is replaced by von Neumann entropy S:

$$\mathcal{I}(A:B) \equiv S(A) + S(B) - S(AB). \tag{2.76}$$

This captures the total correlations between the two subsystems A and B.

The same can't be said for Eq. (2.74), because the expression $S(B|A)$, introduced in Eq. (2.74), is ambiguous. Unlike the classical case, there are many possible quantum measurements that can be performed on system A to assign an actual "value" to it and that affect its state differently. Let $\{\Pi_i\}$ be a projective measurement on A, where Π_i are projection operators such that $\sum_i \Pi_i = \mathbb{I}$ and i labels the possible outcomes of the measurement. In the following, we identify Π with $\Pi \otimes \mathbb{I}$ when it is acting on the whole system.

After the measurement, with unknown result, the state ρ_{AB} is transformed to

$$\rho'_{AB} = \sum_i \Pi_i \rho_{AB} \Pi_i. \tag{2.77}$$

Alice observes the outcome i with probability $p_i = \mathrm{Tr}(\Pi_i \rho_{AB})$ and Bob has the conditional state $\rho_{B|i} = \mathrm{Tr}_A(\Pi_i \rho_{AB})/p_i$. We can then define the quantum analog of Eq. (2.75),

$$S(B|\{\Pi_i\}) \equiv \sum_i p_i S(\rho_{B|i}), \tag{2.78}$$

and thus introduce the classical correlations

$$\mathcal{J}(A:B)_{\{\Pi_i\}} \equiv S(B) - S(B|\{\Pi_i\}). \tag{2.79}$$

To define a measure of the total classical correlations which is independent of the chosen measurement, we maximize the conditional entropy over all possible projective measurements:

$$\mathcal{J}(A:B) \equiv \max_{\{\Pi_i\}} \left[J(A:B)_{\{\Pi_i\}} \right] = S(B) - \min_{\{\Pi_i\}} S(B|\{\Pi_i\}). \tag{2.80}$$

These are the ingredients for the definition of quantum discord, which we state below:

> We define *quantum discord* to be the difference between the total correlations (2.76) of the quantum bipartite system AB and the classical correlations (2.80), that is
>
> $$\mathcal{D}(B|A) \equiv \mathcal{I}(A:B) - \mathcal{J}(A:B) = \min_{\{\Pi_i\}} S(B|\{\Pi_i\}) + S(A) - S(AB), \tag{2.81}$$
>
> where $S(X)$ is the von Neumann entropy of system X,
>
> $$S(B|\{\Pi_i\}) = \sum_i p_i S(\rho_{B|i}) = \sum_i \mathrm{Tr}(\Pi_i \rho_{AB}) S\left[\frac{\mathrm{Tr}_A(\Pi_i \rho_{AB})}{\mathrm{Tr}(\Pi_i \rho_{AB})} \right], \tag{2.82}$$
>
> and the minimization is carried over all possible projective measurements on the system A.

With this definition, quantum discord has the following properties:

1. It is not symmetric in general: $\mathcal{D}(B|A) \neq \mathcal{D}(A|B)$. This is a direct consequence of the fact that conditional entropy is not symmetric.

2. It is non-negative, $\mathcal{D} \geq 0$, as a consequence of the convexity of conditional entropy.

3. It is invariant under local unitary operations. This means that it is the same for the state ρ_{AB} and the state $(U_A \otimes U_B)\rho_{AB}(U_A \otimes U_B)^\dagger$ where U_A and U_B are unitary operators acting locally on A and B, respectively. Indeed, von Neumann entropy is invariant under unitary transformations and the result obtained from the measurement $\{\Pi_i\}$ on the state ρ_{AB} can be obtained from the measurement $\{U_A \Pi_i U_A^\dagger\}$ on its transformed state.

4. It is upper bounded by the entropy of the measured subsystem: $\mathcal{D}(B|A) \leq S(A)$. For a two-qubit system, this implies $\mathcal{D}(B|A) \leq 1$.

In order to better understand the kind of correlations described by quantum discord we report the form of the states with vanishing discord for both the parties A and B, which are also called *classical states*:

$$\rho = \sum_{ij} p_{ij} \left|\theta_i\right\rangle \left\langle\theta_j\right| \otimes \left|\eta_j\right\rangle \left\langle\eta_j\right|, \tag{2.83}$$

where $|\theta_i\rangle$ and $|\eta_j\rangle$ are orthonormal bases of system A and B, respectively, and p_{ij} is a joint probability distribution for the indices i, j.

2.2.4 Quantum discord for a two-qubit system

As can be seen from Eq. (2.81), an optimization procedure is required to calculate quantum discord. This is a hard task in general, and only in a few specific cases the optimal measurement can be found analytically. An explicit formula cannot be found even for a general two-qubit state (which is characterized by 15 real parameters). However, there are analytical results for specific classes of states. In particular we are interested in the formula for states with maximally mixed marginals, proved by Luo [70]. We will use this result in the following chapters, so a brief review is in order.

We defined the Bell diagonal states in Eq. (2.46), with the parameters a_i. The total correlations (2.73) can be evaluated easily: since $S(\rho_A) = S(\rho_B) = 1$,we have

$$I(A:B) = S(\rho_A) + S(\rho_B) - S(\rho_{AB}) = 2 + \sum_{i=1}^{4} \lambda_i \log \lambda_i, \tag{2.84}$$

where λ_i are the eigenvalues of ρ and are equal to the coefficients c_i of Eq. (2.47).

The classical correlations (2.80) can be maximized analytically and one finds [70] that

$$\mathcal{J}(A:B) = \frac{1+a}{2}\log(1+a) + \frac{1-a}{2}\log(1-a), \tag{2.85}$$

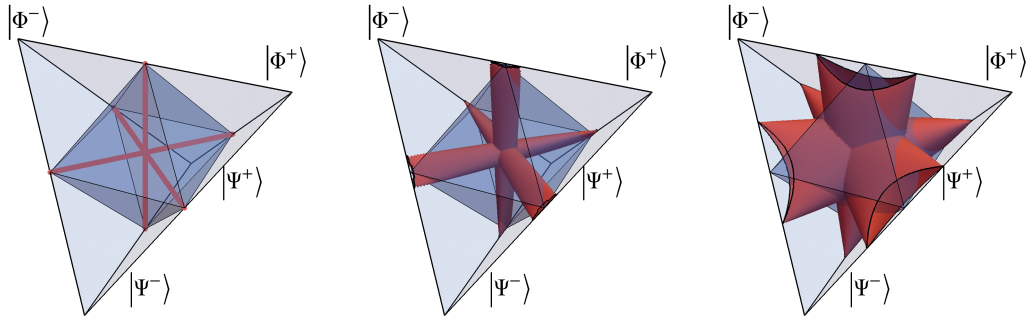

(a) $\mathcal{D} = 0$ (b) $\mathcal{D} = 0.01$ (c) $\mathcal{D} = 0.1$

Figure 2.4: (a) Zero-discord states and (b-c) Surfaces of equal discord in the Bell diagonal state tetrahedron.

where $a = \max(|a_1|, |a_2|, |a_3|)$. Thus we can write the analytical expression for the quantum discord

$$\begin{aligned}\mathcal{D}(B|A) &= I(A:B) - \mathcal{J}(A:B) = \\ &= 2 + \sum_i c_i \log c_i - \frac{1+a}{2}\log(1+a) - \frac{1-a}{2}\log(1-a). \end{aligned} \tag{2.86}$$

Finally, we note that for Bell diagonal states quantum discord is symmetric, i.e. $\mathcal{D}(B|A) = \mathcal{D}(A|B) \equiv \mathcal{D}(AB)$.

States with zero quantum discord It can be shown [71] that most of the states in the Hilbert space have non-zero quantum discord, that is, the set of states with only classical correlations has measure zero and is nowhere dense in the Hilbert space. This means that most of the separable states have non-classical correlations, even if they aren't entangled.

Even though it is difficult to calculate quantum discord, some criteria have been found for identifying zero-discord states, also known as *classical states* [72]. Using any of these criteria we can easily find the classical states for two-qubit systems with maximally mixed marginals. In the Bloch diagonal form, Eq. (2.46), they have two of the three coefficients a_i equal to zero, hence in the Horodecki diagram they lie on the cartesian axes inside the tetrahedron (see Fig. 2.4a). The classical states are of course separable states.

In Figure 2.4 we also show the surfaces of equal discord in the Horodecki diagram for two values of discord. The surfaces appear as intersecting tubes that enclose the axes $a_1 = 0$, $a_2 = 0$ and $a_3 = 0$: for increasing values of the discord they get closer to the Bell states, while for vanishing discord they collapse to the three axes.

2.3 Open quantum systems

We have seen in Subsection 2.1.1 that one of the postulates of quantum mechanics states that the evolution of closed, isolated quantum systems is described by unitary operations. As discussed in the Introduction, however, most systems of interest in quantum

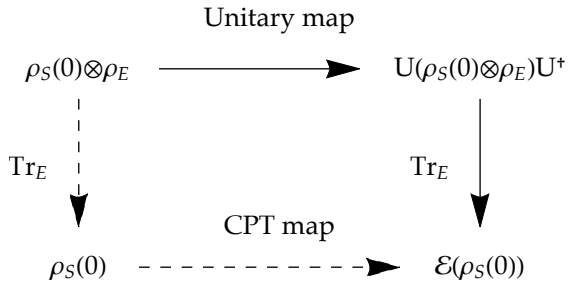

Figure 2.5: A commutative diagram showing the dynamics of a open quantum system. The initial state is a tensor product between the initial state of the system $\rho_S(0)$ and the initial state of the environment ρ_E (top left corner). By following the solid arrows, we first apply a unitary evolution to both the system and environment. To obtain the state $\rho_S(t)$ we apply a partial trace with respect to the environment. By following the dashed arrows, we trace out the environment from the beginning, then we apply a completely positive and trace preserving map $\mathcal{E}$ to $\rho_S(0)$.

technologies can not be considered isolated or closed, because they interact with the surrounding environment. This interaction is often too relevant to be neglected, and hence the theory above fails at giving a proper description of the quantum dynamics.

The theory of *open quantum systems* was developed to address the problem of describing the dynamics of a system interacting with its environment. The starting point is to consider the system, which we label S, and its environment E, as two subparts of a global quantum system, $S+E$ that can be considered closed and isolated. We thus have a state space $\mathcal{H} = \mathcal{H}_S \otimes \mathcal{H}_E$. The global system undergoes unitary evolution, as prescribed by the postulates of quantum mechanics, but it can be seen that the state of the system S undergoes a different dynamics, that is described by a more general quantum map $\mathcal{E} : \mathcal{S}(\mathcal{H}_S) \to \mathcal{S}(\mathcal{H}_S)$ so that, if ρ_S is the initial state of the system,

$$\rho_S' = \mathcal{E}(\rho_S) \tag{2.87}$$

is the final state. The map $\mathcal{E}$ is also called *quantum channel* or *quantum operation* and must have a few properties that ensure that the final state ρ_S' is still a valid density operator. $\mathcal{E}$ must be

- *Convex-linear* on the set of density operators: $\mathcal{E}(\sum_i p_i \rho_i) = \sum_i p_i \mathcal{E}(\rho_i)$, where $\rho_i \in \mathcal{S}(\mathcal{H})$ and $\sum_i p_i = 1$.
- *Completely positive*. $\mathcal{E}(\rho_S)$ must be a positive operator for any operator ρ_S of the system S and, moreover, if we introduce a second system R, with arbitrary dimension, then state $(\mathcal{I} \otimes \mathcal{E})(\rho)$ is positive for any density operator ρ of the composite system $S+R$, where $\mathcal{I}$ is the identity operation on the system R.
- *Trace-preserving*: $\mathrm{Tr}[\mathcal{E}(\rho_S)] = 1$, i.e. the final state must be a proper, normalized density matrix.[1]

[1] This property can be relaxed if we consider quantum maps that involve measurements, but we are not interested in this scenario, and we refer the reader to [2] for further details.

A quantum map with the above properties naturally arises by considering the unitary dynamics of the global system $S+E$, described by the unitary operator U, and then tracing out the environment E:

$$\mathcal{E}(\rho_S) = \mathrm{Tr}_E[U\rho_{SE}U^\dagger]. \tag{2.88}$$

Usually the initial state of the global system is assumed to be factorized, i.e. $\rho_{SE} = \rho_S \otimes \rho_E$.

A way of representing quantum maps that is much relevant to the following discussion is the *Kraus representation*, or operator-sum representation. According to Kraus theorem, a map $\mathcal{E}$ has the above properties if and only if it can be written as

$$\mathcal{E}(\rho) = \sum_i E_i \rho E_i^\dagger, \tag{2.89}$$

where the *Kraus operators* E_i satisfy the completeness relation

$$\sum_i E_i^\dagger E_i = \mathbb{I}, \tag{2.90}$$

which ensures that the output state has unit trace: $\mathrm{Tr}[\mathcal{E}(\rho)] = 1$.

Notice that Eq. (2.89) is equivalent to (2.88). Indeed, assume that the initial state is $\rho_{SE} = \rho_S \otimes |e_0\rangle\langle e_0|$, where $|e_0\rangle$ is a state belonging to some orthonormal basis $\{e_k\}$ of the environment. Then we can write the partial trace in Eq. (2.88) explicitly to obtain

$$\mathcal{E}(\rho_S) = \sum_k \langle e_k|U(\rho_S \otimes |e_0\rangle\langle e_0|)U^\dagger|e_k\rangle \tag{2.91}$$

$$= \sum_k E_k \rho_S E_k^\dagger, \tag{2.92}$$

where we define the operators $E_k \equiv \langle e_k|U|e_0\rangle$, acting on the principal system S. It is evident that the E_ks satisfy the completeness relation: $\sum_k E_k^\dagger E_k = \sum_k \langle e_0|U^\dagger|e_k\rangle\langle e_k|U|e_0\rangle = \langle e_0|U^\dagger U|e_0\rangle = \langle e_0|\mathbb{I}_{SE}|e_0\rangle = \mathbb{I}_S$, where we used the unitarity of U and the completeness of the basis $\{e_k\}$. The assumption of a pure initial state for the environment does not involve a loss of generality, since, if ρ_E were mixed, we would be allowed to consider a bigger environment where, by purification, the initial state was pure, without affecting the dynamics of the principal system.

We have introduced above a quantum map $\mathcal{E}$ that does not depend on time, i.e. it describes the output of an operation. If we are interested in the time evolution of the principal system, we need a family of quantum maps parametrized by the time $t \geq 0$: $\mathcal{E}_t$, where $\mathcal{E}_{t=0}$ is obviously the identity.

A description of the time evolution of an open quantum system that is complementary to that of quantum operations involves a differential equation for the density operator, that generalizes the Liouville-von Neumann equation (2.25), and that is generally referred to as the *master equation*:

$$\frac{d\rho_S}{dt} = -\frac{i}{\hbar}[H_S(t), \rho_S] + \mathcal{D}[\rho_S]. \tag{2.93}$$

The term $\mathcal{D}[\rho_S]$, called *dissipator*, is a superoperator added to the equation that accounts for the non-unitary evolution of the system. The form of the dissipator depends on the specific physical model that one intends to describe. A wide body of literature is devoted to the microscopic derivation of master equations for a variety of quantum systems.

2.3.1 Quantum non-Markovianity

An important class of master equations is the *Gorini-Kossakowski-Sudarshan-Lindblad* [73–75] form[2]

$$\frac{d\rho_S}{dt} = -i[H_S(t), \rho_S(t)] + \sum_k \gamma_k(t) \left[V_k(t)\rho_S(t)V_k^\dagger(t) - \frac{1}{2}\left\{V_k^\dagger(t)V_k(t), \rho_S(t)\right\}\right], \quad (2.94)$$

where $\gamma_k(t) \geq 0$ and the $V_k(t)$ are called Lindblad operators. The curly brackets denote the anti-commutator: $\{A, B\} = AB + BA$.

Eq. (2.94) describes the most general quantum dynamics that allows the definition of a divisible quantum map. *Divisibility* is the property of a completely positive quantum map to satisfy the composition law

$$\mathcal{E}(t_3, t_1) = \mathcal{E}(t_3, t_2)\mathcal{E}(t_2, t_1), \quad (2.95)$$

with $\mathcal{E}(t_3, t_2)$ and $\mathcal{E}(t_2, t_1)$ completely positive for any $t_3 \geq t_2 \geq t_1$. Here $\mathcal{E}(t', t)$ denotes the map that describes the dynamics of the system from time t to time t'.

The main feature of a divisible map is the absence of memory effects. Eq. (2.95) tells us that the evolution of the system depends only on its current state, and not on its previous evolution. We have seen in Chapter 1) that this concept, in the theory of classical stochastic processes, is known as *Markovianity*.

Although in classical probability theory the notion of a Markovian process is well defined, its quantum generalization is not straightforward, as it is based on concepts of classical probability that can't be applied in quantum mechanics, essentially because of the disturbance caused by the measurement process. The Lindblad master equation (2.94) is one of the possible approaches that are followed in the literature, but there are other non-equivalent ways of defining Markovianity (e.g. algebraic definition, semigroup property) for quantum processes and it is object of active research and debate, as can be seen in recent reviews on the topic [8, 10].

Proving the divisibility of a quantum map is a very difficult task in general, especially when the full analytic form of the map is missing. A large body of research work in this field is thus devoted to detecting and quantifying the "degree" of non-Markovianity of a quantum process, by providing witnesses and measures that are non-zero when the quantum process is non-Markovian. Most of these measures are reviewed in [10]. In this thesis, we focus on the BLP measure [76], one of the most used in the literature, based on the exchange of information between the open system and its environment, and on the divisibility of the dynamical map describing the open system's time evolution, and the RHP measure [77], based on the entanglement between the quantum system and an ancillary system.

2.3.2 The BLP measure

The BLP measure, introduced in 2009 by Breuer, Laine and Piilo [76], is based on the idea that memory effects in the dynamics of open systems are linked to the exchange of

[2]Equation (2.94) is actually a generalization of the Gorini-Kossakowski-Sudarshan-Lindblad equation, which originally features time independent Hamiltonian H_S, decay rates γ_k and Lindblad operators V_k.

information between the open system and its environment: while in a Markovian process the open system continuously loses information to the environment, a non-Markovian process is characterized by a flow of information from the environment back into the open system.

Formally, the BLP measure looks at how the distinguishability between states of the open quantum system is affected by its interaction with the environment. If the distinguishability between two different initial states of the system decays in time, it means that information is lost to the environment and *vice versa*.

To quantify the distinguishability between states, the BLP measure considers the trace distance, that we defined in Subsection 2.2.1. We already stated that the trace distance has an operational interpretation related to the probability of error in the discrimination between two different quantum states. Moreover it has another property that is relevant to our discussion: it is contractive under the action of completely positive maps, i. e.

$$D(\rho_1, \rho_2) \geq D\left(\mathcal{E}(\rho_1), \mathcal{E}(\rho_2)\right) \tag{2.96}$$

for any map $\mathcal{E}$ and for any pair of states ρ_1 and ρ_2. The proof is quite easy and can be found on [2]. Equation (2.96) means that no quantum operation can increase the distinguishability between a pair of quantum states.

If a quantum evolution is Markovian, its divisibility property, Eq. (2.95), implies that at any intermediate time between the initial and final time, the map can be split into two completely positive maps, for which the trace distance is contractive. It follows that the trace distance between two states of the systems must be less or equal than the initial one, i.e. it must be monotonically decreasing in time.

But if a quantum map is non-Markovian, Eq. (2.95) does not hold, meaning that the intermediate evolution steps are not completely positive: thus, the trace distance between two different states is allowed to have a non-monotonic behavior.

To be quantitative, let us consider two initial states of the system ρ_1 and ρ_2 and let us write $\rho_i(t) = \mathcal{E}_{t,0}(\rho_i)$. In view of the above discussion, the rate of change of the trace distance

$$\sigma_{\rho_1,\rho_2}(t) = \frac{d}{dt} D(\rho_1(t), \rho_2(t)) \tag{2.97}$$

is zero or negative for a Markovian quantum map, while it can be temporarily positive for a non-Markovian one. When $\sigma_{\rho_1,\rho_2}(t) > 0$, the distinguishability between $\rho_1(t)$ and $\rho_2(t)$ is increasing, meaning that there is a temporary backflow of information from the environment to the principal system.

The BLP measure is then defined as

$$\mathcal{N}_{\text{BLP}} = \max_{(\rho_1,\rho_2)} \int_{\sigma>0} dt\, \sigma_{\rho_1,\rho_2}(t). \tag{2.98}$$

The time integral is over all the intervals in which $\sigma_{\rho_1,\rho_2}(t) > 0$. The maximum is taken over all pairs of states, because we want $\mathcal{N}_{\text{BLP}}$ to be a property of the quantum map.

Whenever $\mathcal{N}_{\text{BLP}} > 0$, the quantum map $\mathcal{E}$ is non-Markovian. On the other hand, $\mathcal{N}_{\text{BLP}} = 0$ is a necessary, but not sufficient condition for $\mathcal{E}$ to be Markovian [78].

Besides the fact that it is not sufficient to prove the Markovianity of a quantum process, the BLP measure has another drawback: it is, in general, not easy to evaluate. To obtain

$\mathcal{N}_{\text{BLP}}$, an optimization over the whole state space $\mathcal{S}(\mathcal{H}_S)$ is required. It has been shown [79] that the states of the optimal pair must lie on the boundary of $\mathcal{S}(\mathcal{H}_S)$ (but need not be pure) and that they must be orthogonal. Although this result greatly reduces the number of free parameters to optimize over, it remains a challenging task for any system of more than a few qubits.

2.3.3 The RHP measure

Rivas, Huelga and Plenio introduced this measure of non-Markovianity in [77]. Consider the quantum system of interest S, and an identical ancillary system A. We prepare the two system in the maximally entangled state

$$|\psi\rangle = \frac{1}{\sqrt{N}} \sum_{n=1}^{N} |n\rangle_S |n\rangle_A \,, \tag{2.99}$$

where $|n\rangle$ are the vectors of a basis of the Hilbert space of the system. We now let the system S interact with the environment, while the ancilla A is left untouched, and evaluate the entanglement of the state $|\psi(t)\rangle$. Since any entanglement measure is a monotone under local CP maps, any increase of an entanglement measure with time denotes that the dynamical map fails to be divisible, i.e. that it is non-Markovian. The RHP is defined quantitatively as

$$\mathcal{N}_{\text{RHP}} = \int_{t_0}^{t_f} \left| \frac{dN(t)}{dt} \right| , \tag{2.100}$$

where $N(t)$ is any entanglement measure (in our case, the negativity).

The advantage of $\mathcal{N}_{\text{RHP}}$ over $\mathcal{N}_{\text{BLP}}$ is that no optimization over the initial pair of states is required, at the cost of increasing the size of the system. The RHP measure, however, maintains the same drawback as the BLP in that $\mathcal{N}_{\text{RHP}} = 0$ is a necessary, but not sufficient condition for the Markovianity of the quantum map. In fact, Ref. [77] introduces another measure that is a necessary and sufficient condition for the non-Markovianity of the quantum map, based on the Choi-Jamiolkowski isomorphism [80, 81]. However, to compute this measure one needs to know the structural form of the dynamical map between any two time instants, which is not the case for our processes.

2.4 Quantum estimation theory

In Subsection 2.1.1 we have discussed measurements in quantum mechanics. If we want to determine the value of a physical observable, we have to implement the corresponding projective measurement and then collect data from repeated experiments in order to evaluate the expected value.

Several quantities of interest in quantum information theory, however, do not correspond to quantum observables and thus can not be measured directly. In these situations one has to infer their value indirectly, by inspecting a set of data coming from the measurement of a different observable, or a set of observables. The analytical tools to find the

optimal measurement strategies and the bound to the achievable precision are provided by the framework of quantum estimation theory (QET).

Broadly speaking, one can think of two estimation strategies: a global strategy, where one seeks the best performance in the estimation of the parameter, averaged over all its possible values, and a local strategy, where one wants the best performance at a fixed value of the parameter. Intuitively, one expects local QET to give better results, as the optimization of the estimation procedure is made around a specific value of the parameter, but the POVM will depend on that specific value. A local estimation scheme must thus be based on some prior knowledge of the parameter. Typically, this knowledge comes from a theoretical prediction, a previous global estimation of the parameter, or an adaptive feedback mechanism where the result of a round of estimation is used as local value for the next round [82].

In this section we quickly review local QET [83–85], which looks for the POVM that minimizes the variance of the estimator as a function of the value of the parameter. The theory applies in general to the simultaneous estimation of an arbitrary number of parameters. Here we restrict for simplicity to the estimation of a single parameter.

Classical estimation theory First, let us start with a classical setting. Let us assume that we are interested in the estimation of a single parameter, having a true value λ. We make repeated experiments on the system and collect a set of data $\{x_1, \ldots, x_M)$. We now define an *estimator*, i.e. a function from the set ξ of measurement outcomes to the space of parameters:

$$\hat{\lambda} = \lambda(x_1, \ldots, x_n). \tag{2.101}$$

We denote by $V(\hat{\lambda})$ the mean square error of the estimator, i.e.

$$V(\hat{\lambda}) = \mathbb{E}\left[(\hat{\lambda} - \lambda)^2\right], \tag{2.102}$$

where $\mathbb{E}[X]$ is the expected value, or mean, of the random variable X.

We say that $\hat{\lambda}$ is an *unbiased* estimator if its expected value is equal to the true value of the parameter: $\mathbb{E}\left[\hat{\lambda}\right] = \lambda$. Hence, for an unbiased estimator, the MSE is equal to the variance $\sigma^2(\hat{\lambda}) = \mathbb{E}\left[\left(\hat{\lambda} - \mathbb{E}\left[\hat{\lambda}\right]\right)^2\right]$. The lower the variance, the better the precision of the estimation process, since it will tend to have values concentrated around the true value of the parameter.

The variance, however, has a lower bound given by the *Cramér-Rao theorem* [86], which states that, for any unbiased estimator $\hat{\lambda}$,

$$V(\hat{\lambda}) \geq \frac{1}{MF(\lambda)}, \tag{2.103}$$

where M is the number of values in the data sample. $F(\lambda)$ is the *Fisher information* (FI):

$$F(\lambda) = \int dx p(x|\lambda) \left[\partial_\lambda \log p(x|\lambda)\right]^2 = \int dx \frac{\left[\partial_\lambda p(x|\lambda)\right]^2}{p(x|\lambda)}, \tag{2.104}$$

where ∂_λ is the derivative with respect to λ. In Equation (2.104), known as the *Cramér-Rao (CR) bound*, $p(x|\lambda)$ is the conditional probability of having the outcome x from an

experiment, given the value of λ, and the integration is over all the possible outcomes. The proof of the CR bound can be found, for instance, in [87].

An estimator for which the equality in Eq. (2.103) holds is said to be efficient. The existence of an efficient estimator is guaranteed only for particular statistical models and particular choices of parametrization. However it is known that maximum-likelihood and Bayesian estimators are efficient asymptotically, i.e., when $M \to \infty$ [87]. At the end of this section we will briefly discuss the Bayesian estimator, that we will employ in Chapter 5.

Quantum Fisher information The above discussion regards a general estimation problem with a set of classical data. In the quantum scenario, the data is collected through a quantum measurement on the state of the system, which depends on the parameter. We thus have a family of quantum states ρ_λ, i.e. a manifold in the set of states $\mathcal{S}(\mathcal{H})$.

If $\{E_x\}$ is a POVM, the conditional probability reads $p(x|\lambda) = \mathrm{Tr}[\rho_\lambda E_x]$. Thus the FI (2.104) reads

$$F(\lambda) = \int dx \frac{\left(\partial_\lambda \mathrm{Tr}[\rho_\lambda E_x]\right)^2}{\mathrm{Tr}[\rho_\lambda E_x]}. \tag{2.105}$$

Upon introducing the symmetric logarithmic derivative (SLD) L_λ as the self-adjoint operator satisfying the differential equation

$$\partial_\lambda \rho_\lambda = \frac{L_\lambda \rho_\lambda + \rho_\lambda L_\lambda}{2}, \tag{2.106}$$

we have

$$\partial_\lambda p(x|\lambda) = \mathrm{Tr}[\partial_\lambda \rho_\lambda E_x] = \mathrm{Re}(\mathrm{Tr}[\rho_\lambda E_x L_\lambda]), \tag{2.107}$$

where we have used the cyclic property of the trace and the Hermiticity of the operators. Equation (2.105) now reads

$$F(\lambda) = \int dx \frac{\left(\mathrm{Re}\,\mathrm{Tr}[\rho_\lambda E_x L_\lambda]\right)^2}{\mathrm{Tr}[\rho_\lambda E_x]}. \tag{2.108}$$

Thus, for a given quantum measurement $\{E_x\}$, Eqs. (2.103) and (2.108) give the classical bound to the precision achieved by proper data processing.

The FI can be optimized over all possible POVMs to obtain the *quantum* bound to the precision achievable in the estimation of the parameter λ. This maximization can be carried out analytically[3] [90] (see also [85]) and one finds that the F is bounded by the so-called *quantum Fisher information* (QFI)

$$Q(\lambda) \equiv \mathrm{Tr}[\rho_\lambda L_\lambda^2] \geq F(\lambda). \tag{2.109}$$

The ultimate bound to the precision achievable in the estimation of the parameter λ in a quantum system is thus given by the *quantum Cramér-Rao* bound

$$V(\lambda) \geq \frac{1}{MQ(\lambda)}. \tag{2.110}$$

[3]We have recently shown, however, that the maximization does not hold if the POVM does intrinsically depend on the parameter λ, or if the measure of the sample space depends on the parameter [88, 89]. This is however not relevant for the estimation problems discussed in this thesis.

The bound above does not depend on the measurement, but only on the geometric structure of the manifold ρ_λ. Moreover it is saturable: there exists a quantum measurement for which the FI (2.105) equals the QFI (2.109). The optimal measurement is made by the set of projectors onto the eigenstates of the SLD L_λ [85].

To obtain the value of $Q(\lambda)$ we need to find the SLD operator. Equation (2.106) is a Lyapunov matrix equation, which admits the solution

$$L_\lambda = 2\int_0^\infty dt e^{-\rho_\lambda t}\partial_\lambda\rho_\lambda e^{-\rho_\lambda t}. \tag{2.111}$$

In the basis of eigenstates of the density matrix, $\rho_\lambda = \sum_n \rho_n |\psi_n\rangle\langle\psi_n|$, we have

$$L_\lambda = 2\sum_{nm}\frac{\langle\psi_m|\partial_\lambda\rho_\lambda|\psi_n\rangle}{\rho_n+\rho_m}|\psi_m\rangle\langle\psi_n|, \tag{2.112}$$

where the sum includes only terms where $\rho_n + \rho_m \neq 0$. It follows that the quantum Fisher information is

$$Q(\lambda) = 2\sum_{nm}\frac{|\langle\psi_m|\partial_\lambda\rho_\lambda|\psi_n\rangle|^2}{\rho_n+\rho_m}. \tag{2.113}$$

An alternative expression for the QFI, which will be useful later, can be obtained by writing $\partial_\lambda\rho_\lambda$ explicitly:

$$\partial_\lambda\rho_\lambda = \sum_n\left[\partial_\lambda\rho_n\ |\psi_n\rangle\langle\psi_n| + \rho_n\left(|\partial_\lambda\psi_n\rangle\langle\psi_n| + |\psi_n\rangle\langle\partial_\lambda\psi_n|\right)\right]. \tag{2.114}$$

Here $|\partial_\lambda\psi_n\rangle = \sum_i \partial_\lambda\psi_{ni}(\lambda)|i\rangle$, where $\psi_{ni}(\lambda)$ are the coefficients of ψ_n with respect to an orthonormal basis $\{|i\rangle\}$ that is independent of λ. From the orthonormality relation $\langle\psi_n|\psi_m\rangle = \delta_{nm}$ it follows that

$$\partial_\lambda\langle\psi_n|\psi_m\rangle = \langle\partial_\lambda\psi_n|\psi_m\rangle + \langle\psi_n|\partial_\lambda\psi_m\rangle = 0 \tag{2.115}$$

and therefore $\mathrm{Re}\langle\partial_\lambda\psi_n|\psi_n\rangle = 0$ and $\langle\partial_\lambda\psi_n|\psi_m\rangle = -\langle\psi_n|\partial_\lambda\psi_m\rangle$. By plugging Eq. (2.114) into Eq. (2.113) and using the above identities, we obtain

$$Q(\lambda) = \sum_n\frac{\partial_\lambda\rho_n^2}{\rho_n} + 2\sum_{nm}\frac{(\rho_n-\rho_m)^2}{\rho_n+\rho_m}|\langle\psi_m|\partial_\lambda\psi_n\rangle|^2. \tag{2.116}$$

Equation (2.116) shows explicitly that the QFI consists of two contributions. The first contribution comes from the classical probability distribution, i.e. from the eigenvalues of the density operator ρ_λ. The second contribution is genuinely quantum, as it comes from the dependence of the eigenvectors on the parameters λ. If the latter contribution vanishes, we recover the classical FI, Eq. (2.104).

A figure of merit that is often used in place of the QFI is the quantum signal-to-noise ratio (QSNR)

$$R(\lambda) = \lambda^2 Q(\lambda). \tag{2.117}$$

$R(\lambda)$ is a dimensionless quantity and thus gives an indication of the estimability of the parameter that is independent of its magnitude.

In Subsection 2.2.1 we introduced the Bures distance. We can know show its link to the quantum Fisher information, and create an interesting link to the information-theoretical content of the latter to the geometrical meaning of the former. Indeed, the family of states ρ_λ parametrized by λ (or a vector $\boldsymbol{\lambda}$ of parameters) is a differentiable manifold in the set of quantum states. The Bures distance is Riemannian, and thus we can define its metric on the manifold ρ_λ:

$$ds_B^2 = D_B^2(\rho_\lambda, \rho_{\lambda+d\lambda}) = g_B d\lambda^2. \tag{2.118}$$

By explicit evaluation of the Bures distance, one finds that the QFI is proportional to the metric tensor (in the single parameter case just a number) of the Bures metric [85]

$$Q(\lambda) = 4g_B. \tag{2.119}$$

Equation (2.119) gives a geometric interpretation of the QFI: the bigger $Q(\lambda)$, the farther apart (in the Bures distance sense) the quantum state is sent by a small variation of the parameter λ, and thus the easier it will be to statistically distinguish between the values λ and $\lambda + d\lambda$.

Bayesian estimator We finally describe an estimator that is commonly used in actual inference tasks, the Bayesian estimator. We have said that, with maximum-likelihood estimators, Bayesian estimators are known to be asymptotically efficient, i.e. they allow to saturate the Cramér-Rao bound for a sufficiently high dimension of the data set. In the Bayesian approach, the unknown parameter λ is treated like a random variable, with an associated probability distribution that is conditioned by experimental data.

Bayes's rule states that

$$p(x|y) = \frac{p(y|x)p(x)}{p(y)}. \tag{2.120}$$

This comes from the fact that the joint probability $p(x, y)$ for two random variables is related to the conditional probability by $p(x, y) = p(x|y)p(y)$, but the joint probability is symmetric under the exchange of variables: $p(x, y) = p(y, x)$.

Now, consider a set of data $\Omega = \{x_i\}_{i=1}^M$, obtained from M measurements of the random variable X, depending on the parameter λ. If we label with $p(\Omega|\lambda)$ the probability of obtaining the set of data Ω when the true value of the parameter is λ, Bayes's rule states that

$$p(\lambda|\Omega) = \frac{p(\Omega|\lambda)p(\lambda)}{\int_\Lambda p(\Omega|\lambda')p(\lambda')d\lambda'}, \tag{2.121}$$

where Λ is the set of possible value of λ. $p(\lambda)$ is called the *a priori* distribution of the parameter, and expresses our initial guess about λ, and $p(\lambda|\Omega)$ is the *a posteriori* distribution, that represents our knowledge of the parameter once we observed the data Ω.

We define the Bayesian estimator as the mean of the posterior distribution $p(\lambda|\Omega)$:

$$\hat{\lambda}_B = \int_\Lambda \lambda p(\lambda|\Omega)d\lambda. \tag{2.122}$$

The variance of the Bayesian estimator quantifies its precision:

$$\sigma^2(\hat{\lambda}_B) = \int_\Lambda [\lambda - \hat{\lambda}_B]^2 p(\lambda|\Omega) d\lambda. \tag{2.123}$$

Summary

- The formalism of density matrices allows a complete description of state of a quantum system, its evolution and the effects of quantum measurements. Moreover, it allows us to describe a quantum system that is interacting with the surrounding environment, by means of completely positive and trace preserving maps or quantum master equations
- Quantum correlations are a resource for quantum information processing. Entanglement is the most important form of quantum correlations. Entangled states cannot be generated using a LOCC scheme and are mathematically defined as non-separable states. However, quantum discord describes a more general kind of quantum correlations, that can be found also in separable states.
- While a definition of Markovianity for classical stochastic processes is well known, its generalization to the quantum case is not straightforward, and is subject of debate and research. A number of different measures have been introduced, based on different concepts. The BLP measure, links the non-Markovianity to a regrowth in the distinguishability between two different states of the quantum system, interpreting it as a backflow of information from the environment. The RHP measure uses a similar idea, but is based on the entanglement between the system and an ancillary system that does not evolve in time.
- Quantum estimation theory provides the tools to determine the precision of the estimation of a non-observable parameter of the system through quantum measurement. The most important quantity in QET is the quantum Fisher information, that is the maximum of the Fisher information with respect to all possible quantum measurements, giving, through the quantum Cramér-Rao bound, the ultimate limit to precision. The Bayesian estimator saturates the Cramér-Rao bound asymptotically.

Chapter 3

Dynamics of qubit systems affected by classical noise

In this chapter we address the dynamics of qubit systems interacting with a classical environment. We start in Section 3.1 with a general discussion of the formal description of such dynamics. Then, we describe known analytical results for the interaction of qubits with longitudinal noise in Section 3.2, and with transverse noise in Section 3.3. In both cases, we discuss the dynamics of quantum correlations, by analyzing in particular negativity and quantum discord, introduced in Section 2.2. Finally, in Section 3.4 we address the non-Markovianity of the quantum dynamics by evaluating the BLP and RHP measures defined in Subsection 2.3.1.

3.1 Interaction with a classical environment

In quantum mechanics, the interaction of a system with the environment is described by means of quantum operations, as we discussed in Section 2.3. The system $\mathcal{H}$ and the environment $\mathcal{H}_{\text{env}}$ are considered as one closed system $\mathcal{H} \otimes \mathcal{H}_{\text{env}}$ which undergoes unitary evolution, then, to obtain the state ρ of the system after the interaction, we take the partial trace with respect to the environment:

$$\mathcal{E}(\rho) = \text{Tr}_{\text{env}}[U(\rho \otimes \rho_{\text{env}})U^{\dagger}] \tag{3.1}$$

where ρ_{env} is the initial state of the environment and U is a unitary operator.

If we want to treat the environment classically, then the partial trace must be replaced by its classical counterpart, the marginal distribution. The coupling to the environment is described by an interaction Hamiltonian which is a functional of a stochastic process $B(t)$. The total Hamiltonian reads

$$H[B(t)] = H_0(t) + H_I[B(t)], \tag{3.2}$$

where $H_0(t)$ is the Hamiltonian of the system and $H_I[B(t)]$ describes the interaction between the system and the environment.

For a given realization of the stochastic process $B(t)$, the unitary operator describing the evolution in the time interval $[0, t]$ is the general solution to the Schrödinger equation (2.6)

$$U[B(t)] = \mathcal{T} \exp\left[-i \int_0^t dt' \, H[B(t')]\right], \tag{3.3}$$

where $\mathcal{T}$ is the time ordering operator. To obtain the actual evolution of the system, we must average over all the possible histories of the stochastic field. The map describing the evolution of the density operator is thus

$$\mathcal{E}(\rho) = \int \mathcal{D}[B(t)]\mathcal{P}[B(t)]U[B(t)]\rho U^{\dagger}[B(t)]. \tag{3.4}$$

Here, the functional integral is over all the possible histories of the stochastic process $B(t)$, weighted by the probability functional $\mathcal{P}[B(t)]$, which of course must satisfy the relation

$$\int \mathcal{D}[B(t)]\mathcal{P}[B(t)] = 1. \tag{3.5}$$

In the following, we will use the more compact notation

$$\mathbb{E}\left[f[B(t)]\right] \equiv \int \mathcal{D}[B(t)]\mathcal{P}[B(t)]f[B(t)] \tag{3.6}$$

to indicate that a certain quantity must be calculated by averaging over all possible histories of the field.

In this way, we have defined a quantum map $\mathcal{E}$ that acts on the states of the systems according to the equation

$$\mathcal{E}(\rho) = \mathbb{E}\left[U\rho U^{\dagger}\right] \tag{3.7}$$

and is a CPT map. Indeed Eq. (3.7) is a Kraus decomposition where the sum is replaced by the functional integral over the histories of the field and the Kraus operators satisfy Eq. (2.90) because of the unitarity of U and the normalization condition (3.5).

We now consider a qubit interacting with a classical environment, described with the method above. We consider the following stochastic Hamiltonian

$$H(t) = H_0 + H_I[B(t)] = \omega_0\sigma_z + \nu\boldsymbol{B}(t)\cdot\boldsymbol{\sigma}, \tag{3.8}$$

where we set $\hbar = 1$, as we will do hereafter. The choice of the z axis is completely arbitrary. By giving the appropriate meaning to the energy ω_0 and coupling term ν, H can describe many different physical systems, like a half-spin particle in a magnetic field directed along the z axis, a Josephson qubit [59] or a semiconducting qubit [91].

The interaction Hamiltonian $H_I = \nu\boldsymbol{B}(t)\cdot\boldsymbol{\sigma}$ depends on the stochastic variable $\boldsymbol{B}(t)$, and the resulting map is to be obtained with Eqs. (3.3) and (3.7). In general, an analytical solution for the quantum map $\mathcal{E}_{B(t)}$ can not be obtained, because $H[B(t)]$ does not commute with itself at different times, because of the algebra of the Pauli matrices and the time dependence of H_I. Analytical solutions are possible only in special cases.

We will also consider two-qubit systems, to study the effects of classical noise on quantum correlations. The prototype Hamiltonian is that of two non-interacting qubits, each of them under the effect of a classical noise:

$$H = H_1(t)\otimes\mathbb{I}_2 + \mathbb{I}_1\otimes H_2(t), \tag{3.9}$$

where $\mathbb{I}_1$ and $\mathbb{I}_2$ are the identity operators for the first and second qubit, and

$$H_i(t) = \omega_0\sigma_z^{(i)} + \nu\boldsymbol{B}_i(t)\cdot\boldsymbol{\sigma}^{(i)}. \tag{3.10}$$

The stochastic processes $\boldsymbol{B}_1(t)$ and $\boldsymbol{B}_2(t)$ can be completely uncorrelated or they can have some sort of correlations. The former case presents itself when the two qubits interact with *independent environments*, i.e. they are sent through different noisy channels, or they are separated enough that they interact with different degrees of freedom of the environment. In the opposite scenario, the two qubits interact with a *common environment*, that is, with a single stochastic field $B(t) = B_1(t) = B_2(t)$.

3.2 Analytical results for longitudinal noise

One case where the analytical solution is always available, at least when the probability distribution of the noise phase (1.13) is known, is the *longitudinal noise*, that is, when $\boldsymbol{B}(t)$ is directed along the z axis. Longitudinal noise has been addressed by many authors. Here we review the solutions for the dynamics and the features of the quantum map resulting from the interaction (see [20] and refs. therein), and present some original contributions [92, 93].

In the case of longitudinal noise the Hamiltonian reads

$$H = (\omega_0 + \nu B(t))\sigma_z. \tag{3.11}$$

We assume that $\mathbb{E}[B(t)] = 0$: the action of the noise term is thus that of perturbing the energy of the qubit from its value ω_0. Obviously, H in (3.11) does commute with itself at different times, so we can write the evolution operator explicitly

$$U[B(t)] = \exp\left[-i\int_0^t H[B(t)]dt\right] = \exp\left[-i(\omega_0 t + \nu\phi(t))\sigma_z\right], \tag{3.12}$$

where $\phi(t) = \int_0^t B(t')dt'$ is the noise phase, defined in Eq. (1.13). Thus the evolution map for the qubit system, reads

$$\begin{aligned}\mathcal{E}(\rho) &= \mathbb{E}\left[U[B(t)]\rho U^\dagger[B(t)]\right] = \\ &= \begin{pmatrix} \rho_{11} & e^{-2i\omega_0 t}\mathbb{E}\left[e^{-2\nu i\phi(t)}\right]\rho_{12} \\ e^{2i\omega_0 t}\mathbb{E}\left[e^{2\nu i\phi(t)}\right]\rho_{12}^* & \rho_{22} \end{pmatrix}.\end{aligned} \tag{3.13}$$

We can move to a frame rotating at the frequency ω_0 around the z axis (i.e. apply the unitary $U_{\omega_0} = \exp[-i\omega_0\sigma_z t]$) to get rid of the terms $e^{\pm 2i\omega_0 t}$. The quantities $\mathbb{E}\left[e^{\pm 2\nu i\phi(t)}\right]$ are the characteristic function of the noise phase ϕ evaluated in $\pm 2\nu$ and hence we can obtain the analytical expression for Gaussian processes and for the RTN. We have

$$\mathcal{E}(\rho) = \begin{pmatrix} \rho_{11} & G(2\nu,t)\rho_{12} \\ G(2\nu,t)\rho_{12}^* & \rho_{22} \end{pmatrix}, \tag{3.14}$$

where $G(\alpha,t)$, sometimes called the *decoherence function*, is given by

$$G_{\text{GN}}(\alpha,t) = \exp[-\frac{\alpha^2}{2}\beta(t)] \tag{3.15}$$

for Gaussian noise, where $\beta(t)$ was introduced in Eqs. (1.18) and (1.19) and, for RTN, by

$$G_{\mathrm{RTN}}(\alpha,t)=\begin{cases} e^{-\gamma t}\left[\cosh|\delta|t+\frac{\gamma}{|\delta|}\sinh|\delta|t\right] & \gamma>\alpha \\ e^{-\gamma t}\left[\cos|\delta|t+\frac{\gamma}{|\delta|}\sin|\delta|t\right] & \gamma<\alpha \end{cases}, \quad \delta=\sqrt{\gamma^2-\alpha^2}, \tag{3.16}$$

that is the function reported in Eq. (1.40). Notice that in both cases $G(\alpha,t)$ is a real function. This is a consequence of $B(t)$ being a zero-mean process.

The map in Eq. 3.14 is called *dephasing map*: the populations ρ_{11} and ρ_{22} of the qubit are left untouched; only the coherences are affected by the interaction with the environment, which conserves the energy of the system. The effect is thus that of altering the quantum information content of the qubit without any exchange of energy. This happens in those physical systems where the typical frequencies of the environment are much smaller than the frequency ω_0 of the qubit and thus does not induce transitions between the energy levels. Dephasing maps are described by the following master equation

$$\frac{d\rho}{dt}=-i[H,\rho]+\frac{\gamma}{2}[\sigma_z\rho\sigma_z-\rho]. \tag{3.17}$$

The two-qubit dynamics can be solved as well. The Hamiltonian in Eq. (3.9), with dephasing noise, gives rise to the evolution operator

$$\begin{aligned} U^{(2)}(t) &= U[B_1(t)]\otimes U[B_2(t)] \\ &= \exp\left[-i(\omega_0 t+\nu\phi_1(t))\sigma_z\right]\otimes\exp\left[-i(\omega_0 t+\nu\phi_2(t))\sigma_z\right]. \end{aligned} \tag{3.18}$$

To simplify the discussion, we assume that the initial state of the system is a Bell-diagonal state, Eq. (2.47). Upon considering the reference frame rotating with frequency ω_0 (i.e., by applying the local unitary transformation $e^{i\omega_0 t\sigma_z}\otimes e^{i\omega_0 t\sigma_z}$, we have

$$\rho(t)=\frac{1}{2}\begin{pmatrix} c_1+c_2 & 0 & 0 & (c_1-c_2)e^{-2i\nu(\phi_1+\phi_2)} \\ 0 & c_3+c_4 & (c_3-c_4)e^{-2i\nu(\phi_1-\phi_2)} & 0 \\ 0 & (c_3-c_4)e^{2i\nu(\phi_1-\phi_2)} & c_3+c_4 & 0 \\ (c_1-c_2)e^{2i\nu(\phi_1+\phi_2)} & 0 & 0 & c_1+c_2 \end{pmatrix}. \tag{3.19}$$

In the case of a common environment, obviously we have $\phi_1=\phi_2$. Upon evaluating the average over all the possible realizations of the noise, Eq. (3.7), we obtain the CPT maps describing the interaction with the classical environment. In the case of independent environments, we have to evaluate the expectation value over two uncorrelated stochastic processes, i.e. we have to evaluate quantities like $\mathbb{E}\left[e^{\pm 2i\nu\phi_1}e^{\pm 2i\nu\phi_2}\right]_{B_1(t),B_2(t)}=\mathbb{E}\left[e^{\pm 2i\nu\phi_1}\right]_{B_1(t)}\mathbb{E}\left[e^{\pm 2i\nu\phi_1}\right]_{B_2(t)}$.

As a result, we have, for independent environments,

$$\mathcal{E}_t^{\mathrm{IE}}(\rho)=\frac{1}{2}\begin{pmatrix} c_1+c_2 & 0 & 0 & (c_1-c_2)G^2(2\nu,t) \\ 0 & c_3+c_4 & (c_3-c_4)G^2(2\nu,t) & 0 \\ 0 & (c_3-c_4)G^2(2\nu,t)^2 & c_3+c_4 & 0 \\ (c_1-c_2)G^2(2\nu,t)^2 & 0 & 0 & c_1+c_2 \end{pmatrix}, \tag{3.20}$$

while for common environments

$$\mathcal{E}_t^{\mathrm{CE}}(\rho)=\frac{1}{2}\begin{pmatrix} c_1+c_2 & 0 & 0 & (c_1-c_2)G(4\nu,t) \\ 0 & c_3+c_4 & (c_3-c_4) & 0 \\ 0 & (c_3-c_4) & c_3+c_4 & 0 \\ (c_1-c_2)G(4\nu,t) & 0 & 0 & c_1+c_2 \end{pmatrix}. \tag{3.21}$$

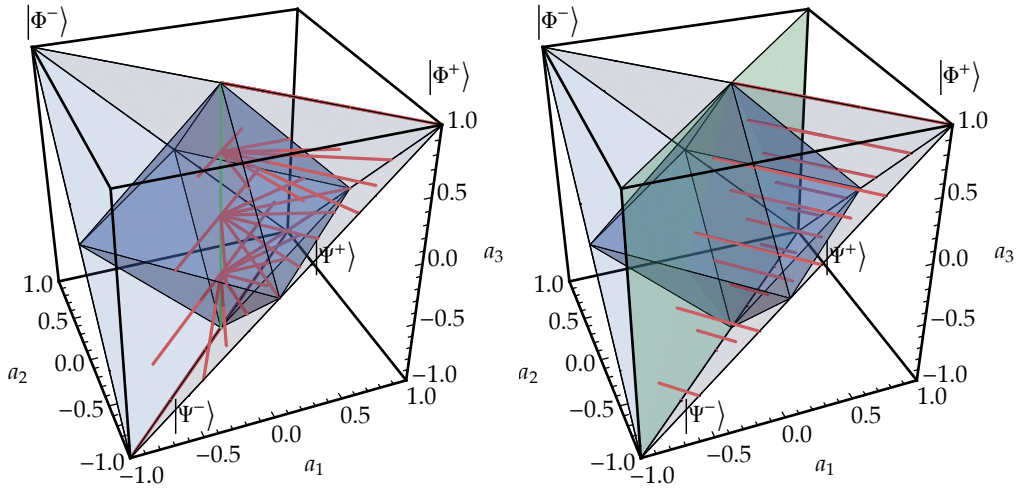

(a) Independent environments

(b) Common environment

Figure 3.1: Trajectories of the system in the Horodecki tetrahedron for two independent environments (a) and for a common environment (b). The initial states are Bell-state mixtures that lie on the surface of the tetrahedron. For independent environments, the trajectories converge to the green line at $a_1 = a_2 = 0$. For a common environment, the trajectories are directed orthogonally to the plane $a_1 = a_2$, shown in green. In both cases, a_3 remains constant.

In the Bloch form, Eq. (2.46), we have respectively

$$\rho_{\text{IE}}(t) = \frac{1}{4}\left(\mathbb{I} + G^2(2\nu, t)a_1\sigma_x \otimes \sigma_x + G^2(2\nu, t)a_1\sigma_y \otimes \sigma_y + a_3\sigma_z \otimes \sigma_z\right) \tag{3.22}$$

$$\rho_{\text{CE}}(t) = \frac{1}{4}\left(\mathbb{I} + \frac{1}{2}[G(4\nu, t)(a_1 - a_2) + a_1 + a_2]\sigma_x \otimes \sigma_x \right.$$
$$\left. + \frac{1}{2}[G(4\nu, t)(a_2 - a_1) + a_1 + a_2]\sigma_y \otimes \sigma_y + a_3\sigma_z \otimes \sigma_z\right) \tag{3.23}$$

The dynamics of the two-qubit system can be visualized by looking at its trajectory in the Horodecki diagram. This is done in Fig. 3.1 for various initial state preparations lying on the surfaces of the tetrahedron. We can see that the trajectories are straight lines converging towards the set of stationary states, which is a line with $a_1 = a_2 = 0$ for the independent-environment case and the plane $a_1 = a_2$ for the common-enviornment case.

3.3 Qubits interacting with transverse noise

The Hamiltonian (3.11), that describes longitudinal noise, allows for a simple analytical solution of the dynamics, if we know the analytical expression of the characteristic function of the stochastic process. But the Hamiltonian in Eq. (3.8) in general does not allow for an explicit solution, due to the fact that it does not commute with itself at different times. In this case, one has to resort to approximations, such as the Dyson series or the Magnus expansion [94], or to numerical simulation, which we address in

Subsection 3.3.3. An exact solution is available, however, for the special case of RTN, which we will cover in the next subsection.

In the following, we specialize to the case of transverse noise, i.e. when $\boldsymbol{B}(t)$ in the Hamiltonian in Eq. (3.8) is orthogonal to the z axis. Without loss of generality, we can assume that $\boldsymbol{B}(t)$ is directed along the x axis, and thus we have the Hamiltonian

$$H = \omega_0 \sigma_z + \nu B(t) \sigma_x. \tag{3.24}$$

The transfer matrix solution and the numerical simulation, however, can be carried out with the general Hamiltonian.

3.3.1 Transfer matrix method

Here we review a method developed by Joynt and collaborators [95, 96], that allows for an analytical solution of the general Hamiltonian (3.8), when the stochastic process describes a RTN. Other analytical solutions for a qubit interacting with RTN with an arbitrary direction are known [97, 98], but this method has the advantage of being generalizable to higher dimensional systems. We also discuss the analytical solution of the two-qubit dynamics, both with common and separate environments.

The key for the success of this method, that allows us to find an analytical solution despite the fact that the Hamiltonian does not commute with itself at different times, is the finite number of states of the environmental noise (two, in the case of RTN).

We consider the time evolution of the Bloch vector $\mathbf{n}(t)$, defined in Eq. (2.37), which can be written by means of a transfer matrix T applied to the initial Bloch vector $\mathbf{n}(0)$ as

$$\mathbf{n}(t) = T(t)\, \mathbf{n}(0). \tag{3.25}$$

Let us discretize the time interval $[0, t]$ in steps of length Δt. We assume that Δt is much smaller than the correlation time $\tau_C = \gamma^{-1}$ of the noise, so that we can consider the fluctuator to be in the same state $s_i = \pm 1$ in the i-th time interval.

We then have

$$T(t) = \mathbb{E}\left[T_{s_n} \cdots T_{s_1}\right], \tag{3.26}$$

where T_{s_i} is the 3×3 transfer matrix from the time instant t_i to time t_{i+1}, when the fluctuator is in the state $s_i = \pm 1$. T_{s_i} has the following expression

$$T_{s_i} = \exp[-2i\Delta t(\omega_0 L_z + s_i \nu \boldsymbol{B} \cdot \boldsymbol{L})], \tag{3.27}$$

where $\boldsymbol{L} = (L_x, L_y, L_z)$ and the L_i are the generators of $SO(3)$, $(L_i)_{jk} = -i\epsilon_{ijk}$, satisfying the commutation relations $[L_i, L_j] = i \sum_k \epsilon_{ijk} L_k$.

We label W the matrix describing the transition probability between the states of the fluctuator after the time Δt. In the case of RTN it is a 2×2 matrix. Its matrix element between the states s' and s reads $W_{s's} = (1 - \gamma\Delta t)\delta_{s',s} + \gamma\Delta t \delta_{s',-s}$. Thus,

$$W = \begin{pmatrix} 1 - \gamma\Delta t & \gamma\Delta t \\ \gamma\Delta t & 1 - \gamma\Delta t \end{pmatrix} = (1 - \gamma\Delta t)\mathbb{I}_2 + \gamma\Delta t \sigma_1. \tag{3.28}$$

Now let us define the 6×6 tensor Γ with element

$$\Gamma_{s_i s_{i-1}} = W_{s_i s_{i-1}} \otimes T_{s_i}. \tag{3.29}$$

The transfer matrix $T(t)$ after the average over all the possible histories of the noise, Eq. 3.26, is given by

$$T(t) = \sum_{s_1,\ldots,s_n} p_{s_1} \Gamma_{s_n s_{n-1}} \cdots \Gamma_{s_2 s_1}, \tag{3.30}$$

where $p_{s_1}(0)$ is the initial probability distribution of the state of the fluctuator. By employing the tensor nature of Γ, Eq. 3.30 can be written equivalently as

$$T = \langle x_f | \Gamma^n | i_f \rangle , \tag{3.31}$$

where $|i_f\rangle$ and $|x_f\rangle$ are vectors in the bidimensional space describing the state of the fluctuator, and describe respectively the initial and final distribution probabilities for the states, i.e. p_{s_1} and p_{s_n}. In our case, where we assume that the noise is in its stationary regime, the two states are equiprobable both in the initial and final distributions, and hence $|i_f\rangle = |x_f\rangle = \frac{1}{\sqrt{2}}(1,1)$. The tensor contraction expressed in Eqs. (3.30) and (3.31) effectively amounts to averaging over the 2×2 blocks of Γ^N, each of which describes the family of evolutions induced by all the noise sequences starting from s_1 and ending with s_n.

In our case, the tensor Γ can be written as

$$\Gamma = \left[(1 - \gamma \Delta t)\mathbb{I}_2 + \gamma \Delta t \sigma_1\right] \otimes \mathbb{I}_3 \times \exp[-2i\Delta t(\omega_0 \mathbb{I}_2 \otimes L_z + \sigma_3 \otimes \nu \boldsymbol{B} \cdot \boldsymbol{L})], \tag{3.32}$$

where σ_i are the Pauli matrices in the space of the fluctuator states and $\times$ denotes a product between 6×6 matrices. The partial inner product in Eq. (3.31) is done on the two degrees of freedom of the fluctuator and the result is a 3×3 matrix. In the continuous limit, i.e. by letting $\Delta t \to 0$, Eq. (3.32) becomes

$$\Gamma \simeq 1 + i\Delta t(\omega_0 \mathbb{I}_2 \otimes L_z + \sigma_3 \otimes \nu \boldsymbol{B} \cdot \boldsymbol{L}) + (\gamma \Delta t \sigma_1 - \gamma \Delta t \mathbb{I}_2) \otimes \mathbb{I}_3 \Delta t \simeq \exp(-\Delta t P), \tag{3.33}$$

where

$$P = (\gamma - \gamma \sigma_1) \otimes \mathbb{I}_3 - 2i\omega_0 \mathbb{I}_2 \otimes L_z - 2i\sigma_3 \otimes \nu \boldsymbol{B} \cdot \boldsymbol{L}. \tag{3.34}$$

Noting that P does not depend on time, we can write $\Gamma^N = \exp(-\Delta t P)^N = \exp(-tP)$, and hence

$$T = \langle x_f | \exp(-tP) | i_f \rangle , \tag{3.35}$$

and the problem is now cast to the diagonalization of the 6×6 matrix P.

Longitudinal case First, we check that the method gives the correct result for the case of longitudinal noise, $\boldsymbol{B} = (0, 0, B)$, for which we already know the solution. In this case the P matrix is

$$P = (\gamma - \gamma \sigma_1) \otimes \mathbb{I}_3 - 2i\omega_0 \mathbb{I}_2 \otimes L_z - 2i\sigma_3 \otimes B L_z. \tag{3.36}$$

By noticing that $[P, \mathbb{I}_2 \otimes L_z] = 0$, we can diagonalize the 2×2 matrices in the subspaces of L_z with eigenvalues $m = 0, \pm 1$. We obtain the following eigenvalues:

$$0, 2\gamma, \gamma - \delta \pm 2i\omega_0, \gamma + \delta \pm 2i\omega_0 \tag{3.37}$$

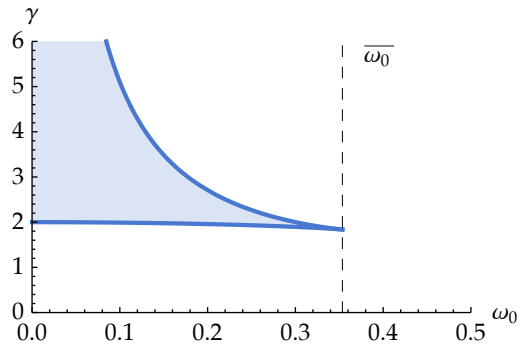

Figure 3.2: Shaded region: values of the parameters ω_0 and γ for which the eigenvalues of the operator P, i.e. the solutions of Eqs. (3.40) and (3.41), are all real, that is there are no oscillating terms in the transfer matrix. The region is bounded by the solutions of Eq. (3.44), which meet at the threshold value $\omega_0 = (2\sqrt{2})^{-1}$, highlighted by the vertical dashed line. For $\omega_0 \to 0$ we recover the dephasing case, with a transition between the two regimes at $\gamma = 2$.

where $\delta = \sqrt{\gamma^2 - 4\nu}$ was defined in (3.16). The resulting transfer matrix, after exponentiating P and evaluating the partial product, is

$$T(t) = \begin{pmatrix} e^{-\gamma t}\left(\cosh\delta t + \frac{\gamma}{\delta}\sinh\delta t\right) & 0 & 0 \\ 0 & e^{-\gamma t}\left(\cosh\delta t + \frac{\gamma}{\delta}\sinh\delta t\right) & 0 \\ 0 & 0 & 1 \end{pmatrix}. \tag{3.38}$$

It is immediate to check that the transfer matrix $T(t)$ in Eq. (3.38) describes the same map of Eq. (3.14) with the decoherence function of (3.16).

Transverse noise We now consider the case where the noise is fully transverse, as in Eq. (3.24). The P matrix reads

$$P = (\gamma - \gamma\sigma_1) \otimes \mathbb{I}_3 - 2i\omega_0 \mathbb{I}_2 \otimes L_z - 2i\sigma_3 \otimes BL_x. \tag{3.39}$$

The eigenvalues μ_i, η_i, $i = 1, 2, 3$, of P satisfy the two equations

$$\mu^3 + 2\gamma\mu^2 + 4(1 + \omega_0^2)\mu + 8\omega_0^2\gamma = 0 \tag{3.40}$$

$$\eta^3 + 4\gamma\eta^2 + 4(1 + \gamma^2 + \omega_0^2)\eta + 8\gamma = 0. \tag{3.41}$$

We notice that we can linearly transform one equation into the other by substituting $\nu = -\mu - 2\gamma$. The inverse of the real parts of these eigenvalues give the decay rate of the Bloch vector components, while the inverse of the imaginary parts give the periods of oscillations.

After exponentiating the matrix P and evaluating the partial inner product, we obtain the transfer matrix. The expression is more cumbersome than in the longitudinal case and we report the matrix elements of $T(t)$ in Appendix A for reference.

In the limiting cases of γ much greater or smaller than the other two parameters, we are able to obtain analytic expressions for the eigenvalues. When $\gamma \gg \omega_0$, i.e. we are in

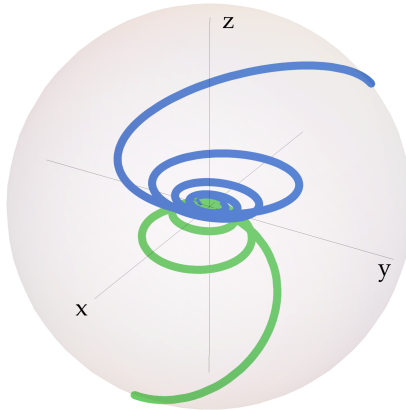

Figure 3.3: Dynamical trajectories in the Bloch sphere for a single qubit affected by RTN with $\gamma = 1/2$ and $\omega_0 = 1$ and for different initial preparations. The initial state is represented by the Bloch vector $\frac{1}{\sqrt{3}}(-1,1,1)$ for the blue trajectory, and by $\frac{1}{\sqrt{2}}(1,0,-1)$ for the orange trajectory. The asymptotic state is the maximally mixed state, that lies at the center of the Bloch sphere.

the fast-noise regime, we find that the greatest decay time is

$$T = \gamma, \tag{3.42}$$

while the oscillation frequency is ω_0, independently of γ. In the opposite limiting case, $\gamma \ll \omega_0$, we find that the longest decay time is

$$T = \begin{cases} \gamma^{-1}(1+\omega_0^2) & \text{if } \omega_0 > 1/\sqrt{2} \\ \frac{1}{2}\gamma^{-1}(1+1/\omega_0^2) & \text{if } \omega_0 < 1/\sqrt{2} \end{cases}, \tag{3.43}$$

while the oscillation frequency is instead $\sqrt{1+\omega_0^2}$. In the intermediate region, by studying the discriminant of Eq. (3.40), we find that for $\omega_0 < (2\sqrt{2})^{-1}$ there is a region of values of γ for which the eigenvalues are all real, i.e. there are no oscillations. This region, shown in Fig. 3.2, is bounded from below and above, respectively, by the two positive solutions $\gamma_{1,2}$ of

$$4\omega_0^2\gamma^4 + \left(8\omega_0^4 - 20\omega_0^2 - 1\right)\gamma^2 + 4\left(\omega_0^2+1\right)^3 = 0. \tag{3.44}$$

For $\omega_0 \to 0$ we have $\gamma_1 \to 2$ and $\gamma_2 \to \infty$, so we recover the transition between fast and slow RTN that is visible in the dephasing case [25, 99]. In fact, by letting $\omega_0 \to 0$ we are implying that the energy gap between the levels of the qubit is far away from the typical frequencies of the noise. A sharp transition between the two regimes is not visible by looking at the time evolution of the Bloch components because the imaginary components tend to zero as the parameters get close to the region, and thus the period of oscillation becomes much larger than the characteristic decay time.

In Fig. 3.3 we show the dynamical trajectories in the Bloch sphere for two different initial preparations. The asymptotic state is the maximally mixed state, with Bloch vector $(0,0,0)$.

3.3.2 Transfer matrix for the two-qubit case

We now write the transfer matrix for the two-qubit dynamics for both the relevant, and opposed, scenarios of independent environments and of a common environment. The generalization of the Bloch vector to the two-qubit case is the Bloch matrix (2.43), which we write as a 15-component vector as follows

$$\mathbf{n}_2 = (\mathbf{a}, \mathbf{b}, R_{11}, R_{12}, R_{13}, R_{21}, R_{22}, R_{23}, R_{31}, R_{32}, R_{33}). \tag{3.45}$$

The action of a unitary transformation on ρ corresponds to the action of a real orthogonal transfer matrix T_2 on $\mathbf{n}_2$. We now derive the transfer matrix for common and independent environments, assuming that the noise is transverse and acting along the x axis.

In the case of independent environments, the transfer matrix is simply

$$T_2^{\text{IE}} = \begin{pmatrix} T & 0 & 0 \\ 0 & T & 0 \\ 0 & 0 & T \otimes T \end{pmatrix}, \tag{3.46}$$

where T is defined in Eq. (3.35).

In the case of a common environment, one can easily see that, when the common fluctuator is in the state $s_i = \pm 1$, the two-qubit transfer matrix has the following block-diagonal form:

$$T_2(s_i) = \begin{pmatrix} T_{s_i} & 0 & 0 \\ 0 & T_{s_i} & 0 \\ 0 & 0 & T_{s_i} \otimes T_{s_i} \end{pmatrix}, \tag{3.47}$$

where T_{s_i} was defined in Eq. (3.27). If we extend the derivation done in the previous subsection for a single qubit, we obtain the following 30×30 matrix:

$$P_2^{\text{CE}} = (\gamma \mathbb{I}_2 - \gamma \sigma_1) \otimes \mathbb{I}_{15} - 2i(\omega_0 \mathbb{I}_2 \otimes Q_z + \nu \sigma_3 \otimes Q_x), \tag{3.48}$$

where the Q_is, with $i = x, y, z$, are 15×15 block-diagonal matrices

$$Q_i = \begin{pmatrix} L_i & 0 & 0 \\ 0 & L_i & 0 \\ 0 & 0 & L_i \otimes \mathbb{I}_3 + \mathbb{I}_3 \otimes L_i \end{pmatrix}. \tag{3.49}$$

The ensemble-averaged transfer matrix for $\mathbf{n}_2$ is then

$$T_2^{\text{CE}} = \langle x_f | \exp(-tP_2) | i_f \rangle , \tag{3.50}$$

where $|i_f\rangle = |x_f\rangle = \frac{1}{\sqrt{2}}(|+\rangle + |-\rangle)$ and the partial inner product is again done on the two degrees of freedom of the fluctuator. An analytic expression for T_2^{CE} cannot be obtained explicitly because we first need to calculate the exponential of P_2, i.e. diagonalize it. However, the exponentiation can be done easily with arbitrary precision once we substitute numerical values.

The transfer matrix method is a very neat solution of the dynamics, but it is effective only when the noise can jump between N_C discrete values. Indeed, the matrix P defined has size $N_C(d^2-1) \times N_C(d^2-1)$, where N_C is the number of levels of the classical noise and d is the dimension of the Hilbert space of the quantum system.

3.3.3 Numerical simulation of the dynamics

We have seen the analytical solutions for the longitudinal noise (both Gaussian and RTN), and we have seen that there is an analytical solution for transverse RTN noise. The latter is possible because the RTN is stepwise constant and has a finite number of values (just two in our case). In general, there is no analytical solution for transverse noise and a numerical algorithm for simulating the dynamics described in Eq. (3.7) is in order. There are two obstacles on our path: the first one is the expectation value over all possible histories of the stochastic process. Numerically, we have to sample this probability space with a large number of realizations of the process, using the simulation algorithms presented in Section 1.4. We thus have

$$\mathcal{E}_t^{N_B}(\rho) = \sum_n^{N_B} \frac{1}{N} U[B_n(t)]\rho U^\dagger[B_n(t)] \underset{N_B\to\infty}{\to} \mathcal{E}_t(\rho) \tag{3.51}$$

The second obstacle is the time-ordering operator in the evolution operator (3.3). To solve the problem, we consider the infinitesimal evolution operator between time t and $t + dt$. In the time dt, we can assume that the Hamiltonian remains constant, and thus commutes with itself. Hence, we can write

$$dU(t) \simeq \exp[-iH[B(t)]dt]. \tag{3.52}$$

We can then apply the operator $dU(t)$ recursively in order to obtain the density operator at time t.

To wrap up, the algorithm for simulating the dynamics of a quantum system interacting with classical stochastic noise

1. Define a discrete set of N_t time instants: $t_0 = 0, t_1, \ldots, t_{N_t}$, with a time step Δt.
2. Sample N_B realizations of the stochastic process on the time instants t_i, using the recipes of Section 1.4.
3. For each realization B_n of the stochastic process, evaluate the infinitesimal evolution operator at time t_i and apply it to the density operator at time t_{i-1}:
$$\rho^{(n)}(t_i) = dU[B_n(t_i)]\rho^{(n)}(t_{i-1})dU^\dagger[B_n(t_i)] \tag{3.53}$$
4. Evaluate the average over the realizations of the stochastic process, as in Eq. (3.51).

In the following we report the code for the evolution of a single qubit under RTN with an arbitrary direction, specified by the unit vector $\boldsymbol{g}$. The code can be easily extended to the two-qubit case.

```
function [rhom, t] = rtn_dynamics(rho0, ... % Initial state
                        tf, ... % Final time
                        nsteps, ... % N. of timesteps t_i
                        nsamples, ... % N. of noise realizations
```

```
                        gamma, ... % Switching rate
                        g, ... % Noise direction vector
                        coupling, ... % Coupling nu
                        omega) % Qubit frequency

% Time vector and time step
t = linspace(0, tf, nsteps);
dt = t(2) - t(1);

% Average density matrix: a 2 x 2 x nsteps array
rhom = zeros(2, 2, nsteps);

for n = 1 : nsamples
   % We generate a realization of the stochastic process.
   % B is a nsteps array

   B = rtn(t, gamma);

   % Density matrix: a 2 x 2 x nsteps array
   rhoi = zeros(2, 2, nsteps);
   rhoi(:, :, 1) = rho0;

      % The function evol_operator() calculates the evolution operator
      % for each timestep t_i. We omit its syntax which is quite trivial
   % U is a 2 x 2 x nsteps array
   U = evol_operator(B, coupling*g, omega, dt);

   % We evaluate the density matrix
   for k = 1 : nsteps - 1
      rhoi(:,:, k+1) = U(:,:, k) * rhoi(:,:, k) * U(:,:, k)';
   end

   % Sum the matrix elements for each realization
   rhom = rhom + rhoi ./ nsamples;
end
```

The analytic solution for the one- and two-qubit dynamic under RTN noise has been compared to the numerical simulations, showing excellent agreement.

3.3.4 Properties of the dynamical map

Equation (3.46) shows that the two-qubit transfer matrix in the case of independent environments is block diagonal. The same can be seen for the matrix T_2^{CE}. This means that if the initial block vector has $\mathbf{a} = \mathbf{b} = 0$, i.e. the state has maximally mixed marginals, then they will be left untouched by the dynamics. Hence, we can apply Eq. (2.86) for quantum discord to the evolved state. Although we don't have an analytic expression for the dynamics in case of other kinds of noise, such as Gaussian noise, we can see that the transfer matrix for an infinitesimal time step is block diagonal as well. Thus, in general,

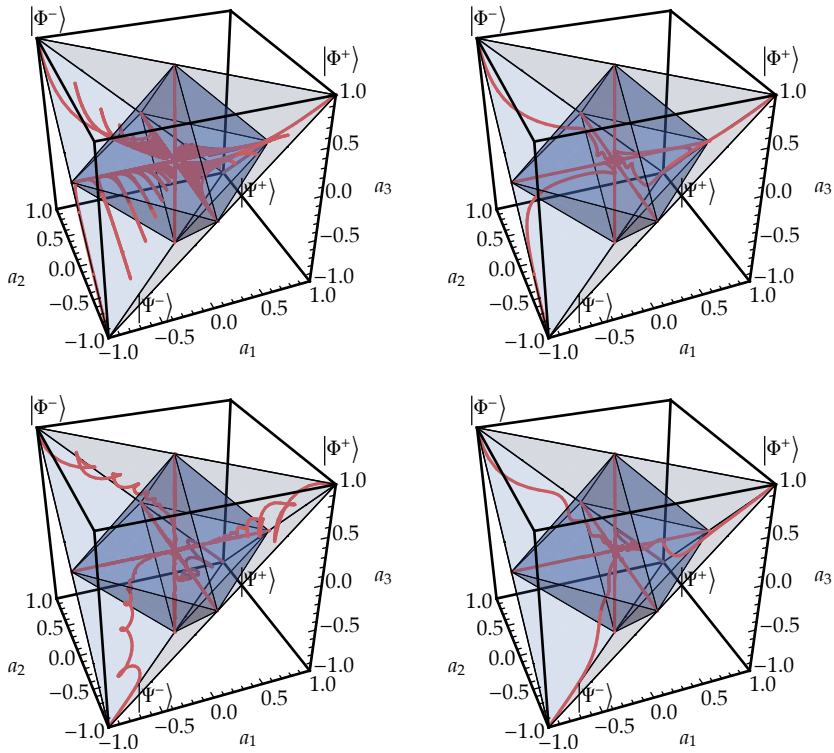

(a) Plots of RTN (above) and OU noise (below) with $\gamma = 0.1$ (left) and $\gamma = 1$ (right). The trajectories converge to the maximally mixed state $\mathbb{I}/4$. They get more convoluted for smaller values of γ, and, for the RTN noise, one can see that they get in and out of the set of separable states, and this corresponds to the sudden death and rebirth of entanglement.

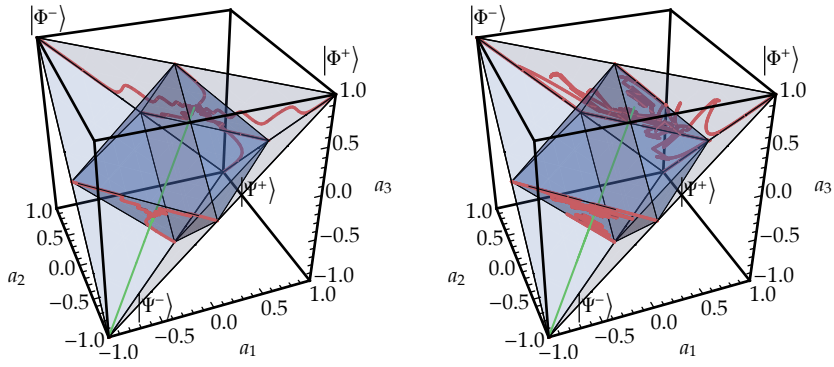

(b) Plots of RTN with $\gamma = 1/2$ (left) and $\gamma = 5$ (right). The solid green line denotes the set of Werner states, which are the only stable states. The trajectories lie on planes that are orthogonal to the green line.

Figure 3.4: Trajectories of a two-qubit system in the Bell-state tetrahedron, starting from different initial states, for (a) independent environments and for (b) common environments, with $\omega_0 = \nu = 1$.

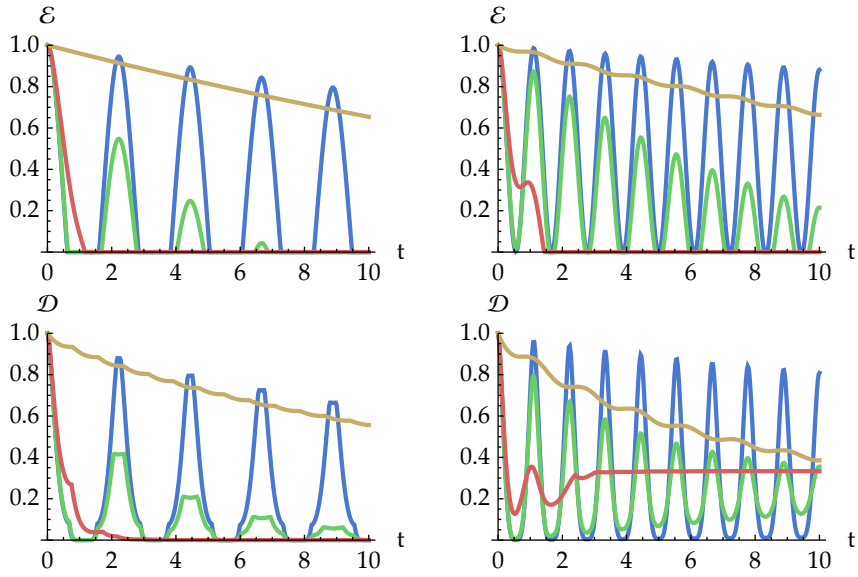

(a) RTN

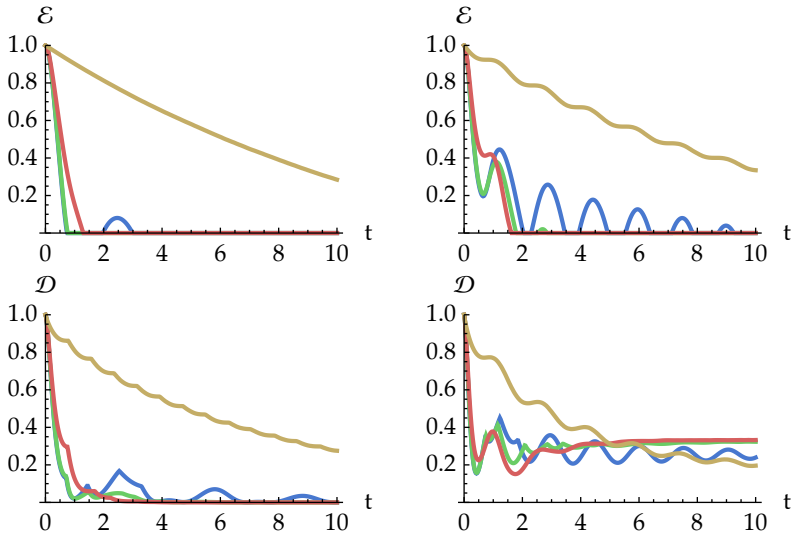

(b) OU

Figure 3.5: Negativity $\mathcal{E}$ and quantum discord $\mathcal{D}$ as functions of time for a two-qubit system initially prepared in the Bell state $|\Psi^+\rangle = 1/\sqrt{2}(|00\rangle + |11\rangle)$ subject to (a) RTN and (b) OU noise, with independent (left) and common (right) environment ($\omega_0 = 1$, $\nu = 1$). Blue: $\gamma = 10^{-2}$; green: $\gamma = 10^{-1}$; red: $\gamma = 1$; yellow: $\gamma = 100$. For both noises, for smaller values of γ, quantum correlations oscillate heavily, with sudden deaths and rebirths of entanglement. The effect is more evident for the RTN. The frequency of oscillations doubles in the common-environment case. For higher values of γ, the correlations decay, possibly with small oscillations, and entanglement dies suddenly.

we can restrict to the set of states with maximally mixed marginals and use Eq. (2.86) for the evaluation of quantum discord.

Upon restricting our choice of the initial state to Bell-state mixtures we are also able to picture the trajectory of the system. In view of the spectral decomposition theorem, the matrix R of Eq. (2.43), if symmetrical, can be diagonalized by means of an orthogonal matrix, to which correspond two local unitary operations on the two qubits [70]. It is straightforward to check that Bell-state mixtures have a symmetric R matrix. One can also see analytically that the transfer matrix for the RTN noise with independent environments, Eq. (3.46), preserves the symmetric nature of the matrix. The same can be seen numerically for T_2^{CE} and also for Gaussian noise. Since all measures of quantum correlations are invariant under local unitary operations, we can always cast R into its diagonal form, and represent the two-qubit states with mixed marginals in the Horodecki tetrahedron introduced in Subsection 2.1.4.

Stationary states For the single-qubit RTN map the only fixed point is the maximally mixed state (with the Bloch vector $\vec{0}$). This can be seen from the fact that none of the eigenvalues of P is zero and thus the transfer matrix doesn't have one as eigenvalue. Figure 3.3 shows two trajectories, both converging to the center of the Bloch sphere. The same generalizes immediately to the two-qubit case with independent environments. The stable state is the maximally mixed state $\rho = \mathbb{I}/4$. In the CE case the P_2 matrix has the eigenvalue zero. The corresponding eigenvector is the generalized Bloch vector with $\mathbf{a} = \mathbf{b} = 0$ and $(c_{ij}) = \mathbb{I}_3$. This means that all the states of the form

$$\rho_p^W = p\,|\Phi^-\rangle\langle\Phi^-| + (1-p)\mathbb{I}/4 \qquad p \in [0,1], \tag{3.54}$$

known as *Werner states* [100], are stationary states of the dynamics. This can also be seen because they satisfy the relation $\rho_p^W = (U \otimes U)\rho_p^W(U^\dagger \otimes U^\dagger)$ for every local unitary U and the CPT map induced by a common reservoir is a convex combination of unitary maps of the form $U \otimes U$. Being the zero eigenvalue of P_2 non-degenerate, these are the only stable states of the map. The same results are seen numerically for the Gaussian noise, although in this case we don't have an analytic expression for the transfer matrix.

3.3.5 Comparison of the dynamics with Gaussian and non-Gaussian noise

In this Section we compare the dynamics induced by Gaussian and non-Gaussian RTN noise and discuss their effects on the decoherence of quantum correlations of a two-qubit system. We start by noticing that the spectrum of the noise (or equivalently, its autocorrelation function) is in general not enough to describe the effect of the noise on the qubit, i.e. the dynamics of the qubit under the influence of OU noise and RTN with the same spectral width and with the same coupling may be, in general, rather different.

In Fig. 3.5 we show how the negativity and quantum discord evolve in time for the two models of noise for different values of the spectral width γ. The initial state is a pure Bell state. For both noises, we can identify two working regimes. In the first one, for small γ (slow noise), quantum correlations oscillate heavily and there are sudden deaths and rebirths of entanglement. This can be seen in the top left diagram of Fig. 3.4a:

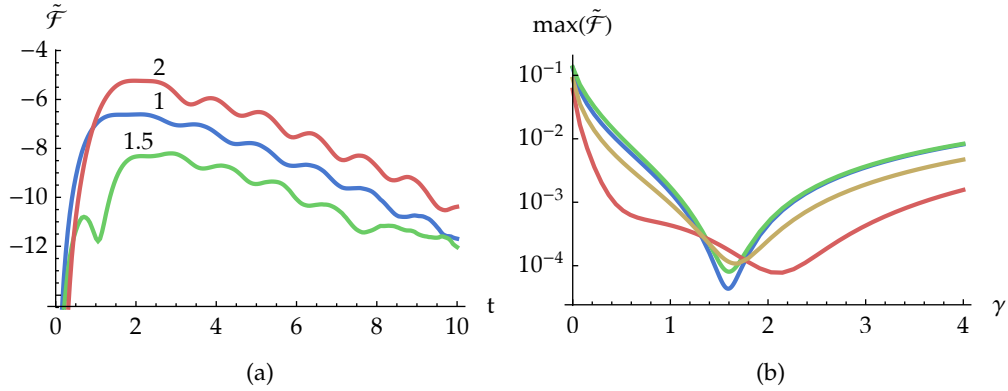

Figure 3.6: (a) Logarithm of the fidelity complement $\tilde{\mathcal{F}}(t)$ between the state of a qubit ($\omega_0 = \nu = 1$) affected by OU noise (with spectral width $\gamma_{\text{OU}} = 1$) and RTN as a function of (rescaled) time, for different values of γ_{RTN}. The qubit is initially prepared in the state $\mathbf{n} = (1, 0, 0)$. We notice that for $\gamma_{\text{RTN}} = 1$, i.e. when the two noises have the same spectrum, the dynamics is different. By tuning γ_{RTN}, the fidelity between the evolved states in the two scenarios may be increased by two orders of magnitude. (b) the maximum of the fidelity complement $\tilde{\mathcal{F}}(t)$ as a function of γ_{RTN} for $\gamma_{\text{OU}} = 1$, initial state set to $\mathbf{n} = (1, 0, 0)$ (blue), $\mathbf{n} = (0, 1, 0)$ (green), $\mathbf{n} = (0, 0, 1)$ (red) and $\mathbf{n} = (1, 0, 1)/\sqrt{2}$ (yellow). We can see that the quality of the simulation depends heavily on the initial state, but that by a suitable choice of γ_{RTN} we can obtain a fidelity which is above 0.999 throughout the evolution of the qubit.

the trajectory of the system repeatedly goes in and out the octahedron of separable states. The frequency of oscillations depends on ω_0 and is doubled if the two qubits are affected by a common environment. In the second regime (large γ, i.e. fast noise), the correlations decay to zero, with sudden death of entanglement and with oscillations. The time constant of the decay is roughly inversely proportional to γ, i.e. the decay is slower for very fast noise. In the common-environment case, we notice that the discord does not vanish in time. The reason is that the stable state of the dynamics does not lie in the set of states with zero discord (cf. Fig. 3.4b).

In order to compare quantitatively the dynamics of the system in the presence of the two kind of noise we introduce the fidelity complement

$$\tilde{\mathcal{F}}(t) = 1 - \mathcal{F}(\rho_{\text{OU}}(t), \rho_{\text{RTN}}(t)), \tag{3.55}$$

where $\mathcal{F}(\rho_{\text{OU}}(t), \rho_{\text{RTN}}(t))$ is the quantum fidelity, Eq. (2.56), between the state of a single qubit affected by RTN and the state of a qubit affected by OU, assuming that the two kinds of noise have the same coupling and spectral width. When this quantity is zero, the two states are identical. In Fig. 3.6a we show the fidelity complement as a function of of time. We can see that $\tilde{\mathcal{F}}(t)$ is not vanishing when the two noises have the same autocorrelation time. However, upon changing γ, we can reduce its value of three orders of magnitude.

Notice that there is an initial regime in which the fidelity complement increases and a second regime in which it vanishes, as the system tends to its asymptotic maximally

mixed state, and hence there is a global maximum of the fidelity complement, $\max[\tilde{\mathcal{F}}(t)]$, which depends on γ_{RTN}. This maximum can be used as a figure of merit of how good the simulation of Gaussian noise is. In the right panel, we show that $\max[\tilde{\mathcal{F}}(t)]$ can be driven very close to zero by a suitable choice of the parameter γ. It should be noticed, however, that the optimal value of the parameter does depend on the frequency of the qubit, on the parameters of the OU noise and also on the initial state of the qubit, as it is apparent upon looking at Fig. 3.6b.

We thus conclude that the effects of non-Gaussian noise on qubits cannot be trivially mapped to that of Gaussian noise and vice versa, as that would require that the optimal value of the parameter be independent of the initial state of the qubit(s). This means that the spectrum alone is not enough to characterize the effect of the noise on the qubit systems. On the other hand, the effect of the two noises is qualitatively similar and the dynamics under the effect of one kind of noise may be quantitatively *simulated* with high (quantum) fidelity with the other kind of noise by suitably tuning the parameters.

3.4 Non-Markovianity of the dynamical map

In this section we discuss the quantum non-Markovianity of the dynamics of qubit systems interacting with classical noise. We start by reviewing the results for the longitudinal noise case, then we evaluate numerically the BLP and RHP measures introduced in Subsection 2.3.1 in the transverse noise case [93].

Longitudinal noise The quantum map originating from the interaction with a classical noise is reported in Eq. (3.14). From Subsection 2.3.1, we recall that the BLP measure of non-Markovianity involves an optimization over all possible pairs of initial states (cf. Eq. (2.98)), and that for single qubits, it is known that the states of the optimal pair are pure and orthogonal. For a pure dephasing map, the optimal pair is easily found [8, 101]. The trace distance between an arbitrary pair of states affected by the map of Eq. (3.14) is

$$D(t) = \sqrt{a^2 + |b|^2 G(t)^2}, \tag{3.56}$$

where $a = \rho_{11}^{(1)} - \rho_{11}^{(2)}$ and $b = \rho_{12}^{(1)} - \rho_{12}^{(2)}$. The time derivative of Eq. (3.56) is

$$D'(t) = \frac{|b|^2 G(t)}{\sqrt{a^2 + |b|^2 G(t)^2}} G'(t). \tag{3.57}$$

In order to obtain the BLP measure, we have to maximize Eq. (3.57). It is easy to find that $a = 0$ and $|b| = 1$, i.e. the optimal pair is made by antipodal states on the equator of the Bloch sphere. For these states the trace distance becomes $D(t) = |G(t)|$.

It is then immediate to see that Gaussian noise will always induce a Markovian dynamics of the qubit: the function $G_{\text{GN}}(t)$ is a monotonically decreasing function, because $\beta(t)$ is a monotonically increasing function of time (cf. Eq. (1.19). On the other hand, with RTN it can be seen immediately by looking at the definition of $G_{\text{RTN}}(t)$ in Eq. (3.16) that the map is Markovian in the regime of fast noise, i.e. when $\gamma > 2\nu$ and $G_{\text{RTN}}(t)$ features hyperbolic functions, while it is non-Markovian in the other regime (slow noise), where the function contains oscillating functions [102].

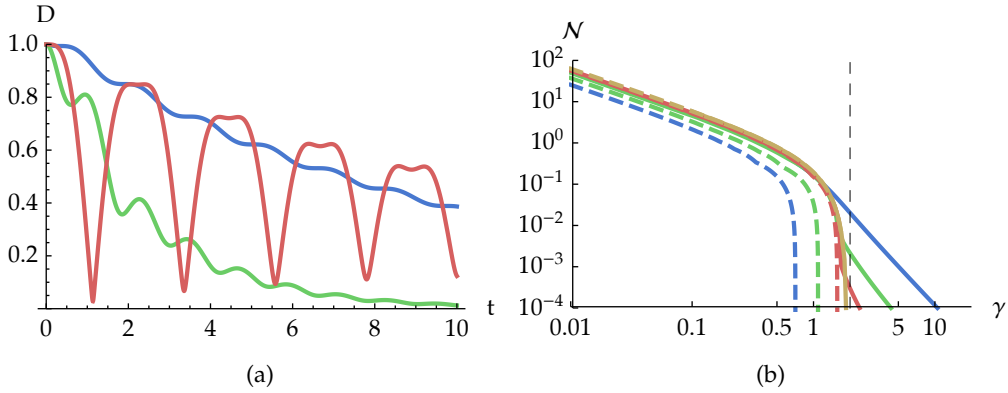

Figure 3.7: (a) Trace distance D between the pairs of states that maximize $\mathcal{N}_{\text{BLP}}$ as a function of time for $\omega_0 = 1$ and $\nu = 1$, with $\gamma = 0.1$ (dotted green), $\gamma = 1$ (dashed orange), $\gamma = 10$ (solid blue). We see that the trace distance oscillates in time: in the intervals in which it increases the map is not divisible. The oscillations get smaller for higher γ: they are barely noticeable in the plot for $\gamma = 10$. (b) Log-log plot of the non-Markovianity measures $\mathcal{N}_{\text{BLP}}$ (solid) and $\mathcal{N}_{\text{RHP}}$ (dashed) as functions of the spectral width γ for a qubit subjected to RTN noise, for $\nu = 1$ and $\omega_0 = 1$ (blue), $\omega_0 = (2\sqrt{2})^{-1}$ (green), $\omega_0 = 0.1$ (red) and $\omega_0 = 0.01$ (yellow). The two measures decrease monotonically for increasing γ. There is a threshold value for γ (that depends on ω_0) above which the RHP measure is zero. The BLP measure, instead, is always non-zero and vanishes for $\gamma \to \infty$, i.e. when $K(t - t') \sim \delta(t - t')$. For small γ, both measures are proportional to $1/\gamma$. For small ω_0 (yellow line), we recover the results obtained for the dephasing, with both measures vanishing at $\gamma = 2$ (vertical dashed line).

Transverse noise In the case of transverse noise, the situation is more complicated because the optimal pair of states can't be determined analytically. Even if with RTN the solution of the dynamics is analytical, the mathematical expressions are more complicated than in the dephasing case. In the following, we evaluate the trace-distance-based BLP measure and the entanglement-based RHP measure for the single-qubit map with RTN noise. A study of the non-Markovianity functions with Gaussian noise is complicated by the fact that the dynamics must be simulated numerically.

For the BLP measure, our numerical results show that the pair of optimal states lies on the equator of the Bloch sphere (i.e. $n_z = 0$), independently on the parameters of the noise. A numerical optimization over the azimuth angle is still in order for computing the measure. The optimal angle depends on the two parameters γ and ω_0 and the dependence is sometimes not smooth. We found that the two measures are in disagreement, i.e. the BLP measure is always non-zero and is vanishing for $\gamma \to \infty$, whereas the RHP measure is vanishing for γ greater than a certain threshold. This is shown in Fig. 3.7b, where the two measures are calculated for a range of values of the switching rate γ and for different values of ω_0. From Fig. 3.7b we can see that both measures depend approximately on $1/\gamma$ at small γ. While the RHP measure suddenly goes to zero for γ above a certain threshold value, which depends on ω_0, the BLP measure only vanishes asymptotically. The BLP measure appears to be independent of ω_0 at small values of γ.

We recall that the two measures only pose a sufficient condition for the dynamical

Stochastic process	Longitudinal noise	Transverse noise
OU	Markovian	Non-Markovian
RTN	Markovian (fast) Non-Markovian (slow)	Non-Markovian

Table 3.1: (Non-)Markovianity of the quantum map for the longitudinal and transverse noise case, with OU noise and RTN.

map to be non-divisible, i.e. non-Markovian. The RHP measure fails to capture the non-Markovian behavior of the map because the trajectory quickly enters the set of separable states, as one can see from Fig. 3.4a. On the other hand, the BLP measure is always non-zero, meaning that the map is non-Markovian, unless we let $\omega_0 \to 0$. In this case we approach the dephasing limit, and the BLP and RHP measures coincide and vanish at $\gamma = 2$ [102]. This is shown in Fig. 3.7b for $\omega_0 = 0.01$ (green line). For non-vanishing ω_0, the non-Markovianity measure vanishes for high values of γ, as one can expect, since the stochastic process that models the noise tends to the Markovian limit, i.e. when $K(t - t') \sim \delta(t - t')$.

In Fig. 3.7a we show, for different values of γ, the behavior of the trace distance $D(t)$ between the pair of states that maximize the integral in the definition of $\mathcal{N}_{\text{BLP}}$, see Eq. (2.98). For smaller values of γ, the oscillations are very pronounced. When γ increases, the oscillations become less appreciable ($D(t)$ seems to decay monotonically in the plot for $\gamma = 10$, solid blue line), but derivative of the trace distance is always positive in the first oscillation.

Given the need to optimize over an angle, and the need to reach very long evolution times in order to capture all the oscillations in the trace distance, evaluating the BLP measure for the Gaussian noise is practically unfeasible. However, initial pairs of states can be found for which the trace distance does not decay monotonically for a very wide range of values of γ, and this allows us to conclude that also Gaussian transverse noise with a Lorentzian spectrum induces non-Markovian quantum dynamics on qubits.

Summary

- We described in detail the dynamics of one- and two-qubit systems affected by classical noise, either Gaussian or non-Gaussian (random telegraph noise).
- We discussed the analytical solution for the longitudinal noise, that induces pure dephasing, and revised some results involving the dynamics of quantum correlations.
- We discussed the transfer matrix method, that allows for an analytical solution also for transverse noise in the case of RTN.
- We analyzed in detail the effects of the transverse noise on a two-qubit system: we showed the trajectories in the Bell state tetrahedron, the dynamics of quantum

correlations and we discussed the non-Markovianity of the map.

- We compared the RTN with numerical simulations of Ornstein-Uhlenbeck Gaussian noise, showing that the power spectral density is not enough to characterize the effect of the noise when it has a non-Gaussian statistics. At the same time, we showed that the effects of RTN can be simulated by OU noise and viceversa by suitably tuning their correlation time.
- We studied the non-Markovianity of the map, with analytical results for the longitudinal case and numerical results for the transverse case for both Gaussian and non-Gaussian noise. The results are summarized in Table 3.1.

Chapter 4

Optical simulation of a classical single-qubit noise channel

In this chapter we discuss an experimental implementation of an optical quantum simulator of the evolution of a qubit interacting with a classical environment. The experiment has been carried out at the Quantum Technology Lab of the Università degli Studi di Milano. Quantum simulators are among the most intriguing and sought implementations of quantum technologies, as they may be exploited to mimic the dynamics of other quantum systems that are less accessible or less controllable [103] and thus study their properties. The inherent parallel structure of quantum simulators make them suitable to solve problems that are intractable on conventional supercomputers, like the simulation of the dynamics of a many-particle system. In particular, optical quantum simulators have attracted much interest as they may be used at room temperature, thanks to the fact that photons do not interact with each other [104–107]. Moreover, photons may propagate in free space or in waveguides, and thus may be used to simulate complex structures with long range interaction.

The quantum simulator that we are going to describe exploits the spectral components of a single-photon state to perform the parallel sum of about one hundred complex numbers. In order to demonstrate the operation of our QS, we run the simulation of two different single-qubit dephasing channels, arising from the interaction of the quantum system with an external classical noise, as described in Section 3.2. We already presented analytical solutions for this model when the noise is Gaussian or RTN, and we will test the experimental setup by comparing it to these known results. The simulator can however implement other kinds of noise for which an analytical solution does not exist even for longitudinal noise, such as $1/f$ noise, that is relevant for solid-state and superconducting quantum systems [19, 20, and refs. therein].

We rewrite the Hamiltonian (3.11) here for convenience:

$$H(t) = H_0 + H_{\text{int}} = \omega_0 \sigma_z + B(t)\sigma_z. \tag{4.1}$$

Here $B(t)$ is the stochastic process describing the classical noise. The environment induces decoherence, but does not exchange energy with the system.

As we said above, the qubit is encoded in the polarization of the photon. We take the horizontal and vertical polarization as the computational basis of the qubit, i.e. $|0\rangle \equiv |H\rangle$ and $|1\rangle \equiv |V\rangle$. We recall that, if the system is initially prepared in the state ρ_0, the state at time t is given by the CPT map $\rho(t) = \mathcal{E}_t(\rho_0) = \mathbb{E}\left[U(t)\rho_0 U^\dagger(t)\right]$, where

$U(t) = \exp[-i\int_0^t H(\tau)d\tau]$ is the evolution operator and as usual we take the expectation value over the realizations of the stochastic process $B(t)$.

4.1 Description of the experimental setup

As discussed in Subsection 3.3.3, in order to obtain the state of the system at any time t, we should compute the average of a sufficiently large collection of independent realizations (sample paths) of the stochastic process $B(t)$. Each sample path is a real scalar function $\phi_r(t) = \int_0^t B_r(\tau)d\tau$, that corresponds to the phase shift induced by a particular realization $B_r(\tau)$, with r running on the sample index. In particular, the qubit state at time $\bar{t}$ will be given by

$$\rho(\bar{t}) = \frac{1}{n}\sum_{r=1}^{n} |\psi_r(\bar{t})\rangle \langle\psi_r(\bar{t})| , \tag{4.2}$$

where $|\psi_r(\bar{t})\rangle = (1/\sqrt{2})\left(e^{-2i\phi_r(\bar{t})}|H\rangle + |V\rangle\right)$.

In Fig. 4.1 we show a schematic diagram of the experimental apparatus. The frequency-entangled two-photon state is generated by parametric down-conversion (PDC) with a diode pump laser at 405.5 nm by using a BBO crystal (1 mm thick). The two photons are then collected by two fiber couplers and sent respectively into a single-spatial-mode and polarization-preserving fiber (SMF) and a multimode fiber (MMF). When the idler photon enters the coupler, it travels entirely through the fiber towards the single photon detector (D2). Conversely, the signal photon, after the short single-mode fiber, enters a 4F system [108], i.e. it propagates in the air, through few optical devices: the gratings G1 and G2 (1714 lines/mm) and the lenses L1 and L2 ($f = 500$ mm).

Between the two lenses are a half-wave plate (H1), that we use for the input state preparation, a spatial light modulator (SLM) that is used simulate the dynamics, and a tomographic apparatus (T) [109, 110] to reconstruct the output state. At the end of the 4F system the signal photon is coupled to a multimode fiber and reaches the single photon detector (D1). Finally an electronic device measures the coincidence counts (CC) and sends them to the computer (PC). The tomographic apparatus (T) is composed of a quarter-wave plate, an half-wave plate and a polarizer. The SLM is a 1D liquid crystal mask (640 pixels, 100 µm/pixel) and is placed on the Fourier plane between the two lenses L1 and L2 of the 4F system (see Fig. 4.1).

In the Fourier plane the spectral components of the signal photon are linearly dispersed (1.82 nm/mm), so that the photon hits as many pixels as possible. The SLM is controlled by the computer (PC) and is used to introduce a different phase $\phi_r(\bar{t})$ for each pixel. When the photon hits the second grating, the various spectral components are recombined, thus effectively averaging over the various realizations, as in Eq. (4.2).

In order to obtain the correct value for the average, the spectrum of the PDC must be as flat as possible, so that the intensity at each pixel is balanced. In order to measure the PDC spectrum we used a 2 mm slit on the Fourier plane of the 4F system. We calibrated the slit using a graduated reference on the Fourier plane and for each slit position (and therefore for each wavelength) we recorded coincidence counts from the detectors. In Fig. 4.2a we show the measured PDC spectrum. We observe that it is selected by the

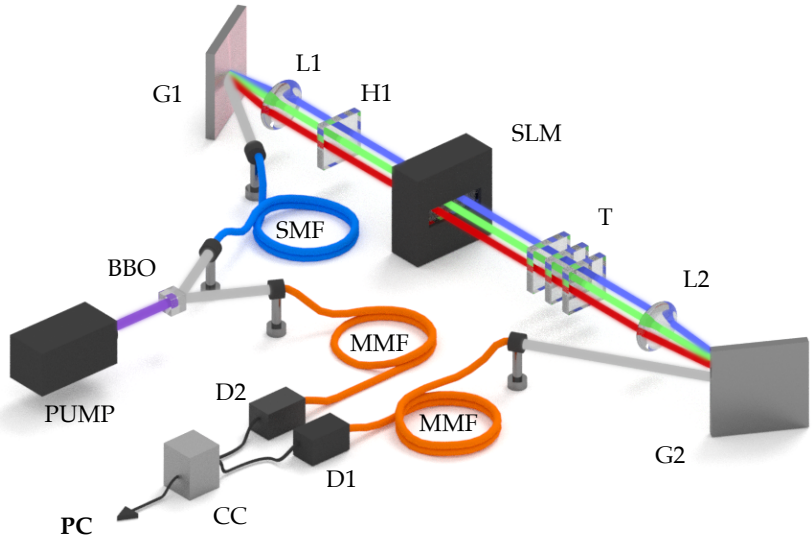

Figure 4.1: Schematic diagram the experimental setup. Two entangled photons are generated via PDC with a pump laser diode at 405.5 nm and a beta barium borate (BBO) nonlinear crystal. The idler photon is collected by a multi-mode fiber (MMF, orange) coupled to a single-photon detector (D2). The signal photon is collected by a single-spatial-mode and polarization preserving fiber (SMF, blue) and enters the 4F system, composed of the two gratings G1 and G2, two lenses L1 and L2, the half-wave plate H1, the spatial light modulator (SLM) and a tomographic apparatus T, composed of a quarter-wave plate, a half-wave plate and a polarizer. The photon then hits the single-photon detector D1. The coincidence counts (CC) are then sent to a PC for data processing.

limited width of the H1 plate mount, in such a way that the intensity of the spectral components impinging on the SLM is almost constant. For this reason we are limited to use $n = 100$ out of the 640 pixel available on the SLM.

Let us give a more formal description of the quantum dynamics in the experimental setup. When leaving the BBO, the signal (s) and idler (i) photon are in the pure state [111]

$$\int d\omega f(\omega) |H\rangle_s \otimes |\omega\rangle_s \otimes |H\rangle_i \otimes |-\omega\rangle_i , \tag{4.3}$$

ω is the spectral shift with respect to the PDC central component $\omega_0 = \omega_p/2$, ω_p being the pump laser frequency. Notice that the polarization and frequency degrees of freedom of the two photons are independent of each other and thus, upon the detection of an idler photon, the conditional state of the signal photon, i.e.

the partial trace over the idler degrees of freedom, is given by the mixed state

$$\rho_{SE} = \rho_S \otimes \rho_E = |H\rangle \langle H| \otimes \int d\omega |f(\omega)|^2 |\omega\rangle \langle \omega| . \tag{4.4}$$

The initial system-environment state is therefore factorized, and this warrants the existence of the reduced dynamics [112]. The polarization of the idler photon encodes a qubit, while the spectral/spatial degrees of freedom may be considered as the environment.

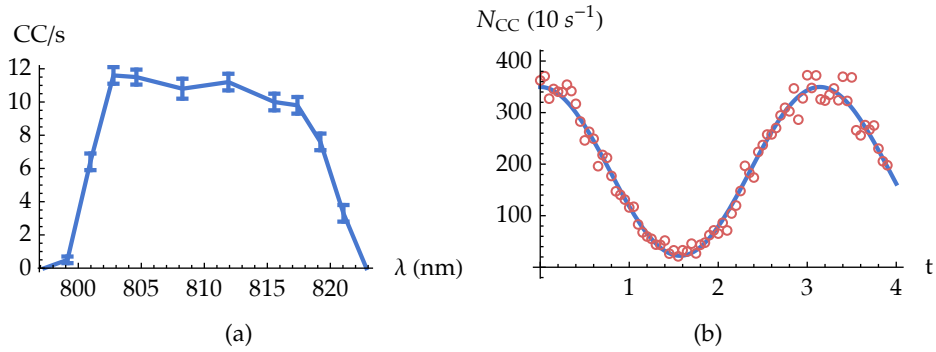

Figure 4.2: (a) The measured spectrum of the PDC. We can see that it is almost flat in the region $802 \div 817\,\text{nm}$. (b) Coincidence counts $N_{cc}(\bar{t})$ in the case of RTN with $\gamma = 0$, the blue line is the fit with the function $N_{cc} = N(1 + p\cos(2\bar{t}))$.

The grating G1 (see Fig. 4.1) disperses linearly the photon spectral components ω, and the lens L1 focuses them on the Fourier plane of the 4F system where the SLM is placed. Each spectral component ω is characterized by a Gaussian spatial profile (60 µm FWHM) centered in the spatial coordinate x. We have a linear relation $\omega = \alpha x$, where $\alpha = 1.82\,\text{nm/mm}$. In order to emphasize that the spectral components are spatially dispersed we use the notation $|x\rangle = |\omega(x)\rangle$.

The half-wave plate H1 rotates the initially horizontal polarization of the signal photon, turning the state of the system to

$$|\psi_S(0)\rangle = (1/\sqrt{2})\,(|H\rangle + |V\rangle)\,. \tag{4.5}$$

We consider $|\psi_S(0)\rangle$ as the initial state for the simulated dynamics.

By labelling with $|\eta_r\rangle$ the r-th pixel of the SLM, we have $|x\rangle = \sum_r \eta_r(x)\,|\eta_r\rangle$, where $|\eta_r(x)|^2$ is the probability that the component x passes through the r-th pixel. In this notation the identity $\mathbb{I} = \sum_r |\eta_r\rangle\langle\eta_r|$ expresses the fact that all detectable components pass through the pixels.

The initial state of the environment then reads $\rho_E = \sum_{r,s} A_{rs}\,|\eta_r\rangle\langle\eta_s|$, where the matrix

$$A_{rs} = \int dx |f(x)|^2 \eta_r(x)\eta_s^*(x) \tag{4.6}$$

is positive definite with trace equal to one. The SLM imprints a pixel-dependent phase on the horizontal polarization component, which we denote by $e^{-2i\phi_r(\bar{t})}$. The unitary interaction operator can therefore be written in the form

$$U(\bar{t}) = \exp\left[-2iP_H \otimes \sum_r \phi_r(\bar{t})P_r\right], \tag{4.7}$$

where $P_H = |H\rangle\langle H|$ and $P_r = |\eta_r\rangle\langle\eta_r|$. As a result,

$$U(\bar{t})\,|H\rangle \otimes |\eta_r\rangle = e^{-2i\phi_r(\bar{t})}\,|H\rangle \otimes |\eta_r\rangle \tag{4.8}$$

$$U(\bar{t})\,|V\rangle \otimes |\eta_r\rangle = |V\rangle \otimes |\eta_r\rangle\,. \tag{4.9}$$

Upon tracing out the environment, from $\rho_{SE}(\bar{t}) = U(\bar{t})\left(\rho_S(0)\otimes\rho_E\right)U(\bar{t})^\dagger$ we obtain the state of the qubit

$$\rho_S(\bar{t}) = \frac{1}{2}\sum_r A_{rr}\begin{pmatrix} 1 & e^{-2i\phi_r(\bar{t})} \\ e^{2i\phi_r(\bar{t})} & 1 \end{pmatrix}, \tag{4.10}$$

so that only the coherences are affected by the dynamics. In our case for the diagonal elements we have $A_{rr} = 1/n$ ($n = 100$) because the selected PDC spectrum is basically rectangular. In general, one can apply corrections to the matrix A_{rr} to compensate inhomogeneities in the spectrum.

In the limit of a large number of noise realizations r, if the phase ϕ_r is sampled according to the probability distribution of the stochastic process $B(t)$, Eq. (4.10) will be equivalent to the dephasing map of Eq. (3.14).

The discussion above starts from the assumption that the initial state is the pure state in Eq. (4.5). However, due to the imperfections of the experimental apparatus, in each realization the state is not exactly pure but rather of the form $\rho_{S,\text{exp}} = p\rho_S + (1-p)\rho_{\text{mix}}$, where $\rho_{\text{mix}} = \frac{1}{2}|H\rangle\langle H| + \frac{1}{2}|V\rangle\langle V|$ is the maximally mixed state, so that the relevant quantity to be measured is

$$\langle H|\rho_{S,\text{exp}}(\bar{t})|V\rangle = \frac{1}{2}\,p\left\langle e^{-2i\phi_r(\bar{t})}\right\rangle_n. \tag{4.11}$$

In our setup, the average over the realizations of the noise is performed by (coherently) collecting the different spatial components $|\omega\rangle$ through the lens L2 and the grating G2 into a multimode fiber. The state reconstruction is performed by the tomographic apparatus T placed between the SLM and the lens L2.

The realizations of the stochastic processes are generated according to the numerical recipes presented in Section 1.4. For the RTN, the initial values $B_r(0)$ are chosen randomly between ±1 with equal probability. For the OU process, gor each realization (i.e. for each pixel) we impose the initial condition $X_r(0) = 0$.

The time step for the simulation is $\delta\bar{t} = 0.001$ (in arbitrary units). The acquisition is done at the time steps $\bar{t}_i = i \times 50\delta$ by assigning the phases $\phi_r(\bar{t}_i) = \int_0^{\bar{t}_i} B_r(\tau)d\tau$ to the pixels and then by reconstructing the state with the tomographic method by performing four projective measurements [109, 110, 113], namely onto the states $|H\rangle$, $|V\rangle$, the circular polarization $|R\rangle = (|H\rangle - i|V\rangle)/\sqrt{2}$ and the $-\pi/4$ diagonal polarization $|DD\rangle = (|H\rangle - |V\rangle)/\sqrt{2}$.

In order to obtain the parameter p, we acquire a reference measure using the RTN with $\gamma = 0$ (that is, static noise). In this case we have $\langle e^{-2i\phi_r(\bar{t})}\rangle = \cos(2\bar{t})$. In Fig. 4.2b we can see the coincidence counts vs. the simulation time $\bar{t}$ in the case of the RTN with $\gamma = 0$. From the fit (blue solid line) with the function $N_{\text{cc}}(\bar{t}) = N(1 + p\,\cos(2\bar{t}))$ we find $p = 0.88 \pm 0.02$ as well as $N = 186 \pm 2$. Thus, in the general case we can write: $\left\langle e^{-2i\phi_r(\bar{t})}\right\rangle_n = (N_{\text{cc}}(\bar{t}) - N)/p$.

Notice that $\langle e^{-2i\phi(\bar{t})}\rangle$ is real-valued because the two considered stochastic processes have zero mean (and indeed, from the tomographic measures, we find that the imaginary part of $\langle e^{-2i\phi_r(\bar{t})}\rangle_n$ is zero within the experimental uncertainty). Thus, in order

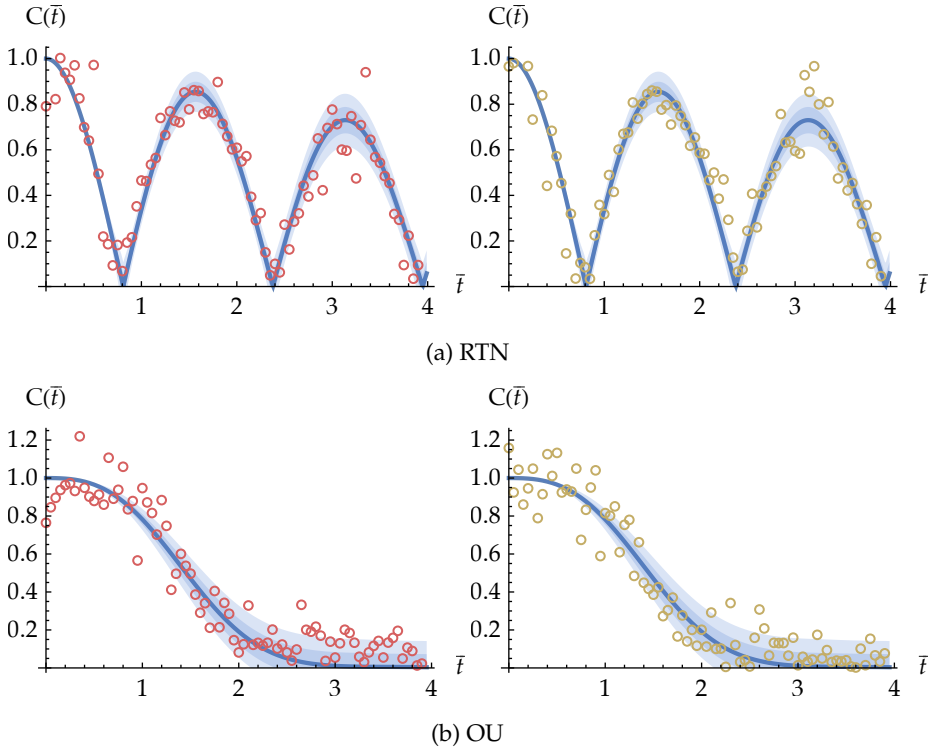

Figure 4.3: Dynamics of the off-diagonal element of $\rho_S(\bar{t})$, $C(t) = |\langle e^{-2i\phi_r(\bar{t})}\rangle_n|$, for RTN (a) and OU (b) with $\gamma = 0.1$. In the left panels the red circles represent the data obtained with tomographic reconstruction of $\rho_{S,\text{exp}}(\bar{t})$. In the right panels, the yellow circles are obtained with a single projection onto the state $|+\rangle$. The blue line is the analytic solution of the model. The shades represent intervals of 1σ (darker) and 2σ (lighter) around the analytic solution, where σ is the standard deviation of paths obtained with 100 realizations of the stochastic process. Note that the noise for small $\bar{t}$ is due to the Poissonian fluctuations on the coincidence counts.

to estimate the trace distance we can perform just one projective measure on the state $|+\rangle = (1/\sqrt{2})(|H\rangle + |V\rangle)$, since we have $\langle +|\,\rho_{S,\text{exp}}\,|+\rangle = \frac{1}{2}\left(1 + p\,\text{Re}\left\langle e^{-2i\phi_r(\bar{t})}\right\rangle_n\right)$.

4.2 Results for Gaussian noise and RTN

In this section we show the results obtained by running simulations of two dephasing channels driven by Ornstein-Uhlenbeck noise or non-Gaussian random telegraph noise, that we already discussed analytically in Section 3.2. Apart from providing a convenient description of many realistic environments, dephasing channels also permit a simple assessment of the non-Markovian character of the reduced dynamics of the system, as we discussed in detail in Chapter 3. Recall that the BLP measure of non-Markovianity for a dephasing channel is based on revivals of the trace distance $D(t) = \frac{1}{2}\|\rho_1(t) - \rho_2(t)\|_1$, between two different initial states. We have seen in Section 3.4 that for a dephasing

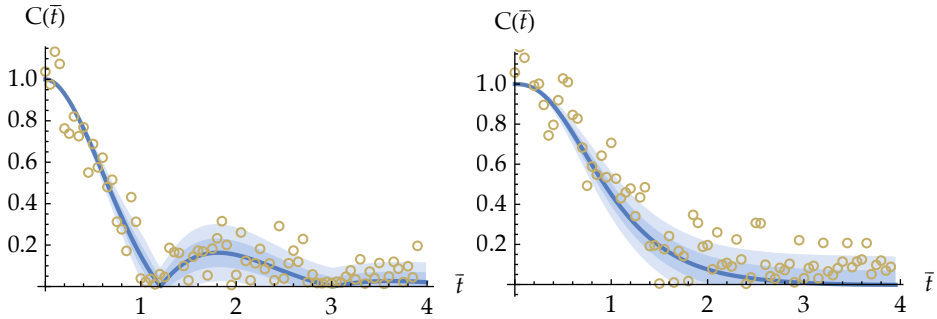

(a) RTN (b) OU

Figure 4.4: Dynamics of the off-diagonal element of $\rho_S(\bar{t})$, $C(t) = |\langle e^{-2i\phi_r(\bar{t})}\rangle_n|$, vs $\bar{t}$ evaluated by the method of the projection onto the state $|+\rangle$ in the case $\gamma = 1$ for RTN (a) and OU (a) stochastic process. The blue line is the analytic solution and the blue shades represent intervals of 1σ (darker) and 2σ (lighter) around the analytical solution, where σ is the standard deviation of paths obtained with 100 realizations of the stochastic process.

channel the non-Markovianity of the map can be assessed by looking at the coherences of the density operator $\rho(t)$, starting from the initial state (4.5).

In Fig. 4.3 we plot the experimental results in the case of the RTN and OU process respectively. In both cases we have $\gamma = 0.1$ in arbitrary units. We note the presence of strong revivals in the RTN case, according to the non-Markovian character of the dynamics. In the OU case the off-diagonal element of $\rho_S(\bar{t})$ decays monotonically, as expected for a Markovian dynamics. We use an acquisition time of 10 s for each measure of coincidence counts. For a pure dephasing dynamics one has:

$$D(t) = |\langle e^{-2i\phi(t)}\rangle| \approx |\langle e^{-2i\phi_r(\bar{t})}\rangle_n| \equiv C(t)\,. \tag{4.12}$$

Notice that in order to obtain the non-Markovianity from the revivals of the trace distance we need the factor $\frac{1}{2}p$. Indeed, while the trace distance is in principle bounded by one, here we estimate its value from the reduced dynamics of the off-diagonal matrix elements, whose actual value depends on the purity of the system state. The latter is known only in average and it is also affected by experimental uncertainty due to the Poissonian statistics of photon counting. The quantity $C(t)$ is shown in Fig. 4.3 as a function of $\bar{t}$ for RTN (a) and OU noise (b), both with $\gamma = 0.1$.

In Fig. 4.3 we can also see the comparison between the tomographic method (red circles, on the left) and the method based on the projection on the state $|+\rangle$ (yellow circles, on the right) in the case of the RTN and of the OU. We note that the two methods indeed give compatible results.

In Fig. 4.4 we can see the results obtained by the projection method on the state $|+\rangle$ and with $\gamma = 1$, for both RTN (a) and OU process (b). Note the decrease of non-Markovianity of the RTN dynamics compared to the case with $\gamma = 0.1$. In turn, the non-Markovianity vanishes when $\gamma \geq 2$ [102]. In the case of the OU noise, the dynamics remains Markovian as expected.

Summary

- We have discussed a proof-of-principle implementation of a photonic quantum simulator of single-qubit dephasing induced by the interaction with classical noise. The qubit is encoded in the polarization of a single photon, and the dynamics is obtained by dispersing the spectral components of the photon with a grating, then applying a different phase shift (sampled according to the probability density of the classical noise) to each component through a spatial light modulator and then coherently collecting the components with a lens and another grating. The advantage of this simulator is that the different realizations of the dynamics are evaluated in parallel, thanks to the quantum nature of the photon.

- As a first example, we have run simulations of dephasing channels driven either by Gaussian (Ornstein-Uhlenbeck) or non-Gaussian (random telegraph) stochastic processes, and compared them to the known analytical solutions. In particular, we have addressed the non-Markovianity of the quantum map.

- Upon increasing the number of pixels in the spatial light modulator one may increase the number of realizations and perform more accurate simulations of noisy channels and complex classical environments. Moreover, the setup can be modified to address the dynamics of two-qubit systems or other forms of noise, such as transverse noise.

Chapter 5

Entangled probes for the spectral properties of Gaussian environments

In Chapter 3 we have discussed the dynamics of one- and two-qubit systems under the influence of classical noise. We have seen that the effect of the environment is that of destroying the quantum coherence and correlations of the system, thus posing a serious limitation to the implementation of quantum technologies. We have also seen that a non-Markovian dynamics allows for at least partial revivals of quantum correlations: this effect can be exploited in the engineering of the environment in order to preserve the quantum resources needed for information processing tasks.

From a somehow complementary standpoint, the very sensitivity of quantum systems to external influence can provide an effective tool to characterize unknown parameters of a given environment [114–117]. Using *quantum probes*, as opposed to classical ones, usually macroscopic and more intrusive, can be very useful in those situations where a high precision is needed, but at the same time the sample must be preserved from unwanted interactions with the probe. For example, the analysis of biological processes requires low-intensity radiation to avoid burning the sample. Indeed, characterizing the noise induced by an external complex system is of great relevance in many areas of nanotechnology, as well as in monitoring biological or chemical processes [118–121]. Besides, it represents a crucial step to design robust quantum protocols resilient to noise [122–127].

The proper framework to address characterization by quantum probes [128, 129], and to design the best working conditions, is given by quantum estimation theory, which we reviewed in Section 2.4. It provides analytical tools to optimize the three building blocks of an estimation strategy (depicted in Fig. 5.1):

1. preparation of the probe system in a suitably optimized state,

2. controlled interaction of the probe with the system for an optimal amount of time t

3. measurement of an optimal observable on the probe.

We recall that the ultimate precision for any unbiased estimator $\hat{\gamma}$ of a certain parameter γ is bounded by the quantum Cramèr-Rao (CR) theorem, stating that $\mathrm{Var}(\hat{\gamma}) \geq [MH(\gamma)]^{-1}$, where M is the number of measurements and $H(\gamma)$ is the quantum Fisher

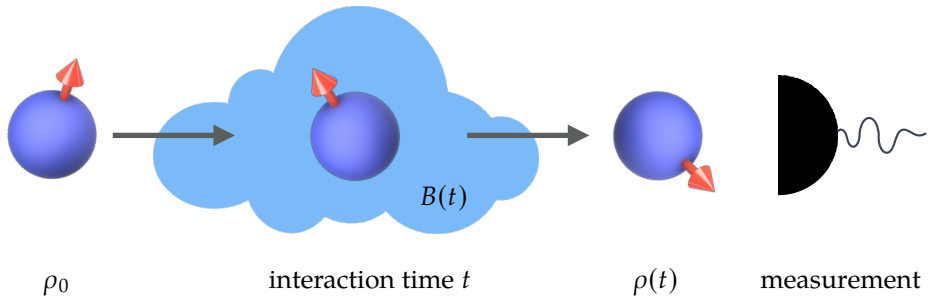

Figure 5.1: A typical quantum probing scheme consists of the preparation of the quantum probe in a certain initial state ρ_0, the interaction of the probe with the environment for a controlled amount of time t, which will leave the probe in the state $\rho(t)$, and finally a quantum measurement on the probe. The experiment is repeated M times to collect classical data over which one can apply a Bayesian estimation procedure. To maximize the precision in the estimation, the experimentalist can thus tune, compatibly with physical and technological limitations of the setup: the initial state ρ_0, the interaction time t and the quantum measurement.

information (QFI), i.e. the superior of the Fisher information over all possible quantum measurements described by positive operator-valued measures (POVMs).

The quantum nature of the probing system allows us to exploit its non-classical resources to allow for better precision in the estimation of the parameter. In particular, quantum features such as entanglement, or squeezing for continuous variable systems, have been proven to be resources that allow to overcome classical limits to precision. In ideal conditions, while for a classical system the variance of the estimator is proportional to M^{-1}, it has been shown that with quantum probes the variance becomes proportional to M^{-2} (this is known as *Heisenberg scaling*) [3, 41, 43, 130]. This quantum-enhanced scaling, however, can be lost in presence of noise [42, 114, 131].

Recently, single-qubit quantum probes have been proposed for the characterization of noise by monitoring decoherence and dephasing induced by the environment under investigation, in particular when the latter can be described in terms of classical stochastic processes [45, 46, 132–134].

In this chapter we review the results obtained in [45] for single-qubit probes used to estimate the spectral properties of a classical environmental noise, and then we present an original contribution [135] that extends this analysis to entangled qubits, and show how they greatly improve the characterization of a broad class of environmental noises compared to any sequential strategy involving single qubit preparation [136–138]. In particular, we show how to improve estimation of the correlation time (i.e. the spectral width) of classical Gaussian noise, described by the Ornstein-Uhlenbeck process (cf. Subsection 1.2.2).

5.1 Single-qubit probe

Let us start by considering a single qubit interacting with a classical longitudinal noise, that induces dephasing. The Hamiltonian is the one that we studied in Section 3.2:

$$H(t) = \omega_0 \sigma_z + \nu B(t) \sigma_z, \tag{5.1}$$

where ω_0 is the energy of the qubit and $B(t)$ is a realization of the stochastic process that describes the noise. The autocorrelation function of $B(t)$ depends on an unknown parameter γ, that we want to estimate. As a paradigmatic example we consider here a zero-mean Ornstein-Uhlenbeck process, where the parameter γ is the spectral width, i.e. the inverse of the correlation time of the process. It is worth noticing that a similar analysis may be carried out for other Gaussian processes, e.g. processes with power-law or Gaussian autocorrelation functions, and that results are qualitatively the same, independently on the choice of the autocorrelation function. We discuss the estimation of the spectral with of RTN in Subsection 5.2.4.

We already know from our previous discussion that, if the qubit is initially prepared in a state described by the density operator $\rho(0)$, the density operator at the time t will be $\rho(t)$ with $\rho_{kk}(t) = \rho_{kk}(0)$, $k = 1, 2$ and

$$\rho_{12}(t) = e^{-2\left[i\omega_0 t + \beta_\gamma(t)\right]} \rho_{12}(0)\,, \tag{5.2}$$

where

$$\beta_\gamma(t) = \nu^2 \int_0^t \int_0^t ds\, dw\, K(s, w) = \frac{\nu^2}{\gamma}(e^{-\gamma t} + \gamma t - 1). \tag{5.3}$$

To find the optimal single-qubit preparation, we can limit our discussion to pure states. This is due to the convexity of the QFI [137]. We then consider the general qubit state

$$|\theta, \phi\rangle = \cos\frac{\theta}{2}\,|0\rangle + e^{i\varphi} \sin\frac{\theta}{2}\,|1\rangle\,. \tag{5.4}$$

Its evolved state under the effect of the noise is (see Section 3.2)

$$\rho_{\theta,\phi}(t) = \frac{1}{2}\begin{pmatrix} 1 + \cos\theta & G_\gamma(t) e^{i\varphi} \sin\theta \\ G_\gamma(t) e^{-i\varphi} \sin\theta & 1 - \cos\theta \end{pmatrix}, \tag{5.5}$$

where we omitted the dependence of $G_\gamma(t)$ on ν, and we moved to the rotating reference frame to get rid of the phase $\omega_0 t$.

To evaluate the QFI, we use Eq. (2.116). We need the eigenvalues and eigenvectors of $\rho_{\theta,\phi}(t)$. The eigenvalues are

$$\rho_\pm = \frac{1}{2}\left(1 \pm \sqrt{G_\gamma^2(t) \sin^2\theta + \cos^2\theta}\right). \tag{5.6}$$

The eigenvectors have rather cumbersome expressions. The overlaps that appear in Eq. (2.116), however, are simple enough to be reported:

$$\langle \rho_\pm | \partial_\gamma \rho_\pm \rangle \quad = 0 \tag{5.7}$$

$$|\,\langle \rho_\pm | \partial_\gamma \rho_\mp \rangle\,|^2 = \frac{\left|\cot\theta\, \partial_\gamma G_\gamma(t)\right|^2}{4\left(G_\gamma(t)^2 + \cot^2\theta\right)^2}. \tag{5.8}$$

Notice that the eigenvalues and the overlaps do not depend on the angle φ. We can finally evaluate the QFI

$$\begin{aligned} Q(\gamma) &= \frac{\sin^2\theta G_\gamma(t)^2 \partial_\gamma G_\gamma(t)^2}{\left(1-G_\gamma(t)^2\right)\left(\sin^2\theta G(\gamma,t)^2+\cos^2\theta\right)} + \frac{\sin^2\theta\cos^2\theta\partial_\gamma G_\gamma(t)^2}{\left(\sin^2\theta G_\gamma(t)^2+\cos^2\theta\right)} \\ &= \sin^2\theta \frac{\partial_\gamma G_\gamma(t)^2}{1-G_\gamma(t)^2}. \end{aligned} \tag{5.9}$$

From Eq. (5.9) it is immediately seen that the optimal states are those with $\theta = \pi/2$. We can choose without loss of generality the state $|+\rangle = \frac{1}{\sqrt{2}}(|0\rangle + |1\rangle)$.

To conclude the discussion of the single-qubit probe, we show that a projection measurement onto the eigenstates of the system is optimal, i.e. it saturates the QFI (5.9). With the state $|+\rangle$, the eigenvalues and eigenvectors of $\rho_\gamma(t)$ read

$$\rho_\pm = \frac{1}{2}\left(1 \pm G_\gamma(t)\right) \tag{5.10}$$

$$|\rho_\pm\rangle = \frac{1}{\sqrt{2}}(|0\rangle \pm |1\rangle). \tag{5.11}$$

The FI for the projection measurement is

$$F(\gamma) = \frac{(\partial_\gamma \rho_+)^2}{\rho_+} + \frac{(\partial_\gamma \rho_-)^2}{\rho_-} = \frac{\partial_\gamma G_\gamma(t)^2}{1-G_\gamma(t)^2}. \tag{5.12}$$

If the noise is Gaussian, as we will consider in the following discussion, $G_\gamma(t) = \exp(-2\beta_\gamma(t))$ and hence

$$Q(\gamma) = \frac{4\partial_\gamma \beta_\gamma(t)}{e^{4\beta_\gamma(t)}-1}. \tag{5.13}$$

5.2 Multi-qubit probes

We now move to the multi-qubit probing scenario. We assume that we can prepare an N-qubit system in an arbitrary initial state. In particular, we consider probes prepared both in the separable state $|+\rangle^{\otimes N}$ and in the generalized GHZ entangled state

$$|\Psi_{\text{N}}\rangle = (|0\rangle^{\otimes N} + |1\rangle^{\otimes N})/\sqrt{2}\,. \tag{5.14}$$

We will also address non-perfect preparation of the probe states in Section 5.4.

We also consider two possible scenarios: in the first, each qubits interacts with an independent realization of the noise. This means that the overall Hamiltonian is

$$H^{(\text{N})}(t) = H_1(t)\otimes\mathbb{I}^{\otimes N-1} + \mathbb{I}\otimes H_2(t)\otimes\mathbb{I}^{\otimes N-2} + \ldots, \tag{5.15}$$

where the realizations of the stochastic processes in each Hamiltonian $H_i(t)$ are uncorrelated, and the expected value of Eq. (2) must be calculated over all possible realizations of $B_1(t),\ldots,B_N(t)$. In the second scenario all the qubits interact with a common environment, i.e. with the same realization of the noise. Then $H_1(t) = \ldots = H_N(t) = H(t)$ and the expected value in Eq. (2) must be calculated over all possible realizations of a single stochastic process $B(t)$.

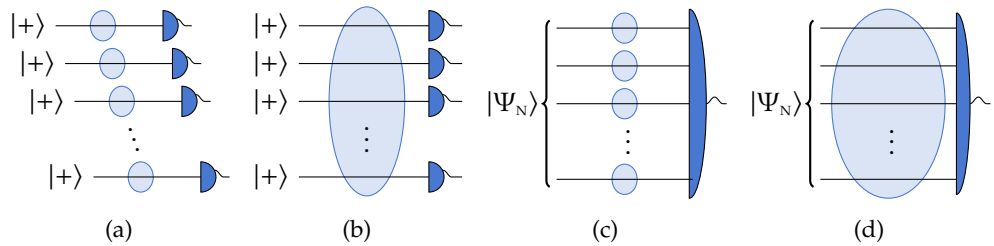

Figure 5.2: Schematic diagrams of possible characterization techniques. In (a) the system is prepared in the separable state $|+\rangle^{\otimes N}$, and each of the probes interact with an independent environment. In (b) the system is prepared in the separable state $|+\rangle^{\otimes N}$, but the probes interact with a common environment. In (c) and (d) the N-qubit system is prepared in the GHZ state $|\Psi_{\rm N}\rangle = (|0\rangle^{\otimes N} + |1\rangle^{\otimes N})/\sqrt{2}$ and the qubits interact with separate and common environments, respectively. At the output, a collective measurement is performed on the qubits.

5.2.1 Comparison of probing schemes

We now discuss the results involving all the four possible probing schemes, that are visually summarized in Fig. 5.2.

Separable probes, independent enviroments Since each qubit interacts with an independent realization of the noise, this scheme amounts to N repetitions of the measurement of a single qubit probe prepared in the optimal state $|+\rangle$ and thus, thanks to the additivity of the QFI,

$$Q_{\rm N}^{\rm SEP,IE}(\gamma,t) = \frac{4N}{e^{4\beta_\gamma(t)}-1}[\partial_\gamma \beta_\gamma(t)]^2. \tag{5.16}$$

Separable probes, common environment In this scenario the dynamics of each qubits is not independent and we need to determine the dynamics of the whole N-qubit state. The QFI has a readable analytical form only for two qubits

$$Q_2^{\rm SEP,CE}(\gamma,t) = \frac{32\left\{e^{8\beta_\gamma(t)}[\sinh 4\beta_\gamma(t)+1]+1\right\}}{3e^{16\beta_\gamma(t)}-2e^{8\beta_\gamma(t)}+1}[\partial_\gamma \beta_\gamma(t)]^2. \tag{5.17}$$

One can easily see that

$$\forall t,\gamma \qquad Q_2^{\rm SEP,IE}(\gamma,t) > Q_2^{\rm SEP,CE}(\gamma,t), \tag{5.18}$$

since $\beta_\gamma(t) > 0$.

We can check numerically that the maximal QFI for separable probes interacting with a common environment is always lower than the maximal QFI for separable probes interacting with independent environments for fixed γ also for $N = 3$ and $N = 4$. The results, shown in Fig. 5.3a, indicate that the ratio between $Q_n^{\rm SEP,CE}(\gamma,t)$ and $Q_2^{\rm SEP,IE}(\gamma,t)$ decreases with N.

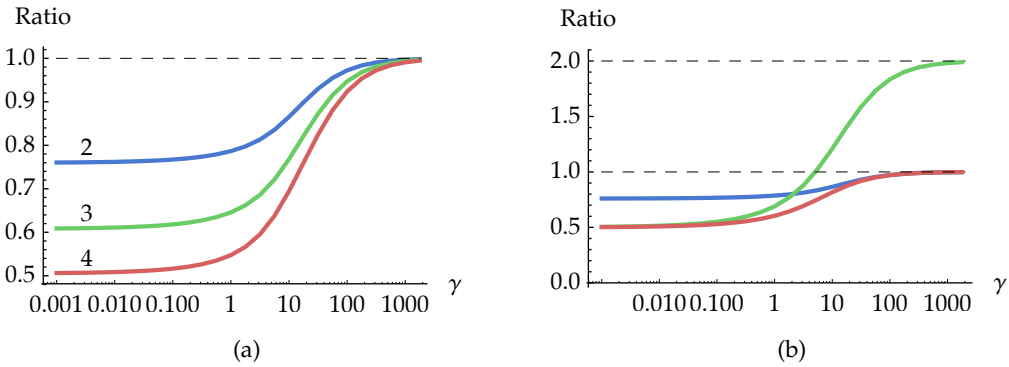

Figure 5.3: (a) Ratio between $Q_N^{SEP,CE}(\gamma, t)$ and $Q_N^{SEP,IE}(\gamma, t)$ for different values of N. The ratio is always lower than one and gets lower as N increases. In the limit $\gamma \gg 1$ the ratio reaches one. (b)Ratios between $Q_{2,max}^{SEP,CE}(\gamma)$ (blue), $Q_{2,max}^{GHZ,CE}(\gamma)$ (green), $Q_{2,max}^{GHZ,IE}(\gamma)$ (red) and $Q_{2,max}^{SEP,IE}(\gamma)$ as functions of γ. We can see that the GHZ probes interacting with common environment achieves a higher maximal QFI than the other schemes. Similar plots can be produced for $N > 2$.

GHZ probes, independent environments In this case, the expected value of the density operator at time t over al possible realizations of the stochastic processes $B_1(t), \ldots, B_N(t)$, in the rotating reference frame, is

$$\begin{aligned}\rho_{GHZ}(t) =& \frac{1}{2}(|0\ldots0\rangle\langle 0\ldots0| + |1\ldots1\rangle\langle 1\ldots1|) + \\ & \frac{1}{2}e^{-2N\beta_\gamma(t)}(|0\ldots0\rangle\langle 1\ldots1| + \text{h.c.})\end{aligned} \tag{5.19}$$

and we find, for the QFI,

$$Q_N^{GHZ,IE}(\gamma, t) = \frac{4N^2}{e^{4N\beta_\gamma(t)} - 1}[\partial_\gamma \beta_\gamma(t)]^2. \tag{5.20}$$

It is quite easy to prove that $Q_N^{GHZ,IE}(\gamma, t) < Q_N^{SEP,IE}(\gamma, t)$ for all t and γ and so we don't have an improvement in the estimation of γ with a probe in the GHZ state if each qubit interacts with an independent realization of the environment.

GHZ probes, common environment If the entangled qubits of the probe are affected by the same realization of the noise, one finds that the expected value of $\rho(t)$ is

$$\begin{aligned}\rho_{GHZ}(t) =& \frac{1}{2}(|0\ldots0\rangle\langle 0\ldots0| + |1\ldots1\rangle\langle 1\ldots1|) + \\ & \frac{1}{2}(e^{-2N^2\beta_\gamma(t)}|0\ldots0\rangle\langle 1\ldots1| + \text{h.c.})\end{aligned} \tag{5.21}$$

and obtains, with the same steps used for the single-qubit probe, the following expression for the QFI:

$$Q_N^{GHZ,CE}(\gamma, t) = \frac{4N^4}{e^{4N^2\beta(t,\gamma)} - 1}[\partial_\gamma \beta_\gamma(t)]^2. \tag{5.22}$$

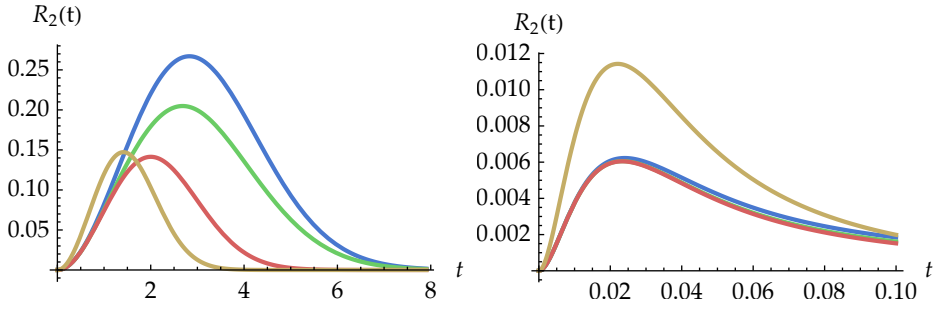

(a) $\gamma = 0.1$ (b) $\gamma = 10$

Figure 5.4: Two-qubit quantum signal-to-noise ratio $R_2(\gamma, t) = \gamma^2 Q_2(\gamma, t)$ as a function of time for two values of the spectral width γ of the noise. The blue line shows $R_2^{\text{SEP,IE}}(\gamma, t)$, the green line $R_2^{\text{SEP,CE}}(\gamma, t)$, the red line $R_2^{\text{GHZ,IE}}(\gamma, t)$ and the yellow line $R_2^{\text{GHZ,CE}}(\gamma, t)$. From the left panel we can see that $Q_2^{\text{SEP,IE}}(\gamma, t) > Q_2^{\text{SEP,CE}}(\gamma, t)$ for all t and that $Q_{2,\text{max}}^{\text{GHZ,CE}}(0.1) > Q_{2,\text{max}}^{\text{GHZ,IE}}(0.1)$. From panel (b) we can see that for high values of γ the GHZ probes interacting with a common environment outperforms the other schemes.

5.2.2 Entangled probes vs separable probes

We have derived the analytical expressions for the four possible measurement schemes. Figure 5.4 shows the dependence on time of the QFI in the four cases and for a small and large value of γ. We can see that the QFI as a function of time has exactly one maximum. Indeed, notice that $\beta_\gamma(t)$ is a monotonically increasing function of t with $\beta_\gamma(0) = 0$ (see Eq. (5.3)). Moreover, the exponential at the denominator guarantees that $Q_{\text{N}}^x(t)$ vanishes at large t. Since also $\partial_\gamma \beta_\gamma(t)$ is a monotonically increasing function of time, we can conclude that $Q_{\text{N}}^x(t)$ has exactly oen maximum. The position of the maximum, however, can not be found analytically, as the equations involved are transcendental. We will have to make do with numerical optimization, which is nevertheless very reliable, given the smooth behavior of $Q_{\text{N}}^x(t)$.

In Fig. 5.3b we show the ratios between the maximal values of the QFI for the various cases and the maximal value for the QFI for separable probes interacting with an independent environment, as functions of γ, in the two-qubit case. We can see that the the ratios are below one except for the scheme involving a joint measurement on entalged probes that interact with a common environment, when γ is above a certain treshold value. Analogous plots may be produced for $N > 2$.

We can now focus on the best schemes for separable probes and for entangled probes. For the former, we have seen that the optimal scheme is to let the probes interact with independent realizations of the environment. The QFI, is

$$Q_{\text{N}}^{\text{SEP}}(\gamma, t) = \frac{4N}{e^{4\beta_\gamma(t)} - 1} [\partial_\gamma \beta_\gamma(t)]^2. \tag{5.23}$$

If the probe is prepared in a GHZ state, the optimal scheme involves the interaction with a common environment, i.e. with the same realization of the noise. The QFI in this

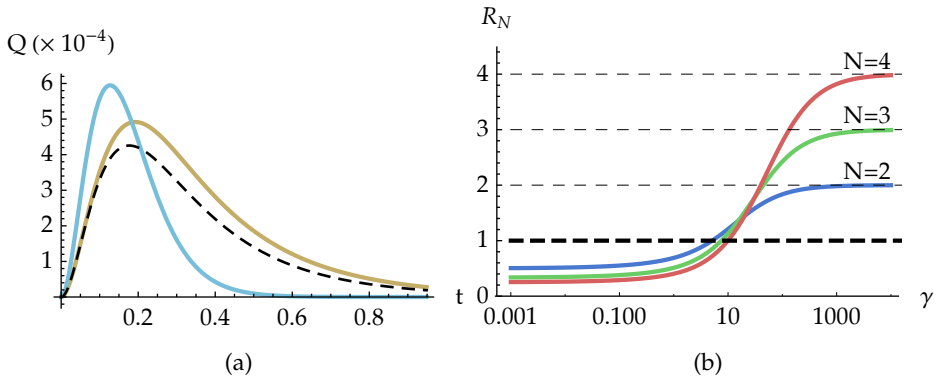

Figure 5.5: (a) the QFI $\mathcal{Q}_2^{\text{SEP}}(t)$ (orange) and $\mathcal{Q}_2^{\text{GHZ}}(t)$ (purple) as function of time for $\gamma = 10$. We also show for comparison the (smaller) QFI for separable two-qubit probes in a common environment (dashed black) . (b) the QFI ratio R_{N} as a function of γ (log scale) for $N = 2$ (blue), $N = 3$ (green) and $N = 4$ (red). For small values of γ, the ratio is below one (black dashed line), and tends asymptotically to $1/N$: in this regime it is more convenient to employ separable states than maximally entangled states. The ratio increases monotonically with γ and exceeds one at a threshold value $\gamma_0(N)$, which depends on N. For asymptotically large γ, the use of N-qubit GHZ states is N times better than the use of N qubits in a separable state.

case reads

$$\mathcal{Q}_{\mathrm{N}}^{\text{GHZ}}(\gamma, t) = \frac{4N^4}{e^{4N^2\beta(t,\gamma)} - 1}[\partial_\gamma \beta_\gamma(t)]^2 \,. \tag{5.24}$$

We have seen that in both cases the QFI has one maximum value, reached when the probe interacts with the environment for an optimal time which we label $\tilde{t}_{\text{SEP}}$ and $\tilde{t}_{\text{GHZ}}$ respectively for the two schemes.

Figure 5.6a shows how the optimal time depends on γ for the two measurement schemes. In the separable case (black line), obviously, the optimal time does not depend on the number of probes. The larger γ, the smaller the optimal time. This is sensible, as greater values of γ mean shorter autocorrelation time and thus faster noise. There are two regimes where the dependence on γ follows two different power laws.

In situations where we can control the interaction time between the probe and the environment, it will be most convenient to set it to the optimal time. Thus, a fair comparison between separable and entangled probes naturally involves the maximal QFI of the two cases. We therefore introduce the QFI ratio as $\mathrm{R}_{\mathrm{N}}(\gamma) = \mathcal{Q}_{\mathrm{N,max}}^{\text{GHZ}}(\gamma)/\mathcal{Q}_{\mathrm{N,max}}^{\text{SEP}}(\gamma)$, and analyze its behavior as a function of γ and N. When $\mathrm{R}_{\mathrm{N}}(\gamma) > 1$, the use of a N-qubit GHZ state improves estimation compared to the use of N uncorrelated probes, e.g. in a sequential strategy.

Figure 5.5 illustrates the main results: the ratio $\mathrm{R}_{\mathrm{N}}(\gamma)$ is larger than one for $\gamma > \gamma_0(N)$, where $\gamma_0(N)$ is a threshold value that depends on N. Moreover, $\mathrm{R}_{\mathrm{N}}(\gamma) \to N$ for $\gamma \gg \gamma_0(N)$. This result is enhanced by the fact that, upon substituting $\tilde{\gamma} = \gamma/\nu$ and $\tau = \tilde{\gamma}t$, we may show that the quantum signal-to-noise ratio (QSNR), Eq. (2.117), does not depend on ν. This means that, if one is able to control the coupling between the probe and the system, one can always tune ν to achieve a situation where $\mathrm{R}_{\mathrm{N}}(\tilde{\gamma}) > 1$. All the figures are

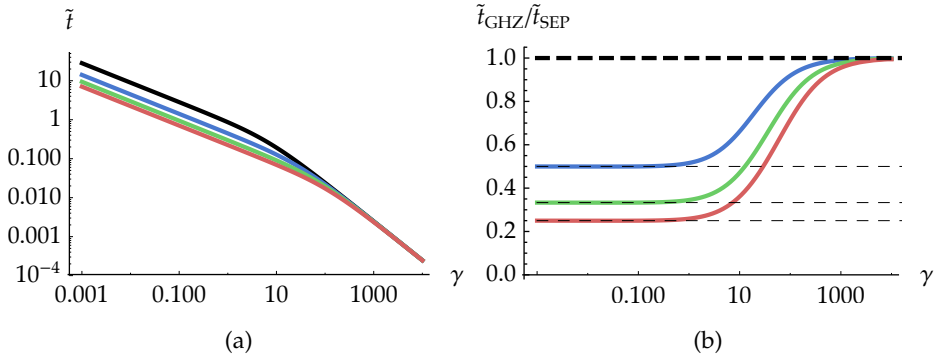

Figure 5.6: (a) Log-log plot of the optimal interaction time $\tilde{t}$ as a function of γ for separable probes (black), and for an entangled probe with $N = 2$ (blue), $N = 3$ (green) and $N = 4$ (red) qubits. (b) The ratio between the optimal time for the GHZ state, $\tilde{t}_{GHZ}$ and for the separable state $\tilde{t}_{SEP}$, for the same values of N.

obtained by setting $\nu = 1$.

5.2.3 Optimality of the GHZ state

Now a question arises: Is the GHZ state $|\Psi_N\rangle$ the optimal one? Are there other states, entangled or not, that allow for even better precision? We are unable to give an analytical answer to this question, because the evaluation of the QFI requires the diagonalization of the density operator. What we know is that that the maximum for the QFI is achieved for an initial pure state, because of the convexity of the QFI [137].

We have thus generated a large number ($n = 10^6$) of random initial pure states, for different values of γ and for $N = 2, 3, 4$. To sample the Hilbert space uniformly, we generated random unitary matrices distributed uniformly according to the Haar measure (the algorithm can be found in Ref. [139]). For each random state, the maximal QFI, $Q_N^{RND}(\gamma)$, resulting from the interaction with a common environment has been numerically evaluated Eq. (2.113). This value is then used to evaluate the corresponding QFI ratio $Q_N^{RND}(\gamma)/Q_N^{SEP}(\gamma)$, and to compare the estimation precision to the precision achievable using N independent qubits interacting with separate environments. Our results indicate that, for $\gamma \gtrsim \gamma_0$, that is, in the region where entanglement is convenient, the GHZ state is indeed the optimal one, thus showing that entanglement is a resource for the estimation of the spectral width of Gaussian noise.

Below the threshold, the GHZ state interacting with a common environment is no longer optimal, and the optimal strategy involves separable probes interacting with independent environments. For completeness, we look for the optimal state in a common environment and find numerically that the extremal state lies in the same family of states that had been identified in [42] as optimal probes to improve frequency estimation. The

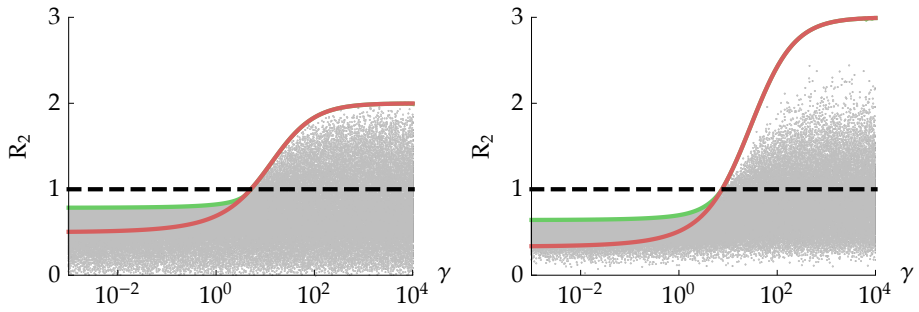

Figure 5.7: The curves in the logplots show the QFI ratio R_2 (top) and R_3 (bottom) as a function of γ for the GHZ state (red) and the optimal state of N qubits in a common environment (green). The two curves coincide above the threshold $\gamma_0(N)$. We also show the QFI ratio for 10^5 randomly generated states (light blue points), uniformly distributed according to the Haar measure.

states of this family, for N qubits, have the form

$$|\Phi_N\rangle = \sum_{k=0}^{\lfloor \frac{1}{2}N \rfloor} a_k \, |k\rangle \, , \tag{5.25}$$

where a_k are normalized real coefficients, $\lfloor \cdot \rfloor$ denotes the integer part, and $|k\rangle$ is an equally weighted superposition of all N-qubit states with a number k or a number $N-k$ of excitations. For instance, for $N = 4$ and $k = 2$,

$$|k\rangle = |0011\rangle + |0101\rangle + |0110\rangle + |1001\rangle + |1010\rangle + |1100\rangle \, . \tag{5.26}$$

The GHZ state belongs to this family with $a_0 = 1/\sqrt{2}$ and all other coefficients set to 0.

Figure 5.7 illustrates our numerical results obtained for two and three qubits. The plots show the QFI ratios R_2 (left) and R_3 (right). The red line is the ratio for the GHZ state, the 10^5 light-blue points correspond to the QFI ratio of randomly generated states and the green line is found by optimizing the QFI over the coefficients a_k of $|\Phi_N\rangle$. We can see that from $\gamma \gtrsim \gamma_0(N)$ the red and green curves coincide, i.e. GHZ states are extremal. We also notice that for $\gamma \gtrsim \gamma_0(N)$ a significant fraction of dots lies above the $r = 1$ dashed line, but the dots are sparse around the solid blue line, meaning that the GHZ state allows for a remarkable gain in the estimation of larger values of γ, compared to the average state in the Hilbert space.

It is worth to emphasize that optimal precision, i.e. the QFI of Eq. (5.24) may be achieved upon implementing a simple rank-2 measurement. Indeed, $\mathcal{Q}_N^{\mathrm{GHZ}}(\gamma)$ corresponds to the Fisher information of a projective measurement $\Pi_\pm = |p_\pm\rangle\langle p_\pm|$ onto the two eigenvectors corresponding to the nonzero eigenvalues of the evolved density operator, which are, respectively

$$p_\pm = \frac{1}{2}\left(1 \pm e^{-2N^2\lambda^2\beta_\gamma(t)}\right) \tag{5.27}$$

$$|p_\pm\rangle = \frac{1}{\sqrt{2}}(e^{-i\omega_0\sigma_z})^{\otimes N}\left(|0\rangle^{\otimes N} \pm |1\rangle^{\otimes N}\right). \tag{5.28}$$

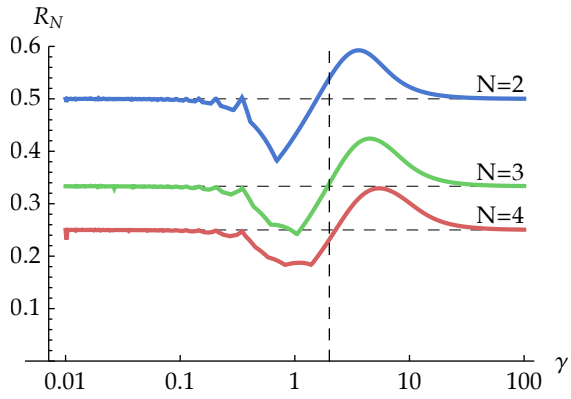

Figure 5.8: The QFI ratio R_N as a function of γ (log scale) for $N = 2$ (blue), $N = 3$ (green) and $N = 4$ (red). For small and large values of γ, the ratio tends asymptotically to $1/N$. There are a minimum and a maximum (well below 1) when γ is around the threshold value $\gamma = 2$ (dashed black line) where the single-qubit dynamics goes from the slow noise regime to the fast noise regime.

5.2.4 Probing the spectral width of RTN noise

As we have seen in Chapter 3, the RTN has the same spectrum as the OU noise, yet its non-Gaussian statistics gives rise to a completely different dynamics. This is particularly evident in the dephasing case, where the RTN has two qualitatively different regimes. In the slow-noise regime, the dynamics is highly non-Markovian and the dephasing function G_{RTN} is oscillating, whereas in the fast-noise regime, it is monotonically decaying.

This in turn reflects to the estimation of the switching rate γ (or equivalently, of the spectral width). The QFI has an oscillating behavior for slow noise, with multiple local maxima, and a single maximum for fast noise. Single-qubit probes for the random telegraph noise have been addressed in Ref. [46], where the optimal interaction time is found for both regimes.

Quite surprisingly, the use of entangled probes in this case is detrimental in both the slow noise case and in the fast noise case. In particular, for asymptotically large values of γ, where the GHZ state is optimal for the Gaussian noise, we find that $R_N = N^{-1}$. We have the same scaling also for asymptotically small values of γ, as can be seen from Fig. 5.8.

The evaluation of the ratio for small values of γ is complicated because of the highly oscillating behavior, but by inspection we see that the ratio is well below one.

5.3 Bayesian estimation

As we saw in Section 2.4, the Cramér-Rao theorem sets a *lower bound* to the precision of any unbiased estimator, and a question arises on how to suitably process data coming from the above rank-2 measurement in order to *saturate* the bound. Bayesian estimators are known to saturate the CR bound for asymptotically large numbers of measurements: in order to assess quantitatively the performance of Bayesian estimation, and to give an

example of its use in quantum metrology, we show the results of simulated experiments on the probing system.

In particular, we simulate the outcomes $\Omega_M = \{x_1, \dots, x_M\}$ of the measurement $\Pi_\pm$ performed at the optimal time $\tilde{t}_{\text{GHZ}}$ by randomly choosing a result according to the probabilities of Eq. (5.27) and we build a Bayesian estimator $\hat{\gamma}$ as the mean value of the *a posteriori distribution* $p(\gamma|\Omega_M)$, starting from a flat prior distribution, i.e. with the *a priori* assumption that the value of γ is equally probable in some interval $[\gamma_a, \gamma_b]$, that is

$$p(\gamma) = \begin{cases} (\gamma_b - \gamma_a)^{-1} & \gamma \in [\gamma_a, \gamma_b] \\ 0 & \text{elsewhere.} \end{cases} \tag{5.29}$$

The two possible outcomes for the projective measurement $\Pi_\pm$ have the probabilities in Eq. (5.27). Thus the probability that the set Ω_M contains m times the outcome Π_+ is given by the binomial distribution

$$p_+(m|\gamma) = p_+(\gamma)^m (1 - p_+(\gamma))^{M-m}. \tag{5.30}$$

Given the set of outcomes $\Omega_M(\overline{m})$, where $\overline{m}$ is the number of measurements that read Π_+, the conditional probability for γ, Eq. (2.120), is

$$p(\gamma|\Omega_M(\overline{m})) = \frac{p_+(\overline{m}|\gamma)(\gamma_b - \gamma_a)^{-1}}{\int_{\gamma_a}^{\gamma_b} p_+(\overline{m}|\gamma)(\gamma_b - \gamma_a)^{-1} d\gamma} = \frac{p_+(\overline{m}|\gamma)}{\int_{\gamma_a}^{\gamma_b} p_+(\overline{m}|\gamma) d\gamma}. \tag{5.31}$$

With $p(\gamma|\Omega_M(\overline{m}))$, we evaluate the mean value and variance of the estimator $\hat{\gamma}$, using Eqs. (2.122) and (2.123).

To simulate the estimation procedure, we extract the random number $\overline{m}$ from the binomial distribution of Eq. (5.30), then we numerically evaluate the integral in Eq. (5.31). This last task is in general tricky, due to the fact that, especially in multiparameter estimation, the probability space can be very large and the *a posteriori* distribution $p_+(\overline{m}|\gamma)$ can be peaked around the expected value of γ. In these cases advanced numerical integration techniques such as Montecarlo sampling must be employed. In the problem at hand, however, simple numerical algorithms are sufficient.

An example is presented in Fig. 5.9, for $\gamma = 10$. We chose $\gamma_a = 0$ and $\gamma_b = 100$ as limits for the flat prior distribution, Eq. (5.29). In Fig. 5.9a we show the estimated value of γ as a function of the number M of measurements, for a single qubit (blue) and a four-qubit GHZ state (green). The error bars show the error $\sqrt{\sigma_\gamma^2}$. We can see that the precision improves with the number of measurements. This is even more apparent in Fig. 5.9b, where the relative error $\epsilon = \sqrt{\text{Var}(\hat{\gamma})}/\hat{\gamma}$ is shown as a function of the number of measurements. We see that with a relatively low number of measurements, of the order of thousands, the bound is saturated and the situation improves by increasing the number of qubits. The proposed scheme thus allows for an effective and achievable estimation of the parameter γ.

5.4 Robustness to noise in the initial state preparation

We have seen how the use of a GHZ state allows for great improvement of the precision of estimation of the spectral width of Gaussian noise. However, it is generally challenging

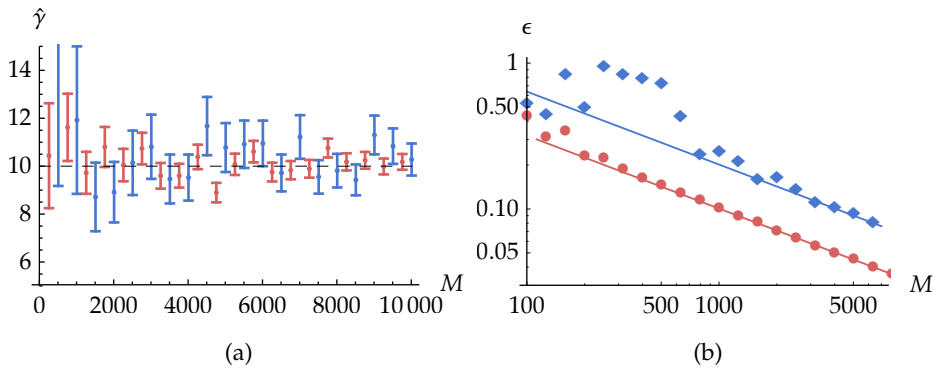

Figure 5.9: (a) Expected value and error from Bayesian estimation as functions of the number of measurements M, for a true value of $\gamma = 10$ (black line), for a single qubit (blue) and a 4-qubit GHZ state (red). Notice that the expected value converges to the true value and the error decreases when M increases. The GHZ state has smaller errors. Here $\gamma_{\max} = 100$. (b) Log-log plot of the relative error $\epsilon = \sqrt{\mathrm{Var}(\hat{\gamma})}/\hat{\gamma}$ of the Bayesian estimator as a function of the number of measurements, for $\gamma = 10$. The lines represent the CR bound for a single-qubit measurement (blue) and for a 4-qubit GHZ state (red). The diamonds (single qubit) and the dots (4 qubits) correspond to the performance of a Bayes estimator applied to simulated experiments. Bayes estimators saturate the CR bound when increasing the number of measurements and very good performances are achieved already for thousands of measurements. The plot also shows that estimation improves with the number of qubits since the CR bound is saturated with a lower number of measurement. Notice that some points are below the CR bound. This is due to the fact that the Bayesian estimator might not be unbiased for finite values of M.

to experimentally prepare the probes *exactly* in the GHZ state. Typically, the preparation involves some noise and the resulting state is not the pure target state. Let us now address the robustness of our scheme against two common models of noise in state preparation: depolarizing noise and dephasing noise.

A partially depolarized state is a mixture between the target state (in our case the GHZ state ρ_{GHZ}) and the maximally mixed state:

$$\rho_p = p\,\rho_{\mathrm{GHZ}} + (1-p)\mathbb{I}/2^N, \tag{5.32}$$

where $0 \leq p \leq 1$. The purity of the depolarized state, as a function of p, is

$$\mu(p) = \frac{1}{2^N}[1 + (2^N - 1)p^2] \tag{5.33}$$

The partially dephased state, on the other hand, is

$$\rho_\delta = \delta\rho_{\mathrm{GHZ}} + \frac{1}{2}(1-\delta)(|0\rangle^{\otimes N}\langle 0| + |1\rangle^{\otimes N}\langle 1|), \tag{5.34}$$

where $0 \leq \delta \leq 1$, with purity

$$\mu(\delta) = \frac{1}{2}\left(1 + \delta^2\right). \tag{5.35}$$

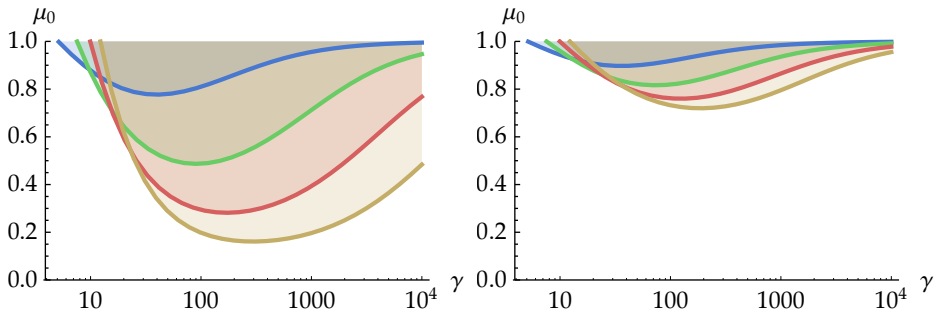

(a) Depolarizing noise (b) Dephasing noise

Figure 5.10: Threshold purity μ_0, as a function of the spectral width γ, above which the use of a depolarized (a) or a dephased GHZ state (b) is more effective than a set of uncorrelated qubits. In the shaded regions above the curve, an imperfect preparation of the GHZ state still allows it to outperform the sequential strategy. The lines correspond to a different number N of qubits: $N = 2$ (blue), $N = 3$ (green), $N = 4$ (red), $N = 5$ (yellow). The threshold μ_0 approaches 1 when $\gamma \to \gamma_0(N)$ and when $\gamma \to \infty$. There is an intermediate region where μ_0 decreases to a minimum, meaning that there is more tolerance in the initial preparation of the probe. When N increases, the minimum of μ_0 decreases and moves to larger values of γ.

In both cases, an analytic expression for the QFI may be found: we have

$$Q_{\mathrm{N}}^{p}(\gamma, t) = \frac{2^{N+2} N^4 \left[(2^N - 2)\, p + 2\right] p^2 [\partial_\gamma \beta_\gamma(t)]^2}{\left[(2^N - 2)\, p + 2\right]^2 e^{4N^2 \beta(t,\gamma)} - 4^N p^2} \tag{5.36}$$

$$Q_{\mathrm{N}}^{\delta}(\gamma, t) = \frac{4N^4 \delta^2}{e^{4N^2 \beta(t,\gamma)} - \delta^2} [\partial_\gamma \beta_\gamma(t)]^2 , \tag{5.37}$$

which are obviously less than $Q_{\mathrm{N}}^{\mathrm{GHZ}}(\gamma)$, being ρ_p and ρ_δ mixed states, but may be still larger than $Q_{\mathrm{N}}^{\mathrm{SEP}}(\gamma)$. Indeed, Figure 5.10 shows that for each value of γ above $\gamma_0(N)$ there is a threshold value for the purity, above which the use of a depolarized or dephased GHZ state still leads to an improvement over the use of N uncorrelated probes. The threshold purity μ_0 is close to one for $\gamma \simeq \gamma_0(N)$ and for $\gamma \gg \gamma_0(N)$, whereas it shows a minimum in the intermediate region, thus allowing for a certain tolerance in the preparation of the initial state of the probe. Besides, this minimum value of the threshold gets lower when increasing the number of qubits. Notice that the threshold purity is much higher for dephasing noise. This is not surprising: the estimation scheme is based on the dephasing induced by the environment, thus the probe is more sensible to an initial dephasing due to noise in the preparation stage.

Summary

- We have discussed the use of qubit systems as probes for the spectral properties of a complex environment described by means of a classical field. The high sensitivity of quantum systems to the effects of environment and their small size may allow

the design of extremely precise and noninvasive probing schemes. The scheme exploits time-dependent sensitivity of quantum systems to decoherence and does not require dynamical control on the probes.

- We have shown that the use of entangled qubits as quantum probes outperforms the sequential use of single-qubit probes. In particular, we have shown that a joint measurement on entangled probes improves the estimation of the correlation time for a broad class of environmental noises when the noise is faster than a threshold value.
- The latter result is enhanced by the fact that, upon controlling the coupling between the probe and the system, the threshold value can be reduced arbitrarily.
- The proposed measurement scheme achieves the Cramér-Rao bound for a relatively low number of measurements, upon employing a Bayesian estimator.
- We have discussed the robustness of the scheme against imperfect preparation of the initial entangled state, by analyzing in detail the depolarizing and dephasing noise. We have showed that there exists a threshold purity of the initial state above which the probing schemes outperforms the sequential scheme.

Chapter 6

Continuous-time quantum walks with spatially correlated classical noise

We now move from few-qubit systems to quantum walks. They are the generalization of classical random walks and describe the propagation of a particle on a discrete graph. As we briefly discussed in the Introduction, their quantum nature, with quantum superposition and interference, allows for features and properties that are not seen in random walks and that are relevant in quantum information processes.

When talking about quantum walks, there are two classes of dynamics that we can consider:

- Discrete-time quantum walks (DTQW): The evolution of the system is step-wise. At each step, a measurement is made on a quantum system, usually referred to as *quantum coin*, and then an operation is applied to the walker, conditional to the outcome of the measurement. The Hilbert space of the walker is thus the tensor product of the space of the position of the particle and of the space of the coin [140].

- Continuous-time quantum walks (CTQW): In this case the evolution is continuous in time and the walker is described by a Hamiltonian, acting on the position space of the particle. The dynamics is thus obtained by solving the Schrödinger equation [141].

Here we focus on continuous-time quantum walks. They have been subject of intense studies, both theoretical and experimental, as they have proven useful for several applications, ranging from universal quantum computation [48], to search algorithms [47, 142], quantum transport [49, 143], quantum state transfer [144] and energy transport in biological systems [145].

Given their relevance in applications, a realistic description of the dynamics of quantum walkers should take into account those sources of noise and imperfections that might jeopardize the discrete lattice on which the CTQW occurs. While the effects of both disorder and dynamical fluctuations have been analyzed in the recent past [53, 54, 146–149], the consequences of spatially-correlated noise on the dynamics of the walker are still unexplored territory.

In this chapter, we present an extension [150] to the model used in Ref. [53], where a quantum walker over a one-dimensional lattice is considered. The hopping amplitudes are assumed to fluctuate in time as a random telegraph noise (RTN) inducing dynamical

percolation, which results in a stochastic time-dependent Hamiltonian. We take a step further and introduce random spatial correlations.

The spatial correlations are introduced as follows: if two adjacent hopping links are subject to spatially correlated fluctuations, then they are affected by the same RTN time evolution. This will lead to the formation of percolation domains within which the tunneling amplitudes evolve according to the same stochastic noise. On a global scale, because of these spatial correlations, the hopping fluctuations will be synchronized domain-wise. Overall, this is perhaps the simplest type of space dependency that one may introduce to the one-dimensional CTQW, as it does not interfere with the local time-dependent part of the noise. The two sources of noise correlations may indeed be treated independently. At the same time, the model allows us to describe the formation of spatial domains and to address percolation effect.

In turn, the motivation for introducing this extra ingredient is two-fold. First, if we aim at a more realistic description of any experimental implementation of a CTQW, we need to take into account sources of noise. This is especially important when studying transport properties in disordered systems in which localization, let it be Anderson or many-body [151–153], represents an obvious obstacle. A renewed interest in this field has spurred deep investigations in highly-engineered experimental setups, such as cold atoms in optical lattices [154, 155], in which complex noise might be efficiently implemented [156].

The second aspect concerns the question of whether the introduction of spatially correlated noise might result in improving certain dynamical features, such as slowing down decoherence or even enhancement of quantum properties. In this respect, memory effects are of primary importance, as they have been shown to improve the performances of numerous protocols in quantum information [157–160] and quantum metrology [128, 161]. They also play a key role in quantum thermodynamics [162] and measurement theory [163]. However, non-Markovian dynamics has been so far widely investigated and understood by focusing on the time/frequency domain [8], e.g. by inspecting quantities such as correlation functions at different times and spectral densities of certain environments. It is this not obvious how, and whether, introducing spatially dependent noise might affect memory effects of a given dynamical map.

6.1 Continuous-time quantum walks

Before discussing the details of the noisy walk, we briefly discuss the noiseless continuous-time quantum walk and show its analytical solution. Here we limit ourselves to the simplest case of a single particle on a linear lattice with N sites, with only first-neighbor links between sites. The quantum description of the lattice requires a set of orthonormal states $|j\rangle_{j=1}^{N}$, where $|j\rangle$ represents a localized state of the particle in the jth node of the lattice.

The Hamiltonian that describes the particle is the discrete Laplacian operator, that describes the free motion of a particle in a periodic potential

$$H_0 = -\sum_j \epsilon \, |j\rangle \langle j| - \nu_0 \sum_j ([|j\rangle \langle j+1| + |j+1\rangle \langle j|]). \tag{6.1}$$

Here ϵ is the onsite energy of each node, v_0 is the coupling coefficient between adjacent sites: we assume that they are constant and independent of the position on the lattice.

H_0 can be diagonalized exactly. If we assume periodic boundary conditions, i. e. we assume that our lattice is a closed loop, then we can move to the Bloch basis $|\psi_k\rangle = \frac{1}{\sqrt{N}} \sum_j \exp(-ikj)\,|j\rangle$ to obtain simple expressions for the eigenvalues and eigenvectors. Upon defining $\theta_n = 2n\pi/N$, we have

$$|\Psi_n\rangle = \frac{1}{\sqrt{N}} \sum_j \exp(-i\theta_n j)\,|j\rangle \tag{6.2}$$

$$E_n = \epsilon + 2v_0 \cos\theta_n, \tag{6.3}$$

with $n = 1, \ldots, N$. Notice that the onsite energy term only gives a shift in the energy levels and does not affect the eigenvectors, so it can be neglected. Knowing the spectral decomposition of H_0, we are able to evaluate $U(t) = \exp(-iH_0 t)$ and its action onto the initial state.

We now focus on an initially localized quantum walker, i. e. we consider as initial state one of the basis states $|\psi(0)\rangle = |\bar{j}\rangle$. The analytical solution for the dynamics is possible (although we don't report the calculations here), and we can study the propagation of the particle. We find that the probability distribution for the particle, given by $\psi_j(t) = |\langle j|\psi_t\rangle|^2$, is highly non-Gaussian, with two peaks that move away from the initial position as time increasing. A very interesting result is that involving the variance of the probability distribution $\sigma^2 = \langle x^2\rangle - \langle x\rangle^2$. Whereas a classical particle exhibits a diffusive behavior, with $\sigma^2 \propto t$, the quantum particle shows a *ballistic propagation*: $\sigma^2 \propto t^2$.

6.2 The model with spatially correlated noise

We now add the noise to the above quantum walk model. We introduce time-dependent stochastic fluctuations on the hopping amplitudes of Eq. (6.1), and we obtain the time-dependent Hamiltonian $H(t)$:

$$H(t) = -\sum_j \big[v_0 + v g_j(t)\big]\Big(|j\rangle\langle j+1| + |j+1\rangle\langle j|\Big), \tag{6.4}$$

in which we neglected the onsite energy term and v is the noise strength and $\{g_j(t)\}_j$ are independent RTN processes that jump between ± 1 according to the switching rate γ. This is the model that was addressed in Ref [53].

We now introduce spatial correlations in the noisy Hamiltonian (6.4) as follows. We assume that two adjacent links of the lattice can be noise-correlated with a certain probability p. Formally, this translates to the following autocorrelation function:

$$\mathbb{E}\left[g_j(t) g_k(0)\right] = \begin{cases} \propto e^{-2\gamma t}, & \text{if } j,k \text{ correlated} \\ 0, & \text{otherwise} \end{cases}. \tag{6.5}$$

For a single noise realization, these spatial correlations will form M domains of lengths $\{L_1, L_2, \ldots, L_M\}$, corresponding to M independent noise evolutions $\{g_1(1), g_2(t), \ldots, g_M(t)\}$

respectively, as shown in Fig. 6.1. The distribution of the domains is random and different for each noise realization: the probability P_M of having M domains in a particular noise realization is described by a binomial distribution

$$P_M = \binom{N-1}{M-1}(1-p)^{M-1}p^{N-M}, \tag{6.6}$$

which corresponds to the following average domain length $\bar{L}$ (as a function of p)

$$\bar{L}_p = \sum_{M=1}^{N}\left(\frac{N}{M}\right)P_M = \frac{p^N-1}{p-1}. \tag{6.7}$$

By continuity, we define $\bar{L}_1 = \lim_{p\to 1}\bar{L}_p = N$. In this case, there is a single noise domain that spans the whole lattice.

So far, the amplitude of the fluctuations ν has been considered a free parameter of the strength of the noise. Here, we are interested in the effects of noise space and time correlations *per se*, rather than in the noise strength. Thus, we set this parameter to $\nu = \nu_0$, meaning that, from now on, we are only going to consider percolation noise: the local hopping amplitudes can switch between 0 and $2\nu_0$ [164], resulting in links that are created and destroyed randomly in time, according to the statistics of the RTN process. Quite obviously, this analysis can be carried out for any value of ν and ν_0.

For each noise realization, the system time evolution is ruled by the operator $U(t) = \mathcal{T}e^{-i\int_0^\tau d\tau H(\tau)}$. The open dynamics of the walker is unraveled by computing the ensemble average of the unitary dynamics over all possible realizations

$$\bar{\rho}(t) = \mathcal{E}_t^{\mathrm{QW}}(\rho_0) = \mathbb{E}\left[U(t)\rho_0 U^\dagger(t)\right]_{\{g(t)\}} \tag{6.8}$$

where $\mathbb{E}[.]_{\{g(t)\}}$ indicates the average taken over an (in principle) infinite number of implementations of the sets $\{g_1(1), g_2(t), \ldots, g_M(t)\}$ and ρ_0 is the (fixed) initial state of the walker. Needless to say, the solution to Eq. (6.8) is analytically out of reach, given the dimension of the Hilbert space and the number of fluctuators.

One could in principle apply the transfer matrix method described in Subsection 3.3.1, suitably generalized to the problem at hand, and numerically diagonalize the matrices. But a quick evaluation of the matrices' sizes gives an idea of the challenge. If we have N sites and N fluctuators (i.e. we are in the case $p = 0$), while the size of the transfer matrix for the quantum walker is $(N^2-1)\times(N^2-1)$, which, for $N = 100$ is at the reach of current computers, the size of the matrix describing the noise state is $2^N \times 2^N \sim 10^{68}$ elements for $N = 100$.

We must thus resort to a numerical approximation of the ensemble-average with the simulation of a finite number of noise realizations R, as we discussed in Equation 3.51. For all the quantities computed in this chapter, the size of the noise sample is $R = 10\,000$, which guarantees statistical robustness of our results. The code for simulating the dynamics is similar to the one presented for qubits: we report it in Appendix B for completeness.

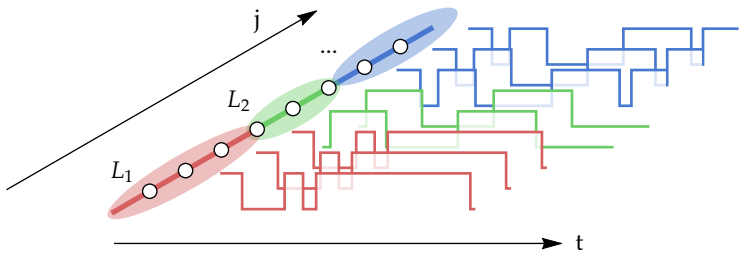

Figure 6.1: Schematic representation of the model. The lattice is divided in random spatial domains $\{L_1, L_2, \ldots, L_M\}$ for a single realization of the noise, generated according to Eq. (6.6) and of average length $\bar{L}_p$. Tunneling amplitudes within the same domain fluctuate synchronously in time and according to the same stochastic process. Different domains evolve independently from each others.

6.3 Non-Markovianity, diffusion and localization

As previously mentioned, the noise-averaged dynamics of the walker can no longer be described by Schrödinger equation and one has to resort to the machinery of open quantum systems. In this respect, a relevant question is whether the open dynamics of the walker is memory-less, i.e. Markovian, or non-Markovian. In Ref. [53] memory effects in the dynamics of the walker in presence of spatially uncorrelated RTN were investigated for some selected initial states leading to the conclusion that decreasing the switching rate γ enhances the memory effects. That scenario corresponds to noise domains of average length $\bar{L} = 1$ and therefore it is a special case study of the more general model introduced in this chapter.

Intuitively, since the non-Markovian dynamics is intrinsically connected to the time-dependency of the environment correlation functions, we can expect that whenever the spatial-uncorrelated noise is Markovian, it will also be Markovian in the spatially-correlated-noise case. This is simply because, as mentioned previously, the spatial correlations in the noise do not interfere with the RTN itself but they only *assist* it. However, if memory effects are present already in the spatially uncorrelated scenario, it is not obvious *a priori* how long-range correlated noise with $\bar{L} > 1$ will affect the non-Markovianity of the quantum map.

We use again the BLP measure (cf. Subsection 2.3.1) to characterize memory effects in the open dynamics of the walker, as was done in [53]. The BLP measure is nearly impossible to compute exactly because it involves a state optimization procedure and the number of parameters to optimize over increases exponentially with the number N of sites in the lattice. Nonetheless, it does provide a rather intuitive interpretation of memory effects in open systems and it still allows to get an insight of the behavior of memory effects by selecting some significant pairs of initial states. Using the RHP measure is out of question, because there are no easy ways of evaluating entanglement for high dimensional systems.

In Ref. [53], the dynamics governed by Eq. (6.4) in absence of spatially correlated noise was analyzed in detail, showing a transition from a diffusive to a localized regime

as a function of the switching rate γ. Furthermore, depending on the strength of the noise, a quantum-to-classical transition was also observed for the fast noise case ($\gamma > 1$), resulting in a Gaussian probability distribution of the walker's state.

Here, we aim at understanding the role of noise spatial correlations in the dynamical behavior of the walker. Specifically, we want to understand whether spatially correlated noise domains help the particle spread over the lattice or whether they instead favor localization. We quantify the extent of noise-induced localization by means of the *inverse participation ratio* (IPR) [165], defined as

$$\mathcal{I}(t) = \sum_{j=1}^{N} \langle j | \bar{\rho}(t) | j \rangle^2 . \tag{6.9}$$

IPR is bounded between $1/N$ and 1 with $\mathcal{I}(t) = 1/N$ meaning complete delocalization and $\mathcal{I}(t) = 1$ corresponding to localization on a single site. The larger the IPR, the more localized the particle is. Using IPR we now investigate how the spatially correlated time-dependent noise affects the diffusive properties of the walker.

6.4 Results

6.4.1 Localized particle

We now present the results on the dynamical properties of the walker in a noisy, spatially correlated lattice. The evolution of the walker is obtained by randomly generating the domains and the noise realizations, computing the single realization unitary dynamics and finally performing the ensemble average (6.8) for a $N = 100$ lattice and for $R = 10\,000$ iterations. First, we will focus on the non-Markovian character of the quantum map, then analyze the diffusive properties of the CTQW. As anticipated above, the maximization involved in the BLP measure is a nearly impossible task for most physical systems. Because of our computational resources and the complexity of the model at hand, this case-study is certainly no exception. However, we can still compute the integral in Eq. (2.98) for some relevant initial pairs of states and gain useful information regarding at least their dynamics.

Since we are interested in the interplay between noise-induced localization and memory effects due to spatially correlated noise, we restrict our attention to pairs of initial states that are localized on adjacent sites and we compute the following quantity

$$n_\tau\left(\gamma, \bar{L}\right) = \int_{\dot{\mathcal{D}}(t)>0} dt\, \frac{d}{dt} D\left(\mathcal{E}_t^{\mathrm{QW}}(\rho_{N/2}), \mathcal{E}_t^{\mathrm{QW}}(\rho_{1+N/2})\right), \tag{6.10}$$

for a fixed final time τ, as a function of γ. In the above equation, $\rho_j = |j\rangle\langle j|$ and $\mathcal{E}_t^{\mathrm{QW}} = \mathcal{E}_t^{\mathrm{QW}}(\gamma, \bar{L})$ is the dynamical map computed via Eq. (6.8) that depends upon the value of the noise switching rate γ and the average domains length $\bar{L}$. The integral over time in Eq. (6.10) is up to the fixed time τ.

In Fig. 6.2a we display $n_\tau\left(\gamma, \bar{L}\right)$ for a $N = 100$ lattice and $\nu_0 \tau = 20$. We choose this truncation time to ensure that the tails of the walker wave-function have not yet reached

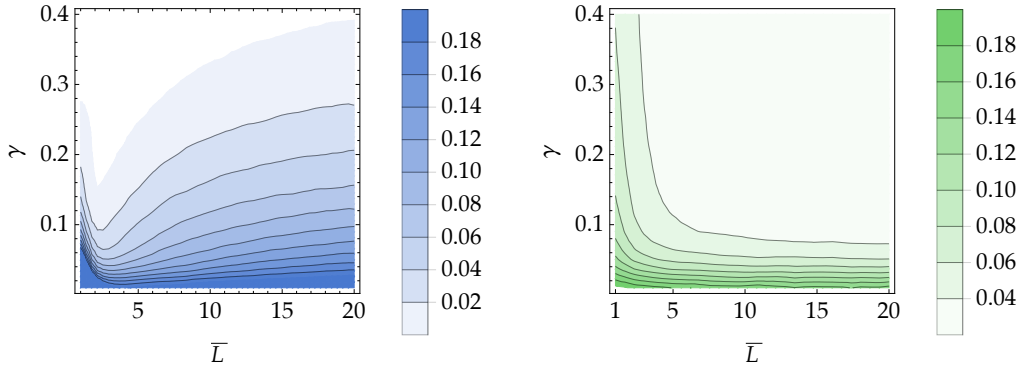

(a) Non-Markovianity

(b) IPR

Figure 6.2: (a) Non-Markovianity $n_\tau(\gamma, \bar{L})$ as a function of the average domain length $\bar{L}$ and switching rate γ for percolation noise. The selected initial states are $|N/2\rangle$ and $|N/2+1\rangle$ with $N = 100$ and $\nu_0\tau = 20$. In the white region, $n_\tau(\gamma, \bar{L}) = 0$. (b) Long-time value of the IPR as a function of average domain length $\bar{L}$ and switching rate γ for percolation noise for the initial states $|N/2\rangle$ for the same values of N and $\nu_0\tau$.

the boundaries of the lattice and therefore we need not to worry about finite-size-induced memory effects. Here we analyze a range of values for γ that are known to generate non-Markovian dynamics, for the same initial states, in the case of non-correlated RTN [53].

The striking feature we immediately notice is that, after a minimum located at $\bar{L} \approx 2$ and independent of γ, as the average domain length $\bar{L}$ is increased, the non-Markovian character evaluated through Eq. (6.10) also increases. Thus spatial correlations in the noise make memory effects stronger, at least for this set of initial states. An intuitive theoretical explanation of this behavior might be the following. The presence of domains with a typical length $\bar{L}$ is effectively equivalent to amplifying the single-link contribution to memory effects proportionally to the size of the domain. The walker experiences a smaller effective lattice of size M with, however, stronger average local disorder. We performed this calculation using increasingly separated localized initial states and found the exact same behavior, with the only difference being a smaller value of $n_\tau\left(\gamma, \bar{L}\right)$.

In Fig. 6.2b, we display the long-time IPR $\mathcal{I}(\nu_0\tau)$ as a function of γ and $\bar{L}$ computed for the initially localized state $|N/2\rangle$. This quantity is defined as the quasi-stationary value that the IPR reaches before boundary effects come into play. Interestingly, for a fixed γ, this has a maximum at $\bar{L} = 1$, similarly to $n_\tau\left(\gamma, \bar{L}\right)$, and decays fast as $\bar{L}$ increases. While uncorrelated slow noise tends to keep the walker localized around its initial position, spatial correlations break the localization and lead to a stronger diffusion of the wave function across the lattice. By increasing the value of the switching rate γ, the IPR becomes smaller as we approach memory-less and more diffusive dynamics. Therefore, while the presence of slow noise ($\gamma < 1$) tends to favor localization, by adding random spatial correlations to the very same noise we can limit this effect and allow the walker to propagate through the lattice while still retaining memory effects in its dynamics. Overall, and perhaps quite unexpectedly, for a small fixed γ, a spatially-correlated RTN

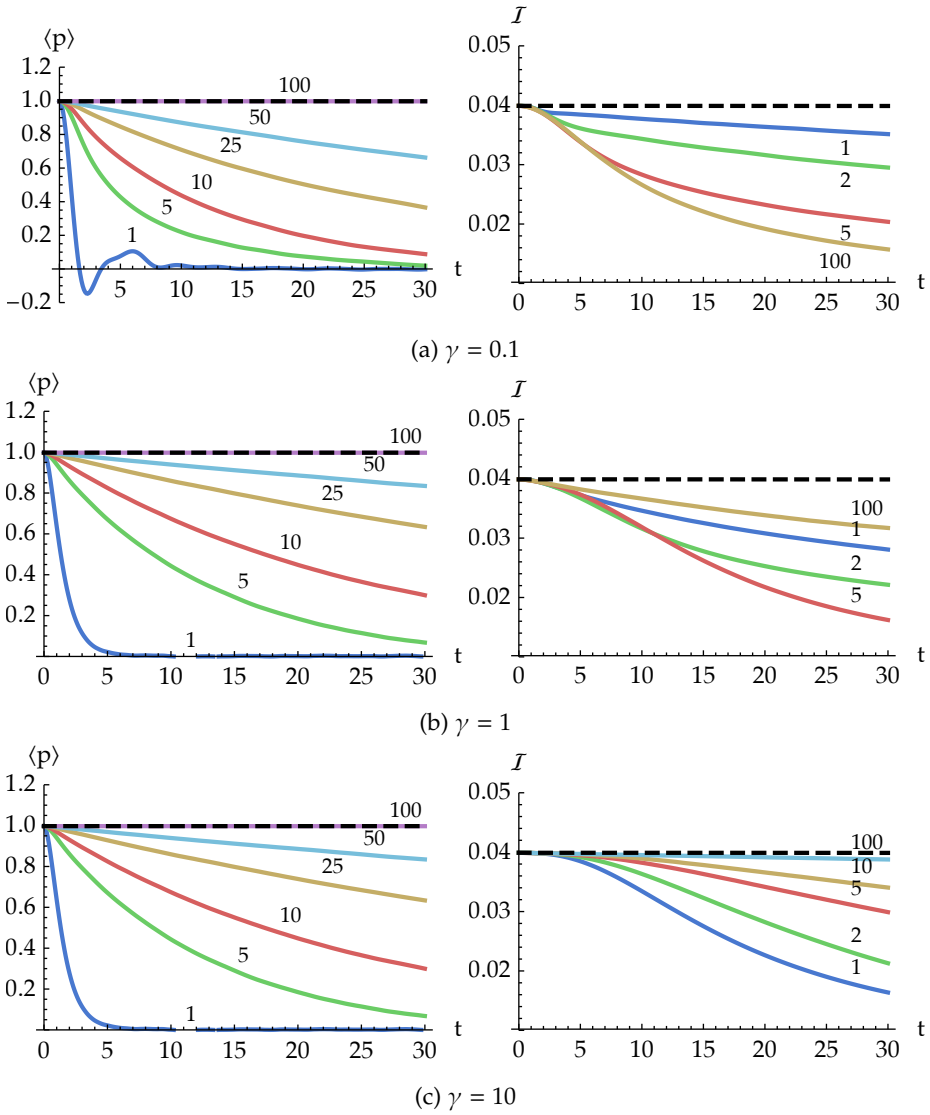

Figure 6.3: Expectation value of the momentum operator $\langle p \rangle$ (left) and IPR $\mathcal{I}$ (right) as a function of time, for different average domain lengths $\bar{L}$, for $\gamma = 0.1$ (a), 1 (b) and 10 (c), with lattice size $N = 100$. The black dashed line indicates the noiseless case. The initial state is Gaussian, Eq. (6.11), with $k_0 = \pi/2$, $\Delta = 10$.

tends to suppress localization while still enhancing memory effects.

6.4.2 Gaussian wave packets

To investigate the transport properties in this setting we turn our attention to an initial Gaussian wave packet, equipped with an average momentum k_0 and spatial spread Δ

$$|\mathcal{G}\rangle = \sum_{j=1}^{N} \left[\frac{1}{\sqrt{2\pi\Delta^2}} e^{-\frac{\left(j-\frac{N}{2}\right)^2}{2\Delta^2}} \right] e^{-ik_0 j} |j\rangle \,. \tag{6.11}$$

We study the behavior of both the IPR and the average momentum operator $\hat{p} = -i\nabla$, computed using the Born rule $\langle \hat{p}(t) \rangle = \mathrm{Tr}\left[\bar{\rho}(t)\,\hat{p}\right]$, which represents the average quantum velocity at which the wave packet travels across the lattice. Figure 6.3 shows the time evolution of these two quantities for three different values of the switching rate γ and different average domain lengths $\bar{L}$. In this case, the effects of the spatially correlated RTN become even clearer. The wave-packet momentum $\langle p \rangle$ (left column) decreases in time, until it eventually vanishes asymptotically, and this decay is faster for smaller values of γ, in agreement with Fig. 6.2b. However, while space-uncorrelated noise leads to a faster reduction of $\langle \hat{p} \rangle$, spatial correlations in the RTN allow the wave-packet to preserve momentum and travel longer across the lattice before stopping. In the limiting case of $\bar{L} = N$ (i.e. $p = 1$), the average momentum $\langle \hat{p} \rangle$ is preserved, as in the noiseless case.

Similarly to the case studied above, the IPR (right column of Fig. 6.3) generally decreases in time. However, there seems to exist a more complicated interplay between γ and $\bar{L}$. For small γ the IPR decays faster for larger values of $\bar{L}$, indicating that spatial correlations break the noise-induced localization, in agreement with our previous results. For larger switching rates γ, instead, the situation is quite the opposite: strong spatial correlations prevent the particle distribution from spreading further, thus preserving the initial IPR, with the limiting case of $p = 1$, i.e. $\bar{L} = N$ that gives the slowest possible decay.

Since the average momentum $\langle p \rangle$ decreases very slowly in time in this regime, the original wave packet can travel across the lattice, maintaining its original shape. This feature is the key ingredient for quantum transport and state transfer, where one wants a quantum state to evolve across a complex network, without losing its quantum properties, so that its quantum information content can be recovered from another point in the network.

Therefore, we have again evidence of how introducing spatial correlations in the noise helps preserving dynamical properties better than in the spatially uncorrelated case. This can surely be exploited to design protocols for state transfer and communication across networks.

Summary

- We have discussed the effects of spatial correlations on the dynamics of continuous-time quantum walks on noisy percolation lattices. The model, which allows us to

address memory effects and transport properties, is based on a stochastic time-dependent Hamiltonian, where the hopping amplitudes between adjacent nodes are described as local random-telegraph processes, which themselves show spatial correlations.

- The presence of strongly spatially correlated noise induces robust memory effects on the quantum map, as compared to the case of uncorrelated RTN. The BLP measure for the non-Markovianity of the map increases with the average length of the domains.
- Spatial correlations lead to localization-breaking, i.e. make the walker able to spread over the network and to reach distant nodes while still undergoing non-Markovian dynamics. This is shown by looking at the evolution of the inverse participation ratio of the walker.
- Spatially correlated RTN improves transport properties of an initially traveling Gaussian packet compared the analogue uncorrelated case.

Conclusions

In this thesis we have discussed and characterized the dynamics of quantum systems interacting with classical noise. We have covered the dynamics of one- and two-qubit systems and presented an experimental simulation of such dynamics. We have also shown a probing technique that allows to estimate properties of the classical noise using entangled qubits. Such a characterization is of great relevance in the quest for developing quantum technologies, as any physical implementation of qubits is affected by the interaction with the environment. Finally we have addressed quantum walks affected by spatially correlated classical noise, covering its diffusion and transport properties.

The interaction with classical noise is relevant in two different aspects. One one hand, there are physical quantum systems that interact with external macroscopic sources of noise that may be treated classically, for example a noisy magnetic field used to control the qubit or macroscopic bistable fluctuators that affect solid state qubits with RTN. On the other hand, the classical description can be an alternative to the usual approach of describing the environment as a quantum bath. In many situations, this description may be challenging or inappropriate. In these cases, modeling the environment with classical random fields, without invoking a quantum environment at all allows to reduce the degrees of freedom and simplify the description. For certain types of dynamics, for example dephasing the decoherence induced by a quantum bath may be equivalently described in terms of stochastic fluctuating classical fields [11].

In particular, we considered one- and two-qubit systems interacting with environments that are modeled by Gaussian stochastic processes and the RTN, which is a non-Gaussian process, and is the basic building block of more complex forms of noise. Among the Gaussian processes, we chose as a paradigmatic example the Ornstein-Uhlenbeck process, that has the same Lorentzian spectrum of the RTN. We first considered the dephasing dynamics induced by longitudinal noise, that is, noise with frequencies that are far away from the typical frequency of the qubit, that effectively alters the quantum coherence of the system without affecting its energy and we reviewed analytical results for the two noises.

We then moved to the case of transverse noise, where the energy of the qubit is not conserved and the dynamics is more complex. We discussed an analytical solution for the RTN that allows us to obtain the exact transfer matrix, and the numerical methods to simulate the Gaussian noise. We showed the trajectories in the Bell state tetrahedron, the dynamics of quantum correlations and we discussed the non-Markovianity of the map. We also highlighted that the two sources of noise, Gaussian and non-Gaussian, give

qualitatively different dynamics, meaning that the power spectral density is not enough to characterize the effect of the noise when it has a non-Gaussian statistics. At the same time, we showed that the effects of RTN can be simulated by OU noise and viceversa by suitably tuning their correlation time. We also underlined once more that the non-Markovianity of the map is connected to temporary revivals of quantum correlations, proving to be a resource for the processing of quantum information.

We have then discussed a photonic quantum simulator of single-qubit dephasing induced by the interaction with classical noise. The qubit is encoded in the polarization of a single photon, and the dynamics is obtained by dispersing the spectral components of the photon with a grating, then applying a different phase shift (sampled according to the probability density of the classical noise) to each component through a spatial light modulator, and then coherently collecting the components with a lens and another grating, effectively averaging over the realizations of the dynamics, which are evaluated in parallel, thanks to the quantum nature of the photon. We presented the results of simulations of dephasing channels driven by Gaussian (Ornstein-Uhlenbeck) or non-Gaussian (random telegraph) stochastic processes, and compared them to the known analytical solutions. In particular, we have addressed the non-Markovianity of the quantum map.

The implementation presented in this thesis is a proof of principle. Upon increasing the number of pixels in the spatial light modulator, one may increase the number of realizations and perform more accurate simulations of noisy channels, or explore more complex forms of classical noise such as $1/f$ noise. Moreover, the setup can be modified to address the dynamics of two-qubit systems, for instance by using both the photons coming from the non-linear crystal as signal. The apparatus could also simulate other forms of noise, such as transverse noise, where analytical solutions lack and one has to resort to numerical simulation.

We then turned to a probing scheme where qubits are used to infer the spectral properties of a complex environment described by means of classical Gaussian dephasing noise. The high sensitivity of quantum systems to the effects of environment and their small size may allow the design of extremely precise and noninvasive probing schemes. In particular, we looked for a quantum improvement in the estimation, by looking at the role of quantum correlations. We have shown that the use of entangled qubits as quantum probes outperforms the sequential use of single-qubit probes. In particular, we have shown that a joint measurement on probes prepared in a GHZ state improves the estimation of the correlation time for a broad class of environmental noises when the noise is faster than a certain threshold value. The variance of the estimator scales proportionally to N^{-2} as opposed to the classical scaling N^{-1}, entanglement is thus a resource for a quantum enhancement in the estimation of the spectral width.

The latter result is enhanced by the fact that, upon controlling the coupling between the probe and the system, the threshold value can be reduced arbitrarily. We have also discussed a simulation of a Bayesian estimation procedure, showing that scheme achieves the Cramér-Rao bound for a relatively low number of measurements, upon employing a Bayesian estimator. We have discussed the robustness of the scheme against imperfect preparation of the initial entangled state, by analyzing in detail the depolarizing and dephasing noise. We have showed that there exists a threshold purity of the initial state

above which the probing schemes outperforms the sequential scheme.

Finally, we have addressed the dynamics of continuous-time quantum walks on noisy percolation lattices and, in particular, we discussed the role of spatial correlations on the memory effects and transport properties of the walker. The model is based on a stochastic time-dependent Hamiltonian, where the hopping amplitudes between adjacent nodes are described as local random-telegraph processes, which themselves show spatial correlations. As a matter of fact, spatially correlated noise results in stronger memory effects in the dynamics and it partly suppresses the localization induced by its randomness, allowing the walker to spread further and faster across the lattice. The analysis provides novel insight into the effects of spatially correlated noise on simple graphs and represents a first step into the understanding of the role of correlated fluctuations on complex networks, which, in turn, are extremely relevant to several quantum information and computation tasks, such as quantum algorithms, quantum communication and models for realistic transport across distant nodes.

The understanding of the dynamics of open quantum systems and the possibility of controlling it are of paramount importance for developing quantum technologies. The behavior of quantum correlations under the influence of complex external environments must be addressed in any physical implementation in order to design devices for quantum information processing. In this sense, quantum non-Markovianity has received increasing attention not only as a theoretical concept, but also as a resource for technology, as it allows for recoherence effects that preserve the quantum correlations that are needed in information processing devices. Experimental advances in the manipulation of many physical systems (such as ultracold atoms, optical, solid state and superconducting quantum systems) opened the door to fascinating new possibilities regarding quantum simulation and reservoir engineering. In this thesis we have covered all these aspects in the specific scenario of quantum systems (qubits or quantum walks over lattices) interacting with classical noise. The results presented here shed some light on the behavior of quantum correlations and the presence of recoherence effects due to the non-Markovianity of the dynamics, and contribute to the general understanding of system-environment interaction. Reservoir engineering and high precision metrology and quantum simulation are key tools that will allow the development of new quantum devices and advances in fundamental research.

Appendix

A Transfer matrix elements for a qubit affected by RTN

Here we write explicitly the nonzero elements of the 3×3 transfer matrix T defined in Subsection 3.3.1, Eq. (3.35). Here μ_i and η_i are the solutions of Eqs. (3.40) and (3.41).

$$\begin{aligned} T_{11} = & \frac{e^{\mu_2 t}\left[\mu_1\mu_3\left(1-2\omega^2\right)-2\omega^2\left(2\gamma^2+\gamma\mu_2-4\omega^2\right)\right]}{4\left[1-\omega^2\left(2\gamma^2+\omega^2\right)\right]+2\gamma\mu_2\left(1-6\omega^2\right)+\mu_2^2\left(1-5\omega^2\right)} \\ & + \frac{e^{\mu_3 t}\left[4-4\omega^2\left(\gamma^2+1\right)+2\gamma\mu_3\left(1-3\omega^2\right)+\mu_3^2\left(1-2\omega^2\right)\right]}{4\left[1-\omega^2\left(2\gamma^2+\omega^2\right)\right]+2\gamma\mu_3\left(1-6\omega^2\right)+\mu_3^2\left(1-5\omega^2\right)} \\ & + \frac{e^{\mu_1 t}\left\{2\gamma\mu_3\omega^2+\mu_2\left[2\gamma\omega^2+\mu_3\left(1-2\omega^2\right)\right]+8\omega^4\right\}}{4\left[1-\omega^2\left(2\gamma^2+\omega^2\right)\right]+2\gamma\mu_1\left(1-6\omega^2\right)+\mu_1^2\left(1-5\omega^2\right)} \end{aligned} \tag{A.1}$$

$$\begin{aligned} T_{12} = -T_{21} = & \frac{\omega e^{\mu_2 t}\left[4\omega^2\left(3\gamma+\mu_2\right)-\gamma\mu_1\mu_3\right]}{4\left[1-\omega^2\left(2\gamma^2+\omega^2\right)\right]+2\gamma\mu_2\left(1-6\omega^2\right)+\mu_2^2\left(1-5\omega^2\right)} \\ & + \frac{\omega e^{\mu_1 t}\left[4\omega^2\left(\mu_3-\gamma\right)+\mu_2\left(\gamma\mu_3+4\omega^2\right)\right]}{8\gamma^2\omega^2-4-2\gamma\mu_1\left(1-6\omega^2\right)-\mu_1^2\left(1-5\omega^2\right)+4\omega^4} \\ & + \frac{\omega e^{\mu_3 t}\left[\mu_3\left(2\gamma^2+\gamma\mu_3-4\omega^2\right)+4\gamma\left(1-2\omega^2\right)\right]}{8\gamma^2\omega^2-4-2\gamma\mu_3\left(1-6\omega^2\right)-\mu_3^2\left(1-5\omega^2\right)+4\omega^4} \end{aligned} \tag{A.2}$$

$$\begin{aligned} T_{22} = 2\gamma\omega^2 \Bigg\{ & \frac{e^{\mu_1 t}\left[\mu_2\left(\gamma-\mu_3\right)+\gamma\mu_3+4\left(1+\omega^2\right)\right]}{\gamma\left\{4\left[1-\omega^2\left(2\gamma^2+\omega^2\right)\right]+2\gamma\mu_1\left(1-6\omega^2\right)+\mu_1^2\left(1-5\omega^2\right)\right\}} \\ & + \frac{e^{\mu_2 t}\left(2\gamma^2+\gamma\mu_2-4+\mu_1\mu_3-4\omega^2\right)}{\gamma\left[8\gamma^2\omega^2-4-2\gamma\mu_2\left(1-6\omega^2\right)-\mu_2^2\left(1-5\omega^2\right)+4\omega^4\right]} \\ & - \frac{\left(2\gamma+\mu_3\right)e^{\mu_3 t}}{4\left[1+2\omega^2(1-\gamma^2)+\omega^4\right]+2\gamma\mu_3\left(1-2\omega^2\right)+\mu_3^2\left(1+\omega^2\right)} \Bigg\} \end{aligned} \tag{A.3}$$

$$T_{33} = 2\omega^2 \left\{ \frac{\left(81 - \eta_1\eta_3\right) e^{\eta_2 t}}{8\left[1 - \omega^2\left(\gamma^2 + \omega^2\right)\right] + 4\gamma\eta_2\left(1 - 4\omega^2\right) + 2\eta_2^2\left(1 - 5\omega^2\right)} \right.$$
$$+ \frac{\left(8 - \eta_2\eta_3\right) e^{\eta_1 t}}{8\left[1 - \omega^2\left(\gamma^2 + \omega^2\right)\right] + 4\gamma\eta_1\left(1 - 4\omega^2\right) + 2\eta_1^2\left(1 - 5\omega^2\right)}$$
$$\left. + \frac{e^{\eta_3 t}\left[4\gamma\eta_3 + 4\left(\gamma^2 - 1 + \omega^2\right) + \eta_3^2\right]}{8\left(\gamma^2\omega^2 - 1 + \omega^4\right) - 2\eta_3\left[2\gamma\left(1 - 4\omega^2\right) + \eta_3\left(1 - 5\omega^2\right)\right]} \right\} \tag{A.4}$$

B Code for simulation of a quantum walk with spatially correlated noise

In this Appendix we report the MATLAB/Octave code that simulates the dynamics of the quantum walk subject to random telegraph noise, with spatial correlations.

The noise domains are generated according to the prescription presented in the main text. Each domain is labeled by an integer number. The $N \times R$ matrix `latticeDef` associates, for each of the R realizations of the noise, each site with its corresponding domain number. The RTN is generated in the same way as we discussed in Section 1.4.

The output of the function is an object containing a vector of time instants `t` and the cell array `rhoAvg`, containing $\bar{\rho}$ at each time instant. All the quantities of interest can be evaluated from $\bar{\rho}$. The code below assumes a particle initially localized in the middle of the lattice. An initial Gaussian wavepacket can also be considered by suitably modifying the initialization of `psi`.

```
function qw = qw_disorder(varargin)
% QW_DISORDER Simulates a 1-particle 1-d quantum walk with RTN noise
% and disordered domains
%
%   qw = qw_disorder() uses default values for the parameters and
%   returns a QuantumWalk struct (see below)
%
%   qw = qw_disorder('param1',value1,'param2',value2, ...) allows to
%           set custom values to the parameters
%
%   PARAMETERS
%
%   latticeSize         size of the lattice
%   noiseRealizations   number of noise histories to average over
%   time                rather selfexplanatory
%   gamma               switching rate of the RTN
%   p                   the probability of correlation between two sites
%   noiseAmp            Amplitude of the noise wrt the coupling
%   onSiteEnergy        selfexplanatory
%   coupling            Couplign between first neighbors
%   DysonOrder          Order of expansion of the Dyson series of U
```

```
%   jumpProb            the prob. of a jump in a time step (default .02)
%   seed                set the seed of the random number generator
%
%   RETURNS
%
%   A struct containing the above parameters and the fields
%
%   t           time vector
%   rhoAvg      A cell array containing the average density operator at
%               each time instant

    % Argument parsing
    ip = inputParser;
    addParameter(ip,'noiseRealizations',500, @isnumeric);
    addParameter(ip,'latticeSize',100,@isnumeric);
    addParameter(ip,'time',10, @isnumeric);
    addParameter(ip,'jumpProb',0.2,@isnumeric);
    addParameter(ip,'gamma', 1., @isnumeric);
    addParameter(ip,'noiseAmp',.9,@isnumeric);
    addParameter(ip,'onSiteEnergy',2,@isnumeric);
    addParameter(ip,'coupling',1,@isnumeric);
    addParameter(ip,'DysonOrder',8,@isnumeric);
    addParameter(ip,'seed',4,@isnumeric);
    addParameter(ip,'p',.0,@isnumeric);

    parse(ip,varargin{:});

    %% Parameters
    qw.N = ip.Results.latticeSize;  % Lattice size
    qw.p = ip.Results.p;
    qw.noiseRealizations = ip.Results.noiseRealizations;
    R = qw.noiseRealizations
    qw.time = ip.Results.time; % Total evolution time

    % jumpProb specifies the probability to have a jump in the timestep
    % It is used to determine the appropriate dt so that we don't miss
    % jumps of the fluctuators, so it must be low (e.g. 0.2 or less)
    qw.jumpProb = ip.Results.jumpProb;

    % Switching rate
    qw.gamma = ip.Results.gamma;

    % Initial position of the particle
    qw.initialPos = floor(qw.N / 2); % Particle localized in the center

    % Array that specifies the spatial noisy domains
    % Each number represents a noise realization. If two sites have
    % the same number then their noise is correlated
```

```
qw.latticeDef = cumsum([ones(1,R); ...
    (rand(qw.N -1,R) < 1-ip.Results.p)]);

domainIndices = qw.latticeDef;

% Parameters of the Hamiltonian
qw.onSiteEnergy = ip.Results.onSiteEnergy;
qw.coupling = - ip.Results.coupling; % First-neighbor coupling str.
qw.noiseAmp = ip.Results.noiseAmp * qw.coupling; % Noise amplitude

Hdiag = qw.onSiteEnergy * ones(qw.N,1);  % On-site energy

% Order of expansion of the Dyson series for
% U = exp (- i H dt)
qw.DysonOrder = ip.Results.DysonOrder;

% Set the seed of the random number generator
rng(ip.Results.seed, 'twister')

% dt for each time step (must be much smaller than the correlation
% time of the RTN because otherwise we miss jumps)
dt = min(.5, qw.jumpProb / qw.gamma);
qw.t = linspace(0, qw.time, floor(qw.time / dt)); % time vector
% Adjust dt so that we have the exact number of timesteps
dt = qw.t(2) - qw.t(1);
timesteps = length(qw.t); % Number of timesteps

% Initial state of the system
psi = zeros(qw.N, R);
psi(qw.initialPos, :) = 1; % Initially localised particle

% Function that returns the intervals between the next jumps.
% It draws n x m numbers from an exponential distribution
rtn_dt = @(n,m) - log(rand(n, m)) / qw.gamma;

% Count the number of spatial domains
domainCount = domainIndices(end, :);

% Initial noise coefficients (equal probability of being +/- c0

% A matrix of randomly chosen +1 and -1
pm = 2 * randi(2, max(domainCount), R) - 1;
nu = qw.noiseAmp * pm(domainIndices); % Initial noise coefficients

r1 = circshift(1: qw.N, [0,  1]);   % [N, 1, ..., N - 1]
l1 = circshift(1: qw.N, [0, -1]);   % [2, ..., N, 1]
```

```
    % Next jump times
    deltat = rtn_dt(max(domainCount), R);

    %% Output variables
    % Density operator
    [qw.rhoAvg{1:timesteps}] = deal(zeros(qw.N));
    qw.rhoAvg{1} = psi(:,1) * psi(:,1)';

    %% Simulation loop
    for ti = 2 : length(qw.t) % Time loop
        for ni = 1 : R % Noise realizations loop

            % At each time step we update the first
            % band diagonal of the Hamiltonian
            Hi1 = qw.coupling + nu(:,ni);

            % We evaluate the evolved psi by Dyson-expanding U,
            % up to a given order
            kQ = psi(:,ni);
            for k = 1 : qw.DysonOrder
                kQ = (-1i * dt) / k * ...
                     (Hdiag.*kQ + Hi1.*kQ(r1) + Hi1(l1).*kQ(l1));
                psi(:,ni) = psi(:,ni) + kQ;
            end

            % We check which of the fluctuators have jumped.
            % If they did, we flip their state and calculate
            % the next jump time, updating the jump-time vector
            jumpdomains = qw.t(ti) > deltat(:,ni);
            jds = sum(jumpdomains);
            if jds > 0
                jumps = qw.t(ti) > deltat(domainIndices(:,ni),ni);
                nu(jumps,ni) = - nu(jumps,ni);
                deltat(jumpdomains,ni) = deltat(jumpdomains,ni) + ...
                                         rtn_dt(jds,1);
            end

            % We build the average density operator
            qw.rhoAvg{ti} = qw.rhoAvg{ti} + ...
                            psi(:,ni) * psi(:,ni)' / R;
        end
    end
end
```

Bibliography

[1] N. Gisin, G. Ribordy, W. Tittel, and H. Zbinden, Rev. Mod. Phys. **74**, 145 (2002).

[2] M. A. Nielsen and I. L. Chuang, *Quantum computation and quantum information* (Cambridge University Press, 2010).

[3] V. Giovannetti, S. Lloyd, and L. Maccone, Nat. Photonics **5**, 222 (2011).

[4] G. Adesso, T. R. Bromley, and M. Cianciaruso, J. Phys. A Math. Theor. **49**, 473001 (2016).

[5] A. Datta, A. Shaji, and C. M. Caves, Phys. Rev. Lett. **100**, 050502 (2008).

[6] B. Dakić, Y. O. Lipp, X. Ma, M. Ringbauer, S. Kropatschek, S. Barz, T. Paterek, V. Vedral, A. Zeilinger, Č. Brukner, and P. Walther, Nat. Phys. **8**, 666 (2012).

[7] H.-P. Breuer and F. Petruccione, *The Theory of Open Quantum Systems* (Oxford University Press, 2002).

[8] H.-P. Breuer, E.-M. Laine, J. Piilo, and B. Vacchini, Rev. Mod. Phys. **88**, 21002 (2016).

[9] C. Addis, B. Bylicka, D. Chruściński, and S. Maniscalco, Phys. Rev. A **90**, 052103 (2014).

[10] Á. Rivas, S. F. Huelga, and M. B. Plenio, Rep. Prog. Phys. **77**, 094001 (2014).

[11] D. Crow and R. Joynt, Phys. Rev. A **89**, 042123 (2014).

[12] J. Helm and W. T. Strunz, Phys. Rev. A **80**, 042108 (2009).

[13] W. M. Witzel, K. Young, and S. Das Sarma, Phys. Rev. B **90**, 115431 (2014).

[14] P. Liuzzo-Scorpo, A. Cuccoli, and P. Verrucchi, EPL **111**, 40008 (2015).

[15] C. Foti, A. Cuccoli, and P. Verrucchi, Phys. Rev. A **94**, 62127 (2016).

[16] W. T. Strunz, Open Syst. Inf. Dyn. **12**, 65 (2005).

[17] A. Pernice and W. T. Strunz, Phys. Rev. A **84**, 62121 (2011).

[18] M. A. C. Rossi, C. Foti, A. Cuccoli, J. Trapani, P. Verrucchi, and M. G. A. Paris, Phys. Rev. A **96**, 032116 (2017).

[19] E. Paladino, M. Y. Galperin, G. Falci, and L. B. Altshuler, Rev. Mod. Phys. **86**, 361 (2014).

[20] C. Benedetti, *Decoherence, non-Markovianity and quantum estimation in qubit systems subject to classical noise*, Ph.D. thesis, Università degli Studi di Milano (2015).

[21] T. Yu and J. H. Eberly, Opt. Comm. **283**, 676 (2010).

[22] B. Bellomo, G. Compagno, A. D'Arrigo, G. Falci, R. Lo Franco, and E. Paladino, Phys. Rev. A **81**, 062309 (2010).

[23] J.-Q. Li and J.-Q. Liang, Phys. Lett. A **375**, 1496 (2011).

[24] C. Benedetti, F. Buscemi, P. Bordone, and M. G. A. Paris, Int. J. Quantum Inf. **10**, 1241005 (2012).

[25] P. Bordone, F. Buscemi, and C. Benedetti, Fluct. Noise Lett. **11**, 1242003 (2012).

[26] R. Lo Franco, B. Bellomo, E. Andersson, and G. Compagno, Phys. Rev. A **85**, 032318 (2012).

[27] R. Lo Franco, B. Bellomo, S. Maniscalco, and G. Compagno, Int. J. Mod. Phys. B **27**, 1345053 (2013).

[28] J.-S. Xu, K. Sun, C.-F. Li, X.-Y. Xu, G.-C. Guo, E. Andersson, R. Lo Franco, and G. Compagno, Nat. Commun. **4**, 2851 (2013).

[29] A. D'Arrigo, R. Lo Franco, G. Benenti, E. Paladino, and G. Falci, Ann. Phys. (N. Y). **350**, 211 (2014).

[30] R. Lo Franco and G. Compagno, "Overview on the phenomenon of two-qubit entanglement revivals in classical environments," in *Lectures on General Quantum Correlations and their Applications*, edited by F. F. Fanchini, D. d. O. Soares Pinto, and G. Adesso (Springer International Publishing, Cham, 2017) pp. 367–391.

[31] J. Li, M. P. Silveri, K. S. Kumar, J.-M. J.-M. Pirkkalainen, A. Vepsäläinen, W. C. Chien, J. Tuorila, M. a. Sillanpää, P. J. Hakonen, E. V. Thuneberg, and G. S. Paraoanu, Nat. Commun. **4**, 1420 (2013).

[32] T. Yu and J. H. Eberly, Opt. Comm. **264**, 393 (2006).

[33] P. Szańkowski, M. Trippenbach, and Y. B. Band, Phys. Rev. E **87**, 052112 (2013).

[34] K. Kakuyanagi, T. Meno, S. Saito, H. Nakano, K. Semba, H. Takayanagi, F. Deppe, and A. Shnirman, Phys. Rev. Lett. **98**, 047004 (2007).

[35] F. Yoshihara, T. Fuse, S. Ashhab, K. Kakuyanagi, S. Saito, and K. Semba, Nat. Phys. , 3906 (2016).

[36] E. Paladino, L. Faoro, G. Falci, and R. Fazio, Phys. Rev. Lett. **88**, 228304 (2002).

[37] J. Trapani and M. G. A. Paris, Phys. Rev. A **93**, 42119 (2016).

[38] J. Trapani, M. Bina, S. Maniscalco, and M. G. A. Paris, Phys. Rev. A **91**, 022113 (2015).

[39] J. Trapani, *Stochastic noise approach to non-Markovian decoherence in continuous variable open quantum systems*, Ph.D. thesis, Università degli Studi di Milano (2017).

[40] S. L. Braunstein, J. Phys. A. Math. Gen. **25**, 3813 (1992).

[41] D. J. Wineland, J. J. Bollinger, W. M. Itano, F. L. Moore, and D. J. Heinzen, Phys. Rev. A **46**, R6797 (1992).

[42] S. F. Huelga, C. Macchiavello, T. Pellizzari, A. K. Ekert, M. B. Plenio, and J. I. Cirac, Phys. Rev. Lett. **79**, 3865 (1997).

[43] V. Giovannetti, S. Lloyd, and L. Maccone, Phys. Rev. Lett. **96**, 010401 (2006).

[44] R. Schnabel, N. Mavalvala, D. E. McClelland, and P. K. Lam, Nat. Commun. **1**, 121 (2010).

[45] C. Benedetti and M. G. A. Paris, Phys. Lett. A **378**, 2495 (2014).

[46] C. Benedetti, F. Buscemi, P. Bordone, and M. G. A. Paris, Phys. Rev. A **89**, 032114 (2014).

[47] A. M. Childs and J. Goldstone, Phys. Rev. A **70**, 22314 (2004).

[48] A. M. Childs, Phys. Rev. Lett. **102**, 180501 (2009).

[49] O. Mülken, V. Pernice, and A. Blumen, Phys. Rev. E **76**, 51125 (2007).

[50] H. Schmitz, R. Matjeschk, C. Schneider, J. Glueckert, M. Enderlein, T. Huber, and T. Schaetz, Phys. Rev. Lett. **103**, 090504 (2009).

[51] M. Karski, L. Forster, J.-M. Choi, A. Steffen, W. Alt, D. Meschede, and A. Widera, Science **325**, 174 (2009).

[52] H. B. Perets, Y. Lahini, F. Pozzi, M. Sorel, R. Morandotti, and Y. Silberberg, Phys. Rev. Lett. **100**, 170506 (2008).

[53] C. Benedetti, F. Buscemi, P. Bordone, and M. G. A. Paris, Phys. Rev. A **93**, 042313 (2016).

[54] I. Siloi, C. Benedetti, E. Piccinini, J. Piilo, S. Maniscalco, M. G. A. Paris, and P. Bordone, Phys. Rev. A **95**, 022106 (2017).

[55] C. W. Gardiner, *Handbook of Stochastic Methods for Physics, Chemistry and the Natural Sciences* (Springer-Verlag, Berlin, 2004).

[56] G. E. Uhlenbeck and L. S. Ornstein, Phys. Rev. **36**, 823 (1930).

[57] C. W. Gardiner and P. Zoller, *The Quantum World of Ultra-Cold Atoms and Light Book 1: Foundations of Quantum Optics* (Imperial College Press, London, 2014).

[58] J. Bergli, Y. M. Galperin, and B. L. Altshuler, New J. Phys. **11**, 025002 (2009).

[59] J. Bergli, Y. M. Galperin, and B. L. Altshuler, Phys. Rev. B **74**, 024509 (2006).

[60] F. W. J. Olver, D. W. Lozier, R. F. Boisvert, and C. W. Clark, eds., *NIST Handbook of Mathematical Functions* (Cambridge University Press, New York, NY, 2010).

[61] T. Yu and J. H. Eberly, Quantum Inf. Comp. **7**, 459 (2007).

[62] A. Rau, J. Phys. A **42**, 412002 (2009).

[63] R. Horodecki, P. Horodecki, M. Horodecki, and K. Horodecki, Rev. Mod. Phys. **81**, 865 (2009).

[64] G. Vidal and R. F. Werner, Phys. Rev. A **65**, 032314 (2002).

[65] H. Ollivier and W. H. Zurek, Phys. Rev. Lett. **88**, 017901 (2001).

[66] S. Barnett, *Quantum information* (Oxford University Press, Oxford, 2009).

[67] A. Peres, Phys. Rev. Lett. **77**, 1413 (1996).

[68] M. Horodecki, P. Horodecki, and R. Horodecki, Phys. Lett. A **223**, 1 (1996).

[69] V. Madhok and A. Datta, Int. J. Mod. Phys. B **27**, 1345041 (2013).

[70] S. Luo, Phys. Rev. A **77**, 042303 (2008).

[71] A. Ferraro, L. Aolita, D. Cavalcanti, F. M. Cucchietti, and A. Acín, Phys. Rev. A **81**, 052318 (2010).

[72] K. Modi, A. Brodutch, H. Cable, T. Paterek, and V. Vedral, Rev. Mod. Phys. **84**, 1655 (2012).

[73] A. Kossakowski, Rep. Math. Phys. **3**, 247 (1972).

[74] V. Gorini, A. Kossakowski, and E. C. G. Sudarshan, J. Math. Phys. **17**, 821 (1976).

[75] G. Lindblad, Commun. Math. Phys. **48**, 119 (1976).

[76] H.-P. Breuer, E.-M. Laine, and J. Piilo, Phys. Rev. Lett. **103**, 210401 (2009).

[77] Á. Rivas, S. F. Huelga, and M. B. Plenio, Phys. Rev. Lett. **105**, 050403 (2010).

[78] E.-M. Laine, J. Piilo, and H.-P. Breuer, Phys. Rev. A **81**, 062115 (2010).

[79] S. Wißmann, A. Karlsson, E.-M. Laine, J. Piilo, and H.-P. Breuer, Phys. Rev. A **86**, 062108 (2012).

[80] A. Jamiołkowski, Rep. Math. Phys. **3**, 275 (1972).

[81] M.-D. Choi, Linear Algebr. Appl. **10**, 285 (1975).

[82] O. E. Barndorff-Nielsen and R. D. Gill, J. Phys. A. Math. Gen. **33**, 4481 (2000).

[83] C. W. Helstrom, *Quantum Detection and Estimation Theory*, Mathematics in Science and Engineering: a series of monographs and textbooks, Vol. 84 (Academic Press, New York, 1976) p. 309.

[84] A. S. Holevo, *Statistical Structure of Quantum Theory*, Lecture Notes in Physics Monographs, Vol. 67 (Springer, Berlin, 2001).

[85] M. G. A. Paris, Int. J. Quantum Inf. **7**, 125 (2009).

[86] H. Cramèr, *Mathematical Methods of Statistics* (Princeton Univ. Press, Princeton, 1946).

[87] E. L. Lehmann and G. Casella, *Theory of Point Estimation*, Springer Texts in Statistics (Springer-Verlag, New York, 1998) p. 590.

[88] L. Seveso, M. A. C. Rossi, and M. G. A. Paris, Phys. Rev. A **95**, 012111 (2017).

[89] M. A. C. Rossi, T. Giani, and M. G. A. Paris, Phys. Rev. D **94**, 024014 (2016).

[90] S. L. Braunstein and C. M. Caves, Phys. Rev. Lett. **72**, 3439 (1994).

[91] M. Hayashi, *Quantum Information: An Introduction* (Springer, New York, NY, 2006) p. 426.

[92] M. A. C. Rossi, C. Benedetti, and M. G. A. Paris, Int. J. Quantum Inf. **12**, 1560003 (2014).

[93] M. A. C. Rossi and M. G. A. Paris, J. Chem. Phys. **144**, 024113 (2016).

[94] W. Magnus, Commun. Pur. Appl. Math. **7**, 649 (1954).

[95] B. Cheng, Q.-H. Wang, and R. Joynt, Phys. Rev. A **78**, 022313 (2008).

[96] R. Joynt, D. Zhou, and Q.-H. Wang, Int. J. Mod. Phys. B **25**, 2115 (2011).

[97] I. A. Goychuk, Phys. Rev. E **51**, 6267 (1995).

[98] I. Goychuk and P. Hänggi, Chem. Phys. **324**, 160 (2006).

[99] P. W. Anderson and P. R. Weiss, Rev. Mod. Phys. **25**, 269 (1953).

[100] R. F. Werner, Phys. Rev. A **40**, 4277 (1989).

[101] Z. He, J. Zou, L. Li, and B. Shao, Phys. Rev. A **83**, 012108 (2011).

[102] C. Benedetti, M. G. A. Paris, and S. Maniscalco, Phys. Rev. A **89**, 012114 (2014).

[103] A. Aspuru-Guzik and P. Walther, Nat. Phys. **8**, 285 (2012).

[104] M. A. Broome, A. Fedrizzi, B. P. Lanyon, I. Kassal, A. Aspuru-Guzik, and A. G. White, Phys. Rev. Lett. **104**, 153602 (2010).

[105] B. P. Lanyon, J. D. Whitfield, G. G. Gillett, M. E. Goggin, M. P. A. Almeida, I. Kassal, J. D. Biamonte, M. Mohseni, B. J. Powell, M. Barbieri, A. Aspuru-Guzik, and A. G. White, Nat. Chem. **2**, 106 (2010).

[106] J. Ma, X. Wang, C. Sun, and F. Nori, Phys. Rep. **509**, 89 (2011).

[107] X. Deng, S. Hao, H. Guo, C. Xie, and X. Su, Sci. Rep. **6**, 22914 (2016).

[108] A. M. Weiner, Rev. Sci. Instrum. **71**, 1929 (2000).

[109] K. Banaszek, G. M. D'Ariano, M. G. A. Paris, and M. F. Sacchi, Phys. Rev. A **61**, 010304 (1999).

[110] D. F. V. James, P. G. Kwiat, W. J. Munro, and A. G. White, Phys. Rev. A **64**, 052312 (2001).

[111] A. Joobeur, B. E. A. Saleh, T. S. Larchuk, and M. C. Teich, Phys. Rev. A **53**, 4360 (1996).

[112] P. Pechukas, Phys. Rev. Lett. **73**, 1060 (1994).

[113] S. Cialdi, A. Smirne, M. G. A. Paris, S. Olivares, and B. Vacchini, Phys. Rev. A **90**, 050301(R) (2014).

[114] B. M. Escher, R. L. de Matos Filho, and L. Davidovich, Nat. Phys. **7**, 406 (2011).

[115] S. Alipour, M. Mehboudi, and A. Rezakhani, Phys. Rev. Lett. **112**, 120405 (2014).

[116] A. Zwick, G. A. Álvarez, and G. Kurizki, Phys. Rev. Appl. **5**, 014007 (2016).

[117] G. A. Paz-Silva, L. M. Norris, and L. Viola, Phys. Rev. A **95**, 022121 (2017).

[118] P. Hänggi and P. Jung, in *Adv. Chem. Phys.*, Vol. 89, edited by I. Prigogine and S. A. Rice (John Wiley & Sons, Inc., 1995) pp. 239–326.

[119] J. M. Taylor, P. Cappellaro, L. Childress, L. Jiang, D. Budker, P. R. Hemmer, A. Yacoby, R. Walsworth, and M. D. Lukin, Nat. Phys. **4**, 810 (2008).

[120] A. K. Mittermaier and L. E. Kay, Trends Biochem. Sci. **34**, 601 (2009).

[121] S. Zhong and H. Xin, Chem. Phys. Lett. **333**, 133 (2001).

[122] J. Bylander, S. Gustavsson, F. Yan, F. Yoshihara, K. Harrabi, G. Fitch, D. G. Cory, Y. Nakamura, J.-S. Tsai, and W. D. Oliver, Nat. Phys. **7**, 565 (2011).

[123] J. Zhang, X. Peng, N. Rajendran, and D. Suter, Phys. Rev. A **75**, 042314 (2007).

[124] M. Ali Ahmed, G. Álvarez, and D. Suter, Phys. Rev. A **87**, 042309 (2013).

[125] I. Almog, Y. Sagi, G. Gordon, G. Bensky, G. Kurizki, and N. Davidson, J. Phys. B **44**, 154006 (2011).

[126] L. Banchi, P. Giorda, and P. Zanardi, Phys. Rev. E **89**, 022102 (2014).

[127] R. Vasile, F. Galve, and R. Zambrini, Phys. Rev. A **89**, 022109 (2014).

[128] A. W. Chin, S. F. Huelga, and M. B. Plenio, Phys. Rev. Lett. **109**, 233601 (2012).

[129] P. Haikka and S. Maniscalco, Open Syst. Inf. Dyn. **21**, 1440005 (2014).

[130] J. J. . Bollinger, W. M. Itano, D. J. Wineland, and D. J. Heinzen, Phys. Rev. A **54**, R4649 (1996).

[131] R. Demkowicz-Dobrzański, J. Kołodyński, and M. Guţă, Nat. Commun. **3**, 1063 (2012).

[132] G. A. Álvarez and D. Suter, Phys. Rev. Lett. **107**, 230501 (2011).

[133] M. G. A. Paris, Phys. A Stat. Mech. its Appl. **413**, 256 (2014).

[134] L. Cywiński, Phys. Rev. A **90**, 042307 (2014).

[135] M. A. C. M. Rossi and M. M. G. A. Paris, Phys. Rev. A **92**, 010302 (2015).

[136] G. M. D'Ariano, P. Lo Presti, and M. G. A. Paris, Phys. Rev. Lett. **87**, 270404 (2001).

[137] A. Fujiwara, Phys. Rev. A **63**, 042304 (2001).

[138] A. Acín, E. Jané, and G. Vidal, Phys. Rev. A **64**, 050302 (2001).

[139] F. Mezzadri, Not. AMS **54**, 592 (2007).

[140] Y. Aharonov, L. Davidovich, and N. Zagury, Phys. Rev. A **48**, 1687 (1993).

[141] E. Farhi and S. Gutmann, Phys. Rev. A **58**, 915 (1998).

[142] S. Chakraborty, L. Novo, A. Ambainis, and Y. Omar, Phys. Rev. Lett. **116**, 100501 (2016).

[143] H. Bougroura, H. Aissaoui, N. Chancellor, and V. Kendon, Phys. Rev. A **94**, 62331 (2016).

[144] D. Tamascelli, S. Olivares, S. Rossotti, R. Osellame, and M. G. A. Paris, Sci. Rep. **6**, 26054 (2016).

[145] M. Mohseni, P. Rebentrost, S. Lloyd, and A. Aspuru-Guzik, J. Chem. Phys. **129**, 174106 (2008).

[146] Y. Yin, D. E. Katsanos, and S. N. Evangelou, Phys. Rev. A **77**, 22302 (2008).

[147] A. Schreiber, K. N. Cassemiro, V. Potočfiek, A. Gábris, I. Jex, and C. Silberhorn, Phys. Rev. Lett. **106**, 180403 (2011).

[148] Z. J. Li and J. B. Wang, Sci. Rep. **5**, 13585 (2015).

[149] T. Chattaraj and R. V. Krems, Phys. Rev. A **94**, 23601 (2016).

[150] M. A. C. Rossi, C. Benedetti, M. Borrelli, S. Maniscalco, and M. G. A. Paris, Phys. Rev. A **96**, 040301 (2017).

[151] P. W. Anderson, Phys. Rev. Lett. **18**, 1049 (1967).

[152] D. M. Basko, I. L. Aleiner, and B. L. Altshuler, Ann. Phys. **321**, 1126 (2006).

[153] R. Nandkishore and D. A. Huse, Ann. Rev. Cond. Matt. Phys. **6**, 15 (2015).

[154] I. Bloch, J. Dalibard, and W. Zwerger, Rev. Mod. Phys. **80**, 885 (2008).

[155] M. A. Cazalilla, R. Citro, T. Giamarchi, E. Orignac, and M. Rigol, Rev. Mod. Phys. **83**, 1405 (2011).

[156] F. Meinert, M. J. Mark, K. Lauber, A. J. Daley, and H.-C. Nägerl, Phys. Rev. Lett. **116**, 205301 (2016).

[157] A. Karlsson, H. Lyyra, E.-M. Laine, S. Maniscalco, and J. Piilo, Phys. Rev. A **93**, 32135 (2016).

[158] B.-H. Liu, X.-M. Hu, Y.-F. Huang, C.-F. Li, G.-C. Guo, A. Karlsson, E.-M. Laine, S. Maniscalco, C. Macchiavello, and J. Piilo, EPL **114**, 10005 (2016).

[159] E.-M. Laine, H.-P. Breuer, and J. Piilo, Sci. Rep. **4**, 4620 (2014).

[160] B. Bylicka, D. Chruściński, and S. Maniscalco, Sci. Rep. **4**, 5720 (2014).

[161] Y. Matsuzaki, S. C. Benjamin, and J. Fitzsimons, Phys. Rev. A **84**, 12103 (2011).

[162] B. Bylicka, M. Tukiainen, D. Chruściński, J. Piilo, and S. Maniscalco, Sci. Rep. **6**, 27989 (2016).

[163] G. Karpat, J. Piilo, and S. Maniscalco, EPL **111**, 50006 (2015).

[164] Z. Darázs and T. Kiss, J. Phys. A **46**, 375305 (2013).

[165] M. Modugno, New J. Phys. **11**, 33023 (2009).